Ph.D. thesis

Synthesis and Strain Analysis of Contracted Porphyrin-related Macrocycles

(環縮小ポルフィリン類縁体の合成と歪み解析)

Graduate School of Chemical Sciences and Engineering,
Hokkaido University

Yuhua Sun

Content

Chapter 4. Synthesis and property investigation of designed [2.2](2,5)pyrrolophane, the cyclo[4]pyrrole with α-β direct linkage

4.1. Introduction
4.2. Synthesis of cyclo[4]pyrrole
4.3. Ring strain analysis
4.4. Property investigation
4.5. Conclusion
4.6. Experimental section
4.7. Reference

Chapter 5. Promising bipyrrole precursor synthesis for elusive cyclic tetrapyrrole with cyclooctatetraene core

5.1. Introduction
5.2. Synthesis of bipyrrole precursor
5.3. Preliminary attempt for homocoupling of bipyrrole
5.4. Conclusion
5.5. Experimental section
5.6. Reference

Chapter 6. Summary and outlook

Chapter 1

General introduction

1.1 Porphyrin and related macrocycles

The first chemical synthesis of porphyrin was found in 1935 by Rothemund[1] with the condensation of pyrrole and aldehyde. Porphyrin keeps attraction for scientists for a long time because of the following two reasons. Firstly, the skeleton of porphyrin is highly related to some important molecules which has crucial roles in life, such as Heme B[2] and Chlorophyll a[3], and the synthesis related process has been a focus of research for a long time[4]. Secondly, the unique electronic structures endow attractive photophysical properties that can be used as photodynamic therapy[5] and gave rise to some new theories like Gouterman four-orbital model[6].

On the other hand, if replace the sp^2 *meso* carbon to sp^3 *meso* carbon, the resulting molecule so called calix[4]pyrrole which was found more earlier than porphyrin by Baeyer[7] in 1886. However, for a century after its discovery, this molecule did not receive much attention because of the blocked conjugation until the report of anion binding ability[8] in 1996, after which it became an important subject of supramolecular research[9].

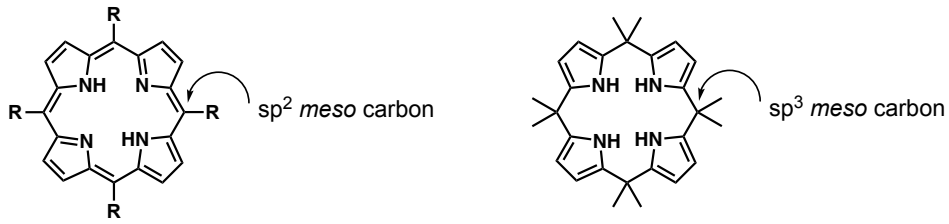

Porphyrin **Calix[4]pyrrole**

Figure 1-1. Structure of porphyrin and calix[4]pyrrole.

Nowadays, both porphyrin and calix[4]pyrrole are important macrocycles and in the recent decades, various analogues of them already be developed that greatly expanded the understanding of related fields. For these novel analogues, a common and widely accepted classification method is to classify them according to molecular size.

In the case of porphyrin (**Figure 1-2**), if the skeleton of tetrapyrrole with four *meso* carbon is not change with only linkage difference, such compounds so called isomeric analogues like N-confused porphyrin[10] that one of the most typical of them. Once increase the number of pyrrole unit and/or the number of *meso* carbon, the resulting compounds so called expanded analogues such as sapphyrin[11]. On the contrary, if decrease the number of

pyrrole unit and/or the number of *meso* carbon, the resulting compounds so called contracted analogues, for example, the subporphyrin[12].

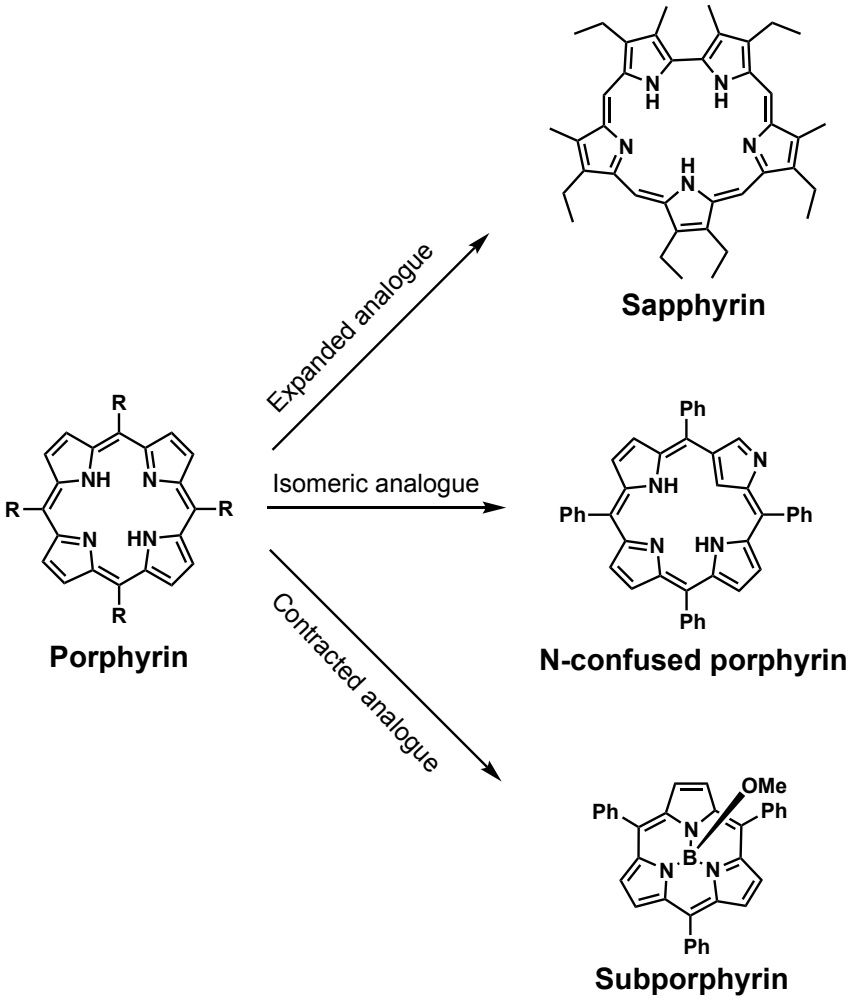

Figure 1-2. Three types of analogues of porphyrin classified by macrocyclic size and the corresponding examples.

With the similar classification method, the analogues of calix[4]pyrrole also can be identified as expanded analogue, isomeric analogue, and contracted analogue. Calix[5]pyrrole[13], N-confused calix[4]pyrrole[14] and calix[3]pyrrole[15] are the representative compounds for these three types of analogues respectively as shown in **Figure 1-3**.

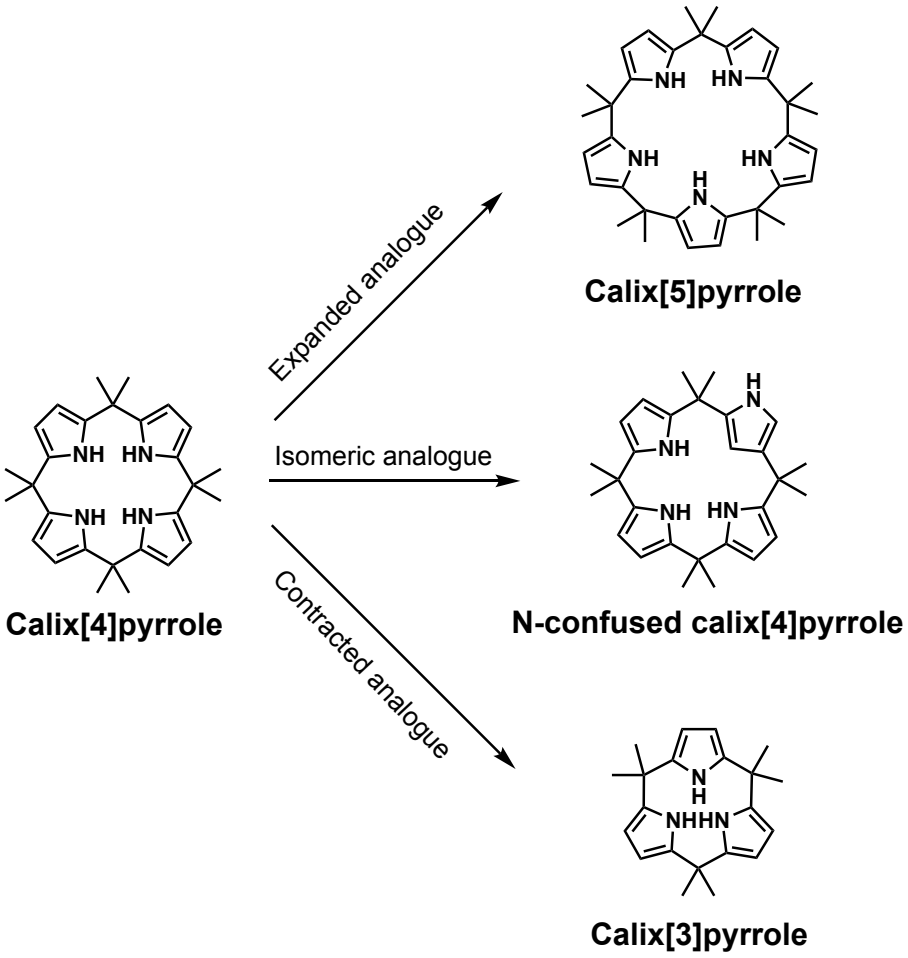

Figure 1-3. Three types of analogues of calix[4]pyrrole classified by macrocyclic size and the corresponding examples.

Besides the conjugated structure and coordination properties which have attracted much attention, these compounds as macrocyclic molecules also have another important fundamental property, ring strain. And the effect of ring strain differs for different types of analogues, which will be discussed in the next section.

1.2 Effect of ring strain on the structure

1.2.1 Effect of ring strain on porphyrin, calix[4]pyrrole and their isomeric analogues

Porphyrin and calix[4]pyrrole were considered as the optimal ring sizes so that these two type molecules can be found from one-pot condensation at a very early time. Such preferential selectivity should be the balance between enthalpy and entropy factors[16] that extremely small ring strain make the formation of them favorable from enthalpy. The small ring strain can be proved by analyzing the single crystal structure of them and comparing bond angle with pyrrole[17] and ideal sp^2 carbon and sp^3 carbon.

According to the planar crystal structure of tetraphenylporphyrin (**Figure 1-4**) reported by Silvers *et al*[18], the bond angles α between pyrrole N–pyrrole alphaC–*meso* C are within the range of 125.64-126.88°, which is close to the bond angle (121.50°) in pyrrole[17]. In addition, the bond angle β of four *meso* carbon between two adjacent pyrroles is 125.55-125.85° that close to the bond angle of ideal sp^2 carbon. According to such small bond bent, the ring strain can be regard has less effect.

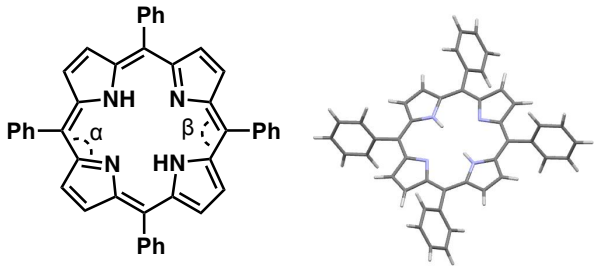

Figure 1-4. Structure of tetraphenylporphyrin[18]. (Solvent molecules are omitted for clarity)

As for calix[4]pyrrole, with the crystal data reported by Gale *et al*[8], the ring strain is almost negligible in this 1,3-alternate conformation (**Figure 1-5**). Because the bond angles α between pyrrole N–pyrrole alphaC–*meso* C are within the range of 121.00-122.00° that very close to the bond angle (121.50°) in pyrrole[17]. And the bond angles β of four *meso* carbon between two adjacent pyrroles are within the range of 109.50-109.90° that also very close to the bond angle of ideal sp^3 carbon.

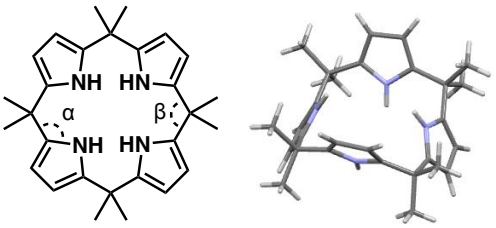

Figure 1-5. Structure of calix[4]pyrrole[8]. (Solvent molecules are omitted for clarity)

The isomeric analogues of porphyrin and calix[4]pyrrole have similar core skeleton sizes so that normally the ring strain is not considered an important factor affecting their structures and properties.

However, once change the ring size become expanded or contracted analogue, the effect of ring strain will appear, and such effect has different influence on expanded and contracted respectively.

1.2.2 Effect of ring strain on expanded analogues

For the expanded analogues of porphyrin, although the change of ring size will increase ring strain, it also makes the macrocyclic structure more flexible. Hence, if there is no force to change their conformation such as coordination with metal ion, plenty of expanded analogues can release the strain by adjust their conformation to allow the bond angles approach their ideal values. For example, the [28]Hexaphyrins(1.1.1.1.1.1)[19] can release the strain by inverting pyrrole subunits (**Figure 1-6**), and the larger-sized [34]octaphyrin(1.1.1.0.1.1.1.0)[20] can release the strain by generating "figure eight" conformation (**Figure 1-7**).

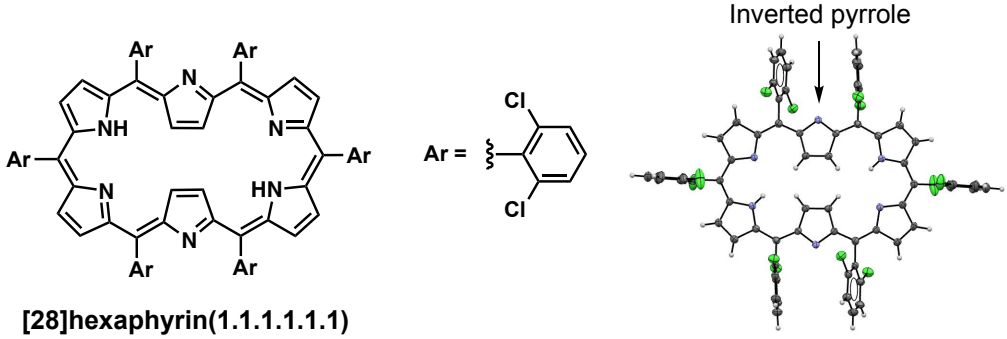

Figure 1-6. Structure of [28]Hexaphyrins(1.1.1.1.1.1)[19].

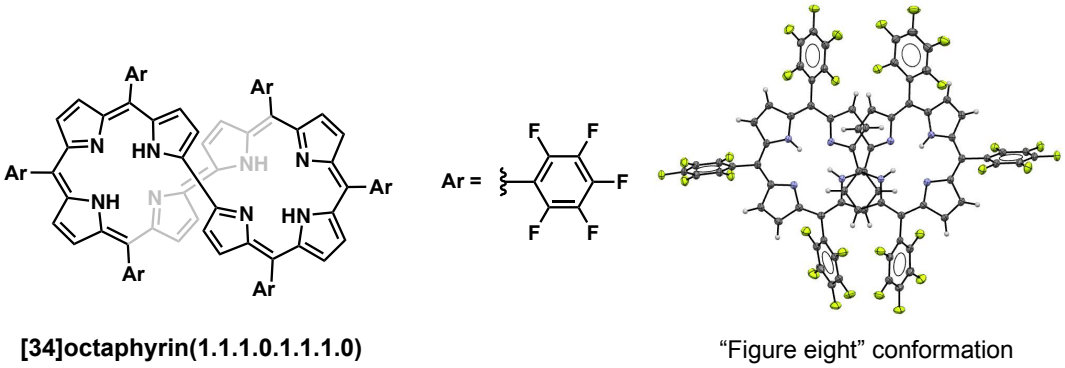

Figure 1-7. Structure of [34]octaphyrin(1.1.1.0.1.1.1.0)[20].

In the case of expanded analogues of calix[4]pyrrole, due to the sp^3 *meso* carbon, the size-increased macrocycles still can keep good flexibility to release strain, like calix[5]pyrrole[13] (**Figure 1-8a**) and calix[6]pyrrole[21] (**Figure 1-8b**) that both molecules shown highly twisted structure to keep low strain energy in the absence of coordinating anions.

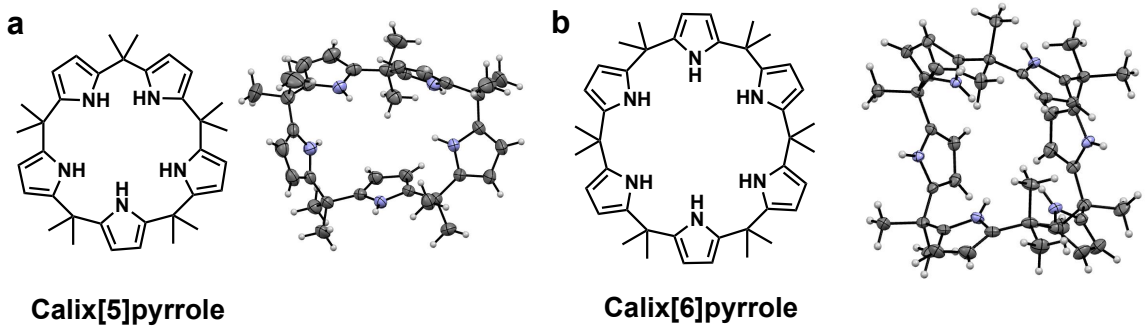

Figure 1-8. Structure of (a) calix[5]pyrrole[13] and (b) calix[6]pyrrole[21]. (Solvent molecules are omitted for clarity)

1.2.3 Effect of ring strain on contracted analogues

On the contrary, the contracted analogues for both porphyrin and calix[4]pyrrole exhibit unique structural features due to the rigid contracted macrocycle. Two typical compounds are subporphyrin and calix[3]pyrrole, as the contracted analogues of porphyrin and calix[4]pyrrole, respectively.

In case of subporphyrin (**Figure 1-9**), the contracted ring size and repulsion of pyrrole-NH within the narrow cavity are believed to cause ring strain, that the free base-type compound[22] exhibits partial cone like core structure and dihedral angles between each pyrroles are 42.88°, 22.69, and 23.94°. Obvious planar bending was also observed in the three pyrrole rings especially for the imine-type pyrrole ring. Despite the non-planar structure, it identified as 14π-aromatic compound (the 14π-conjugate circuit is marked in bold). The presence of aromaticity provides additional stability so that both free base-type or boron(III)-complex of subporphyrin retain porphyrinic properties while the unique 14π structure has a significant impact on the optical and electrochemical properties[12,22,23].

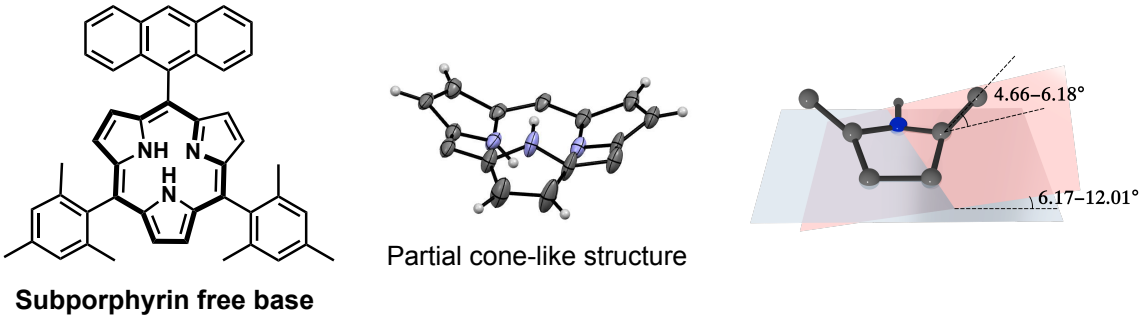

Figure 1-9. (a) Structure of subporphyrin free base[22]. Substituents on the *meso* carbons and solvents were omitted to clearly show the core structure.

While for the calix[3]pyrrole[15] which is contracted analogue of calix[4]pyrrole, the same obvious pyrrole deformation observed (**Figure 1-10**) from the crystal structure. However, unlike subporphyrin, calix[3]pyrrole exhibits a unique reactivity due to the lack of additional stabilizing effects from the aromaticity, which will be introduced in next section.

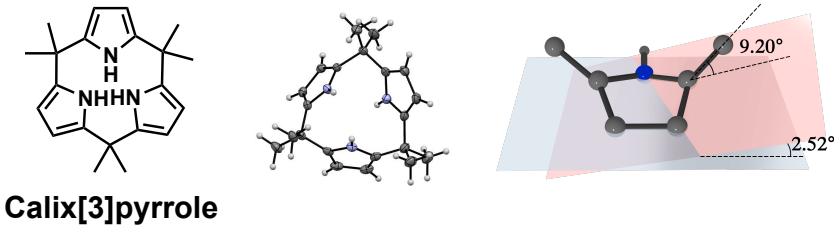

Figure 1-10. Structure of calix[3]pyrrole[15]. (H_2O is omitted for clarity)

1.3 Strain-induced property and synthetic challenge for contracted analogues

It is reasonable to image that some unique properties should be affected by the unusual ring strain. Indeed, in the work of calix[3]pyrrole has shown the effect of ring strain on the reactivity[15]. Calix[3]pyrrole was found can conduct strain-induced ring-expansion reaction under acidic condition (**Scheme 1-1**). Such a novel discovery indicates that the relationship between contracted porphyrin-related macrocycles and ring strain is an emerging field worthy of further investigation. Ring strain can be another factor, besides conjugation structure and coordination ability, that enables the functionalization of porphyrin-related molecules.

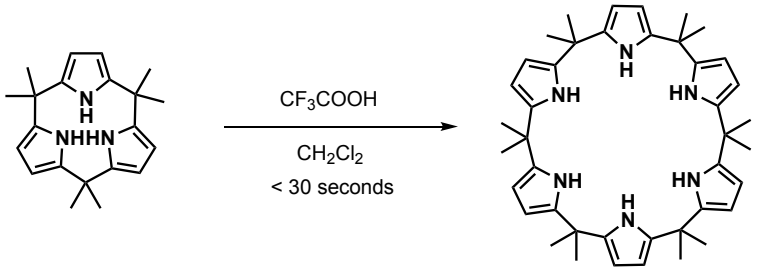

Scheme 1-1. Strain-induced ring-expansion reaction of calix[3]pyrrole under acidic condition[15].

And the ring strain induced unusual property and reactivity of other macrocycles further proved the attraction, such as bioorthogonal chemistry[24], ring-opening polymerization[25], and cycloparaphenylene field[26]. Therefore, the objective of this thesis is to develop novel contracted porphyrin-related macrocycles for further discover and illustrate the relationship between structure/property and ring strain.

However, such research is not easy because it suffered from the synthetic challenge. As introduced in 1.1 section, the most conventional method for synthesizing porphyrin[1] or calix[4]pyrrole[7] is the condensation between pyrrole and aldehyde or ketone. However, the contracted analogues like subporphyrin or calix[3]pyrrole never observed in these conditons (**Scheme 1-2**). The ring strain makes the formation of them not favorable from the perspective of enthalpy. These contracted compounds were obtained with well-designed synthetic routes.

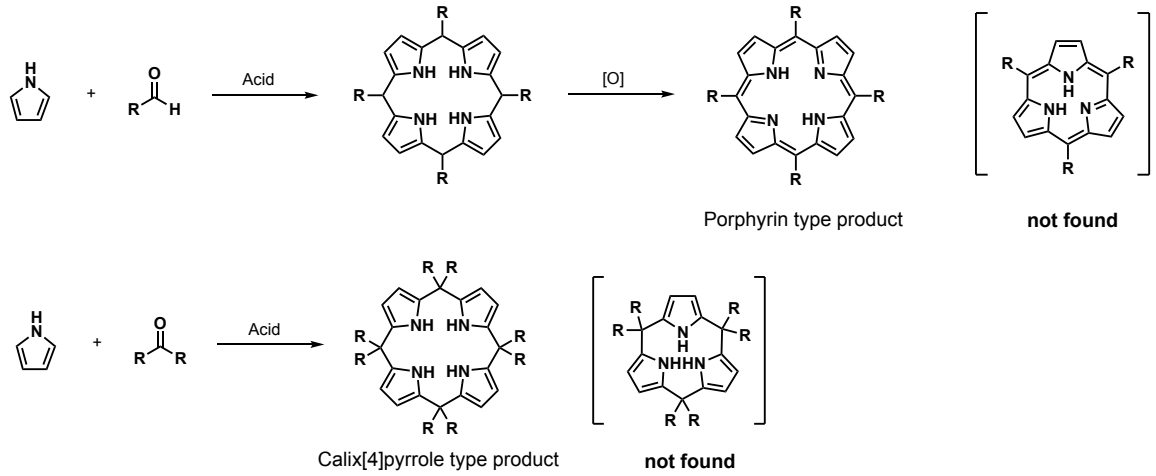

Scheme 1-2. Conventional condensation reaction for porphyrin type and calix[4]pyrrole type compounds.

For example, subporphyrin boron(III)-complex was obtained from boron-templet method (**Scheme 1-3a**) that central boron atom can mitigate steric repulsion of the pyrrole-NH protons so that improve the efficiency of cyclization[12]. The synthesis of subporphyrin free base[22] used another strategy that the compound without boron center was furnished by the transition metal-catalyzed coupling reactions for the direct cyclization (**Scheme 1-3b**). Another example concerns calix[3]pyrrole, this molecule was obtained from Paal-Knorr reaction of cyclic hexaketone (**Scheme 1-3c**) that made the cyclic precursor with less ring strain firstly, then use the formation of an aromatic subunit to overcome the strain energy[15].

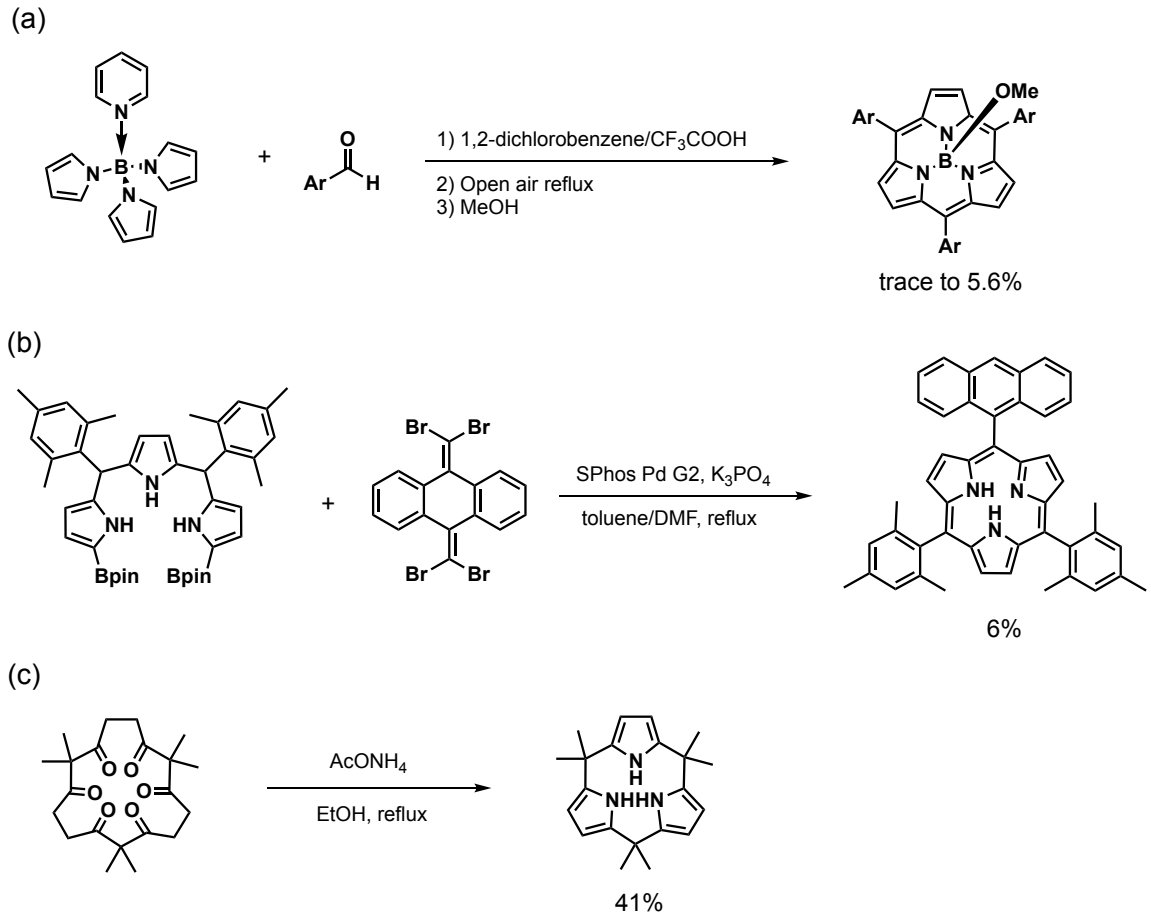

Scheme 1-3. (a) Boron-templet method for synthesizing subporphyrin boron(III)-complex [12]; (b) Suzuki-Miyaura coupling reaction used for cyclization step of subporphyrin free base[22]; (c) Synthesis of calix[3]pyrrole from cyclic hexaketone[15].

Further, a recent work has shown that homologues with different ring strains can produce extremely different results in the synthesis process (**Scheme 1-4**). The ring strain of calix[1]furan[2]thiazole[27] was calculated 2.7 kcal mol^{-1} lower than calix[3]pyrrole because there is no hydrogen atoms repulsion in the central cavity. The reduced ring strain allowed direct cyclization synthesis by Hantzsch thiazole synthesis and provided an impressive 60% yield.

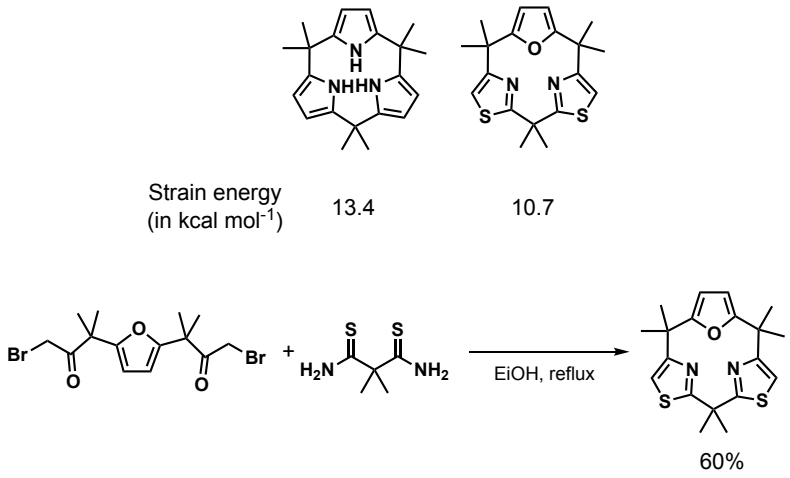

Scheme 1-4. Strain energy comparison of calix[3]pyrrole and calix[1]furan[2]thiazole and synthesis of calix[1]furan[2]thiazole[27].

These examples demonstrated the limitation of conventional synthetic routes in synthesizing contracted analogues and the effect of ring strain on synthetic process. The synthetic difficulties mean that synthetic methods for these of highly strained macrocycles, including the applicability limits of existing strategies and new methodologies, are also important subjects to investigate. Therefore, the effect of ring strain on synthesis will also be discussed in this thesis.

1.4 Method for ring strain analysis

As mentioned above, ring strain apparently plays an important role in the research about contracted analogues because it is highly related to the properties of compounds. Moreover, by investigating ring strain, synthetic methodologies and predictive results can be designed specifically for this purpose. Therefore, the analysis of ring strain will be an important part in this thesis.

In this thesis, the investigation about ring strain will consist of both experimental and theoretical method. The experimental method will mainly involve qualitatively comparing the ring strain between different compounds through single-crystal structures. And the theoretical method will mainly be used for quantitative analysis of ring strain. This includes using density functional theory (DFT) methods to investigate energy changes in the system before and after the reaction, as well as specific analyses of individual compounds. In particular, this thesis will employ a recently reported new method so called StrinViz[28] which will detailed introduced in Chapter 3.

1.5 Overview of this thesis

The objective of this thesis is investigating novel contracted porphyrin related macrocycles to further reveal the effect of ring strain on synthetic process and properties for the development of new synthetic methodology and new strain-induced functionalization. The author firstly investigated the applicability of existing synthetic strategies for highly strained calix[2] type macrocycle. Then, the author investigated analytic character of StrainViz method comparing with conventional homodesmotic reaction method, and used this strain visualization method for strain evaluation for calix[2]pyrrole and novel designed [2.2](2,5)pyrrolophane type macrocycle. With the designed synthetic route, cyclo[4]pyrrole was successfully furnished and the properties was investigated detailed. Finally, for another situation of four pyrrole direct connected with less ring strain, elusive tetrapyrrole-fused cyclooctatetraene compound, the authors proposed a feasible synthetic route and furnished the construction of promising bipyrrole precursor in multiple steps under mild reaction conditions.

In chapter 2, the ring tightening approach towards calix[2] type macrocycle was investigated. The synthesis of two precursor, cyclic tetraketone and furanophane, was performed successfully. Treating these two precursor with Paal-Knorr conditions was found can't provide target calix[2] type macrocycle that different from the result of calix[3] type macrocycle with same strategy. The theoretical calculation indicated an insurmountable energy increase in this process that difficult to overcome by conventional thermal reaction condition.

In chapter 3, the StrainViz method with strain visualization was compared with conventional homodesmotic reaction method. And the investigation with StrainViz method for calix[2]pyrrole and novel designed [2.2](2,5)pyrrolophane type macrocycle were performed. The newly designed structure, consisting of four directly linked pyrroles, is expected to enable redox-driven flexible π-conjugated macrocycle.

In chapter 4, the author furnished the synthesis and property investigation of designed [2.2](2,5)pyrrolophane type macrocycle, so called cyclo[4]pyrrole. The designed synthesis was a 6-step route combined carbonyl related reaction and Suzuki-Miyaura coupling. The strained molecular structure of cyclo[4]pyrrole was detailed researched by crystal structure and calculation. The difficulties caused by ring strain to alternative synthetic routes were also discussed. As expected, a combination of electrochemical methods and theoretical

calculations confirmed that the molecule underwent redox-driven changes in molecular conformation and electronic structure.

In chapter 5, a feasible synthetic route was proposed for the elusive cyclic tetrapyrrole with cyclooctatetraene core that another situation of four pyrrole direct connected with less ring strain. The tetrapyrrole-fused cyclooctatetraene structure was evaluated by calculation in advance and a promising bipyrrole precursor was furnished in multiple steps under mild reaction conditions.

Chapter 6 summarized the work in this thesis and described some perspectives for future.

1.6 Reference

[1] Rothemund, P. Formation of Porphyrins from Pyrrole and Aldehydes. *J. Am. Chem. Soc*. **1935**, *57*, 2010-2011.

[2] Kadish, K. M.; Smith, K. M.; Guilard, R., Eds. Biochemistry and Binding: Activation of Small Molecules. *The Porphyrin Handbook*, 1999; Vol. 4.

[3] Kadish, K. M.; Smith, K. M.; Guilard, R., Eds. Chlorophylls and Bilins: Biosynthesis, Synthesis, and Degradation. *The Porphyrin Handbook*, 1999; Vol. 13.

[4] Senge, M. O.; Sergeeva, N. N.; Hale, K. J. Classic Highlights in Porphyrin and Porphyrinoid Total Synthesis and Biosynthesis. *Chem. Soc. Rev*. **2021**, *50*, 4730-4789.

[5] Giuntini, F.; Boyle, R.; Sibrian-Vazquez, M.; Vicente, M. G. H. Porphyrin Conjugates for Cancer Therapy. *Handbook of Porphyrin Science*, **2013**, *27*, 303-416.

[6] Gouterman, M.; Wagnière, G. H.; Snyder, L. C. Spectra of Porphyrins: Part II. Four Orbital Model. *J. Mol. Spectrosc*. **1963**, *11*, 108-127.

[7] Baeyer, A. Ueber ein Condensationsproduct von Pyrrol mit Aceton. *Ber. Dtsch. Chem. Ges*. **1886**, *19*, 2184-2185.

[8] Gale, P. A.; Sessler, J. L.; Král, V.; Lynch, V. Calix[4]pyrroles: Old Yet New Anion-Binding Agents. *J. Am. Chem. Soc*. **1996**, *118*, 5140-5141.

[9] Kim, D. S.; Sessler, J. L. Calix[4]pyrroles: Versatile Molecular Containers with Ion Transport, Recognition, and Molecular Switching Functions. *Chem. Soc. Rev*. **2015**, *44*, 532-546.

[10] Furuta, H.; Asano, T.; Ogawa, T. "N-Confused Porphyrin": A New Isomer of Tetraphenylporphyrin. *J. Am. Chem. Soc*. **1994**, *116*, 767-768.

[11] Sessler, J. L.; Cyr, M. J.; Lynch, V.; McGhee, E.; Ibers, J. A. Synthetic and Structural Studies of Sapphyrin, a 22-π-electron Pentapyrrolic "Expanded Porphyrin". *J. Am. Chem. Soc*. **1990**, *112*, 2810-2813.

[12] Inokuma, Y.; Yoon, A. S.; Kim, D.; Osuka, A. *meso*-Aryl-Substituted Subporphyrins: Synthesis, Structures, and Large Substituent Effects on Their Electronic Properties. *J. Am. Chem. Soc*. **2007**, *129*, 4747-4761.

[13] Cafeo, G.; Kohnke, F. H.; Parisi, M. F.; Nascone, R. P.; Torre, G. L. L.; Williams, D. J. The Elusive β-Unsubstituted Calix[5]pyrrole Finally Captured. *Org. Lett*. **2002**, *4*, 2695-2697.

[14] Nishiyabu, R.; Palacios, M. A.; Dehaen, W.; Anzenbacher, P. Synthesis, Structure, Anion Binding, and Sensing by Calix[4]pyrrole Isomers. *J. Am. Chem. Soc*. **2006**, *128*, 11496-11504.

[15] Inaba, Y.; Nomata, Y.; Ide, Y.; Pirillo, J.; Hijikata Y.; Yoneda, T.; Osuka, A.; Sessler, J. L.; Inokuma, Y. Calix[3]pyrrole: A Missing Link in Porphyrin-Related Chemistry. *J. Am. Chem. Soc*. **2021**, *143*, 12355-12360.

[16] Watanabe, K.; Pati, N. N.; Inokuma, Y. Contracted Porphyrins and Calixpyrroles: Synthetic Challenges and Ring-contraction Effects. *Chem. Sci*. **2024**, *15*, 6994-7009.

[17] Nygaard, U.; Nielsen, J. T.; Kirchheiner, J.; Maltesen, G.; Rastrup-Andersen, J.; Sørensen, G.O. Microwave Spectra of Isotopic Pyrroles. Molecular Structure, Dipole Moment, and ^{14}N Quadrupole Coupling Constants of Pyrrole. *J. Mol. Structure* **1969**, *3*, 491-506.

[18] Silvers, S. J.; Tulinsky, A. The Crystal and Molecular Structure of Triclinic Tetraphenylporphyrin. *J. Am. Chem. Soc*. **1967**, *89*, 3331-3337.

[19] Sankar, J.; Mori, S.; Saito, S.; Rath, H.; Suzuki, M.; Inokuma, I.; Shinokubo, H.; Kim, K. S.; Yoon, Z. S.; Shin, J.; Lim, J. M.; Matsuzaki, Y.; Matsushita, O.; Muranaka, A.; Kobayashi, N.; Kim, D.; Osuka, A. Unambiguous Identification of Möbius Aromaticity for meso-Aryl-Substituted [28]Hexaphyrins(1.1.1.1.1.1). *J. Am. Chem. Soc*. **2008**, *130*, 13568-13579.

[20] Naoda, K.; Osuka, A. Structural and Aromaticity Control of [34]Octaphyrin(1.1.1.0.1.1.1.0) by Protonation and Deprotonation. *Asian J. Org. Chem*. **2017**, *6*, 1205-1208.

[21] Cafeo, G.; Kohnke, F.H.; La Torre, G.L.; White, A.J.P.; Williams, D.J., From Large Furan-Based Calixarenes to Calixpyrroles and Calix[n]furan[m]pyrroles: Syntheses and Structures. *Angew. Chem. Int. Ed*. **2000**, *39*, 1496-1498.

[22] Liu, L.; Kim, J.; Xu, L.; Rao, Y.; Zhou, M.; Yin, B.; Oh, J.; Kim, D.; Osuka, A.; Song, J. Synthesis of Subporphyrin Free Bases. *Angew. Chem. Int. Ed*. **2022**, *61*, e202214342.

[23] Kobayashi, N.; Takeuchi, Y.; Matsuda, A. *meso*-Aryl Subporphyrins. *Angew. Chem. Int. Ed*. **2007**, *46*, 758-760.

[24] Agard, N. J.; Prescher, J. A.; Bertozzi, C. R. A Strain-Promoted [3 + 2] Azide−Alkyne Cycloaddition for Covalent Modification of Biomolecules in Living Systems. *J. Am. Chem. Soc*. **2004**, *126*,15046-15047.

[25] Bielawski, C. W.; Robert H. Grubbs, R. H. Living Ring-Opening Metathesis Polymerization. *Prog. Polym. Sci*. **2007**, *32*, 1-29.
[26] Darzi, E. R.; Jasti, R. The Dynamic, Size-dependent Properties of [5]-[12]cycloparaphenylenes. *Chem. Soc. Rev*. **2015**, *44*, 6401-6410.
[27] Watanabe, K.; Shibata, K.; Ichino, T.; Ide, Y.; Yoneda, T.; Maeda, S.; Inokuma, Y. Strain-based Design, Direct Macrocyclization, and Metal Complexation of Thiazole-Containing Calix[3]pyrrole Analogues. *Inorg. Chem. Front*. **2024**, *11*, 3548-3554.
[28] Colwell, C. E.; Price, T. W.; Stauch, T.; Jasti, R. Strain Visualization for Strained Macrocycles. *Chem. Sci*. **2020**, *11*, 3923-3930.

Chapter 2

Synthetic exploration for calix[2] type macrocycles from cyclic ketone precursors

Abstract

The preparation of calix[n] type macrocyclic molecules via cyclic polyketone precursors has been proven to be a promising synthetic strategy, even for highly strained calix[3] type macrocycles. In this chapter, the applicability of this strategy toward more strained calix[2]pyrrole and calix[2]furan was investigated. The synthesis of corresponding precursors, 3,3-dialkylated pentane-2,4-diones and its furanophane derivative were furnished from linear tetraketone precursor. The ring strain of the two precursors was analyzed though single crystal X-ray diffraction data. Finally, the synthesis of calix[2] type molecules was attempted, and the results were explained by theoretical calculations and related reaction mechanism.

2.1 Introduction

The preparation of calix[n] type macrocyclic molecules via cyclic polyketone precursors is a conventional and promising synthetic strategy, which can provide expanded analogue like calix[6]pyrrole[1] and contracted analogue like calix[3]pyrrole[2]. The synthesis of strained calix[3]pyrrole is particularly noteworthy. In this Paal-Knorr reaction, the formation of aromatic rings is thought to overcome the increased macrocyclic strain so that driving the reaction forward. Since the unique reactivity of calix[3]pyrrole due to large ring strain has been discovered, it is expected to look for analogues with larger strain and investigate their potential unique properties. Therefore, the synthetic exploration for calix[2] type macrocycles was conducted with same synthetic strategy in this chapter.

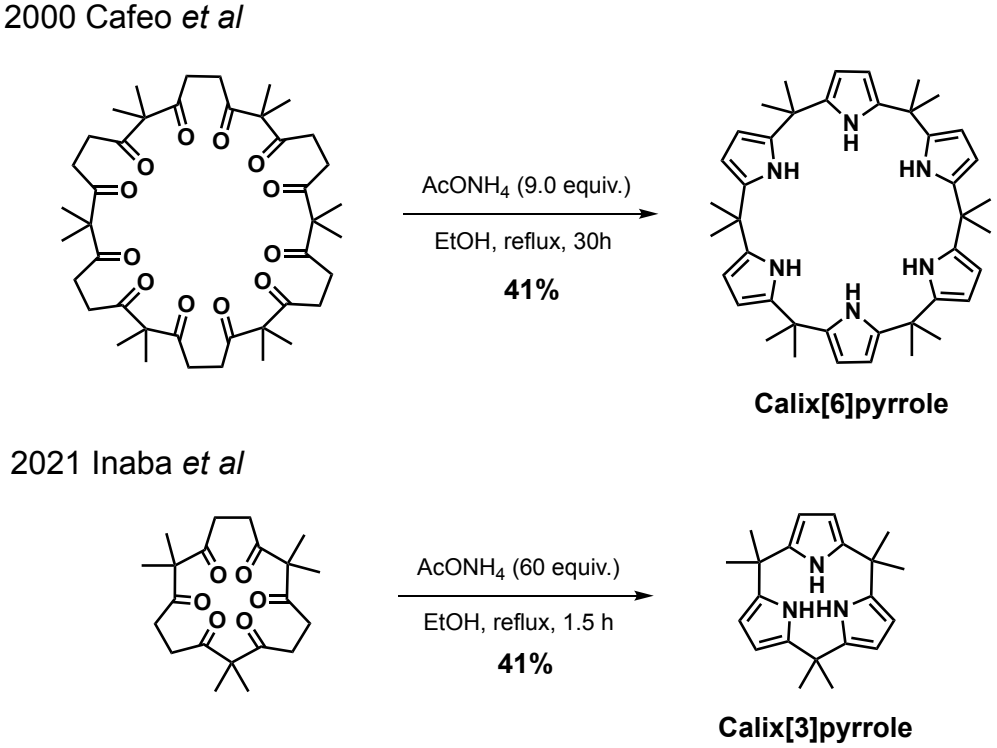

Scheme 2-1. Synthesis of calix[6]pyrrole from cyclic dodecaketone and synthesis of calix[3]pyrrole from cyclic hexaketone.

3,3-dialkylated pentane-2,4-diones (**1**) is a reasonable precursor for the target calix[2]pyrrole (**Scheme 2-2**) with the same strategy. Therefore, the work in this Chapter is started from the synthesis of compound **1**.

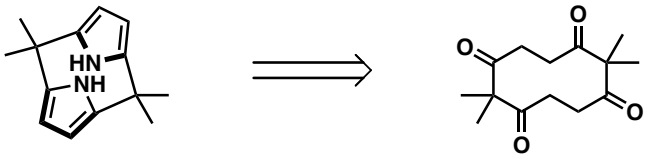

Calix[2]pyrrole **1**

Scheme 2-2. Retrosynthetic analysis of calix[2]pyrrole.

2.2 Construction and structural analysis of cyclic ketone precursors

Cyclic tetraketone precursor was obtained from linear tetraketone **2** via the furanophane **4** intermediate (**Scheme 2-3**). The starting material compound **2** and followed furan formation in toluene with *p*-toluenesulfonic acid (*p*-TsOH) were previous reported[3]. The next step was intramolecular cyclization that firstly generated lithium enolate by excess amount of lithium diisopropylamide (LDA), then add $CuCl_2$ into the reaction to give furanophane **4** in 12% yield. Since the yield of cyclization was not satisfied, several reagents were used in place of $CuCl_2$ including copper(II) triflate, iodine, and $NiCl_2$ for enolate coupling. However, these conditions can't provide better yield. Oxidative furan ring-opening reaction was proceeded by treatment furanophane **4** with *m*-chloroperbenzoic acid (*m*CPBA) at 0ºC to give **5** in 69% yield. Subsequent reduction of the C=C double bond was realized by Pd/C catalyzed hydrogenation and provided target cyclic tetraketone **1** in 43% yield.

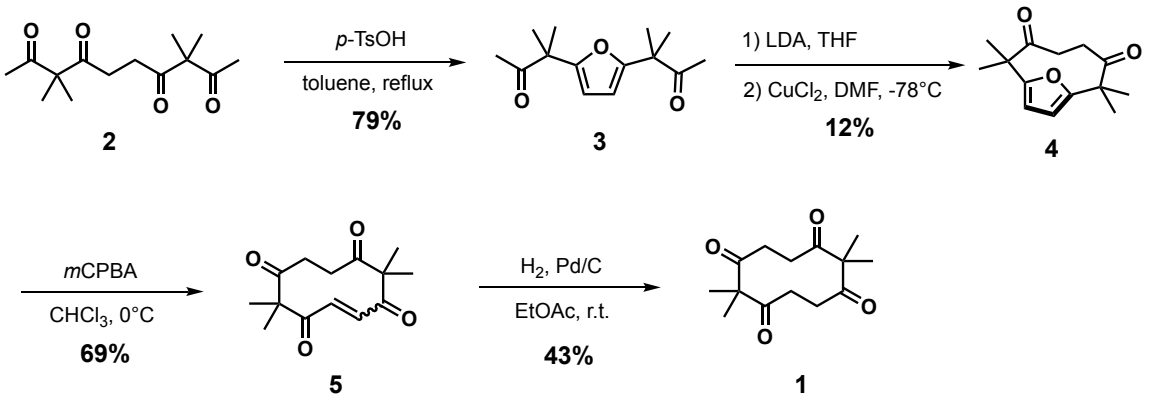

Scheme 2-3. Synthetic route for cyclic tetraketone **1**.

Besides target compound **1**, furonophane **4** was also considered a possible precursor for generating calix[2] type macrocycles. Before attempting to synthesize calix[2] type macrocycles, the ring strain of the two possible precursors was firstly evaluated in view of their small ring size.

The evaluation was conducted by their X-ray single crystal structures. The crystal structure of compound **1** (**Figure 2-1**) revealed its Ci-symmetric conformation in which two 1,4-diketone units adopted a gauche conformation with a torsion angle of 60.7º. Such similar gauche conformation is commonly observed for other larger-sized cyclic

polyketones like cyclic hexaketone precursor[2] for calix[3]pyrrole. And unusual distortion was not found by analyzing other structural parameters such as bond lengths and angles around the carbonyl groups. While the single crystal X-ray analysis of furanophane **4** showed a highly strained structure (**Figure 2-2**). The ethylene unit in **4** adopted an almost eclipsed conformation which was considered for reducing the distortion around the rigid furan part because deformation of furan moiety was distinct.

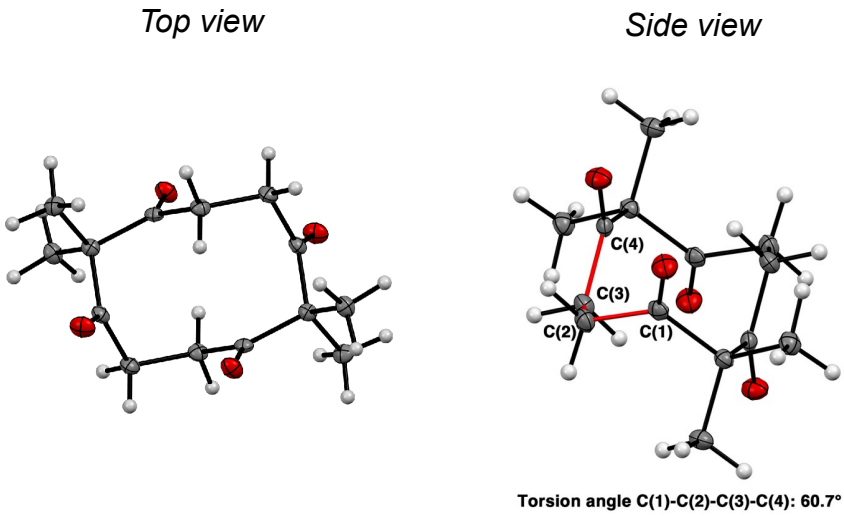

Figure 2-1. Crystal structure of compound **1**. Thermal ellipsoids are drawn at the 50% probability level.

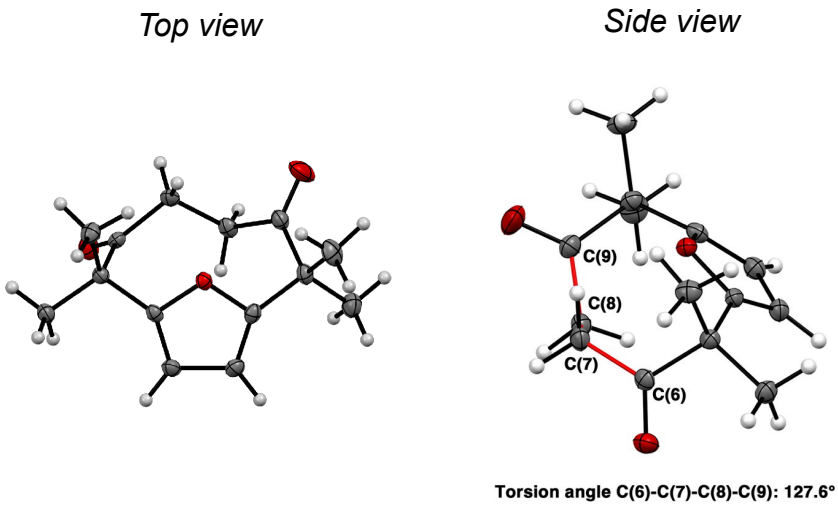

Figure 2-2. Crystal structure of furanophane **4**. Thermal ellipsoids are drawn at the 50% probability level.

Deformation angles α and β around the furan ring of **4** that are defined by the deviation angles between the mean planes of O−C(3)−C(4) and O−C(2)−C(3), and the mean plane O−C(2)−C(3) and a C(2)−C(*meso*) bond, respectively (**Figure 2-3**). These deformation angles were calculated to be α = 3.69º and β = 16.00º, the largest among the known calix[n]furan macrocycles and precursors that compared in **Table 2-1**.

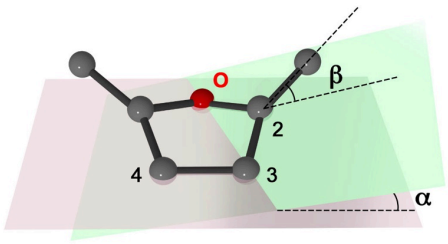

Figure 2-3. Diagram of definition of deformation angles α and β.

Table 2-1. Deformation state of furan-embedded macrocycles. Compound **4** and **8** were synthesized in this work, compound **6** and **7** were reported by Inaba *et al*[2], compound **9** was reported by Hazell[4].

Compound	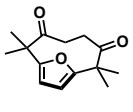 4	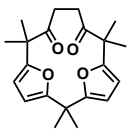 6	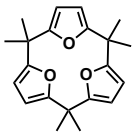 7	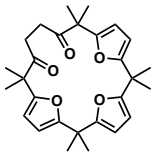 8	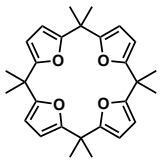 9
Deformation angle α (°)	3.69	0.72	1.95	0.33	0.32
Deformation angle β (°)	16.00	2.37	6.53	1.81	0.68
Conformation and torsion angle of ethylene bridge	Eclipsed 127.6	Anti 165.3	-	Anti 176.2	-

[a] Since the diketone part of **8** was disordered in the crystal structure, angles and conformation were calculated from the major disorder part.

Nonetheless, the ^{1}H NMR spectrum of compound **4** showed a singlet signal for the ethylene protons at 2.17 ppm, indicating flexibility of the bridging chain part in solution. In addition, compound **1** exhibited two singlet signals in the ^{1}H NMR spectrum at 2.69 and 1.30 ppm assignable to the ethylene and methyl protons, respectively that also indicated flexible chain in solution. According to the reaction mechanism of Paal-Knorr[5], such flexibility is necessary for the formation of a five-membered aromatic ring from a 1,4-diketone.

2.3 Attempts of calix[2] type macrocycles synthesis

With the two precursors in hand, Paal-Knor pyrrole synthesis of compound **1** and Paal-Knorr furan synthesis of compound **4** were investigated.

For the Paal-Knor pyrrole synthesis of compound **1** (**Scheme 2-4**), the conventional condition[1,2] that reflux in ethanol with excess amount of ammonium acetate was conducted firstly. However, complicated mixtures that exhibited many proton signals around 2-3 ppm in ^{1}H NMR spectrum were obtained which suggested that intramolecular aldol-type condensation reactions may happened. Since the enormous ring strain of the product calix[2]pyrrole was easily imagined, higher temperature reaction condition was also attempted to overcome the ring strain of product, but only very complicated mixture was generated that no obvious evidence indicated formation of target product. Further, the room temperature condition also be checked that intramolecular aldol product still generated which indicated this small cyclic ketone is highly susceptible to intramolecular addition reactions.

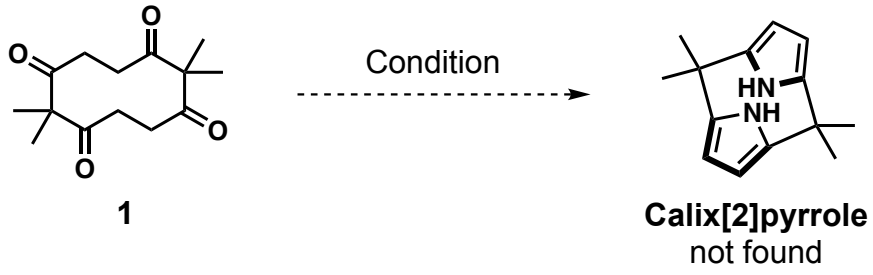

1 **Calix[2]pyrrole** not found

Condition 1: NH_4OAc (40 equiv.), EtOH, reflux

Condition 2: NH_4OAc (40 equiv.), ethylene glycol, 150°C

Condition 3: NH_4OAc (40 equiv.), EtOH, room temperature

Scheme 2-4. Synthetic exploration for calix[2]pyrrole from compound **1**.

Like the situation of compound **1**, the formation of calix[2]furan from furanophane **4** was also not successful (**Scheme 2-5**). Both Brønsted acid and Lewis acid conditions were attempted for Paal-Knorr furan formation. Methanesulfonic acid and chlorotrimethylsilane used as catalyst respectively while both reactions provided unidentified product. Here should be mentioned that chlorotrimethylsilane as catalyst successfully provide

calix[3]furan **7** from compound **6**[2] but in the case of compound **4**, not furan formed product be found.

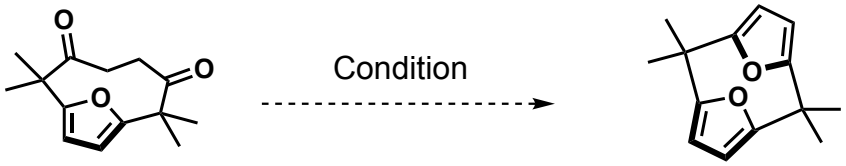

4 **Calix[2]furan** not found

Condition 1: CH_3SO_3H, MeCN, reflux

Condition 2: $SiMe_3Cl$, MeOH, reflux

Scheme 2-5. Synthetic exploration for calix[2]furan from compound **4**.

Due to the increased ring strain, the formation of calix[2]type molecules is obviously not favorable in view of energy. Therefore, theoretical calculations (**Figure 2-4**) were performed to explain the destabilization energy changes from compound **1** to the calix[2]type molecules at the B3LYP/cc-pVTZ level. After structure optimization of related molecules, the destabilization energy (ΔE) between cyclic oligoketones and its related products was evaluated using following equations:

$$\text{Furan system } \Delta E = -\{E_{\text{all-Ketone}} - (E_{\text{nFuran}} + nE_{H2O})\}$$

$$\text{Pyrrole system } \Delta E = -\{(E_{\text{all-Ketone}} + nE_{NH3}) - (E_{\text{nPyrrole}} + 2nE_{H2O})\}$$

where $E_{\text{all-Keton}}$ is the energy of the optimized cyclic ketone, E_{H2O} is the energy of the optimized water molecule, E_{nFuran} is the energy of the optimized cyclic ketone-n-furan, E_{NH3} is the energy of the optimized NH_3 molecule, and E_{nPyrrole} is the energy of the optimized cyclic ketone-n-pyrrole.

From compound **1**, although the energy of first aromatic ring formation seems not unrealistic (around 20 kcal mol^{-1}), the corresponding compound can't be observed. Instead, some intramolecular addition product generated as mentioned above. The possible reason is that the 1,4-diketone moiety requires a considerable amount of additional energy to rotate to eclipsed conformation for completing the Paal-Knorr reaction[5], while the energy barrier of intramolecular aldol reaction is smaller. As for the energy increase of second

aromatic ring formation, the extremely large values (more than 100 kcal mol^{-1}) are as expected which looks difficult to overcome by conventional thermal chemical condition.

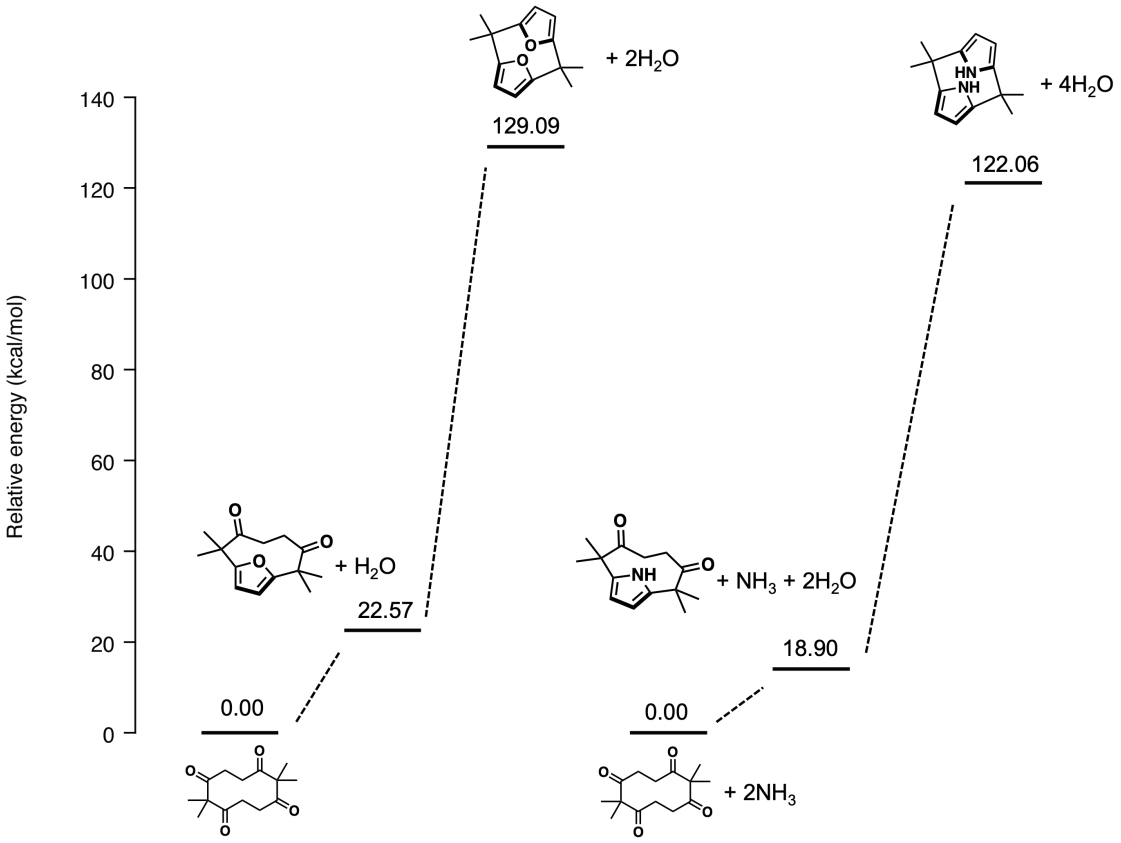

Figure 2-4. Destabilization energies ΔE diagram upon the furan formation reaction from compound **1** and ΔE upon the pyrrole formation reaction from compound **1**.

2.4 Conclusion

In conclusion, cyclic tetraketone **1** and strained furanophane **4** as plausible precursors for calix[2]type molecules were synthesized and their ring strain state were analyzed by X-ray single crystal structures. However, Paal-Knorr-type reaction using **1** and **4**, did not proceed target calix[2]type molecules while the conditions successfully worked for synthesis of calix[3]pyrrole or calix[3]furan. Theoretical calculations revealed that the second aromatic ring formation had a remarkably large destabilization energy ($\Delta E > 100$ kcal/mol) that seems unrealistic to overcome with conventional thermal reactions. Although Paal-Knorr approaches using a cyclic tetraketone were found to be difficult, the attempts showed that synthesis of calix[2]type macrocycles is a more challenging task that require novel synthetic methodology. Despite the difficulty, calix[2]type macrocycles are still attractive to explore their properties derived from extremely high strain.

2.5 Experimental Section

2.5.1 General information

All reagents were purchased from Fujifilm Wako pure chemical corporation, TCI Co., Ltd., Kanto chemical Co., Inc., or Sigma-Aldrich Co., and used without further purification unless otherwise mentioned. All ^{1}H and ^{13}C NMR spectra were recorded using JEOL JMN-ECS400 spectrometer and chemical shifts were reported in parts per million (ppm) relative to an internal standard tetramethylsilane (δ = 0.00 ppm for ^{1}H NMR in $CDCl_3$), a solvent residual peak (δ = 77.16 ppm for ^{13}C NMR in $CDCl_3$). Infrared spectra were measured using a JASCO Co. FT/IR-4600. ESI-TOF-MS spectra were recorded on a Thermo Scientific Executive spectrometer. Elemental analyses were carried out using an Exceter Analytical, Inc. CE440 or MICRO CORDER JM10. Thin layer chromatography was performed on a silica gel sheet, MERCK silica gel 60 F254. Preparative scale separations were performed by means of gravity column chromatography over silica gel (Wakosil® 60. 64 ~ 210 μm). Single crystal X-ray diffraction data were obtained using Rigaku XtaLAB P200 diffractometer equipped with a PILATUS200K detector, which uses a multilayer mirror (MoK_α radiation λ = 0.71073 Å or CuK_α radiation λ = 1.54184 Å) or a Rigaku XtaLAB Synergy-R/DW instrument equipped with a HyPix-6000HE detector, which uses a monochromated mirror. All structures were solved using a dual-space algorithm (SHELXT) and refined using full-matrix least-squares method (SHELXL)[6,7].

Theoretical calculations were performed with Gaussian 16 Rev. C01[8]. Structures of the macrocycles were optimized at the B3LYP/cc-pVTZ level of theory with Grimme's D3BJ dispersion correction[7], referring to their single crystal X-ray structures. The initial structures of calix[2]pyrrole and calix[2]furan modified from the crystal structure of cyclic tetraketone **1**, and structural optimizations were attempted under the same conditions as above. After optimization, the destabilization energy (ΔE) between cyclic oligoketones and its related products was evaluated using the equations shown in the main text. Note: NH_3 and water molecules were included for stoichiometry to evaluate the destabilization of furan/pyrrole ring formation, although the ring formation conditions in the real systems are different from the evaluation scheme above.

2.5.2 Synthetic procedures

· Synthesis of furanophane **4**

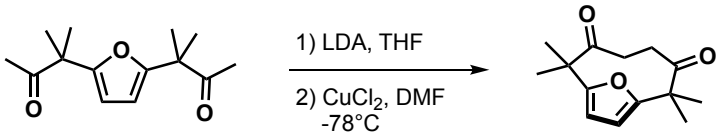

3 **4**

In a 500 mL three-neck flask equipped with a dropping funnel and nitrogen gas inlet/outlet, lithium diisopropylamide (2.0 M in THF/ heptane/ethylbenzene, 35.0 mL, 70.0 mmol) was added and cooled to –78 ºC. A solution of compound **3** (5.00 g, 21.2 mmol) in anhydrous THF (105 mL) was added dropwise using a dropping funnel over 15 min while keeping the solution temperature at –78 ºC. After 15 min of stirring, a solution of $CuCl_2$ (9.41 g, 70.0 mmol) in anhydrous DMF (154 mL) was added all at once. The reaction mixture was stirred for 1 h at –78 ºC in a cooling bath, and then allowed to reach room temperature. The reaction was quenched by adding a 3% aqueous solution of hydrochloric acid (200 mL), transferred to a separatory funnel, and extracted with diethyl ether (250 mL × 3). The combined organic layer was washed with a 3% aqueous solution of hydrochloric acid (250 mL × 2) and dried over anhydrous sodium sulfate. After evaporation under reduced pressure, the crude product was purified by silica gel column chromatography (column diameter: 5.0 cm, height: 15 cm, eluent: ethyl acetate/hexane = 1/10) to give furanophane **4** (592 mg, 2.52 mmol, 12% yield) as white solids.

^{1}H NMR ($CDCl_3$, 400 MHz, 298 K): δ = 6.27 (s, 2H, furyl), 2.17 (s, 4H, ethylene), 1.44 ppm (s, 12H, dimethylmethylene); $^{13}C\{^1H\}$ NMR ($CDCl_3$, 100 MHz, 298 K): δ = 209.9, 158.8, 110.3, 51.2, 34.5, 21.4 ppm; IR (ATR, neat): 2923, 2867, 2851, 1712, 1693, 1457, 1259, 1029, 1015 cm^{-1}; HR-ESI-TOF-MS: m/z calcd. for $C_{14}H_{18}O_3Na^+$: 257.1148 $[M+Na]^+$; found 257.1148; Elemental analysis calcd.(%) for $C_{14}H_{18}O_3$: C 71,77, H 7.74, N 0.00; found: C 71,75, H 7.82, N 0.02; mp: 86-91 ºC; TLC: R_f = 0.30 (Ethyl acetate/hexane = 1/10).

· Synthesis of compound **5**

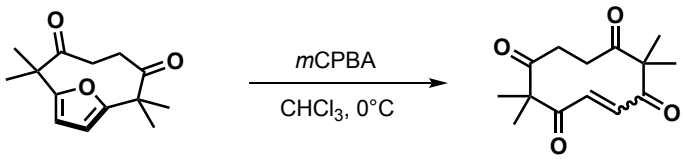

4 **5**

In a 100 mL round-bottomed flask, **4** (400 mg, 1.71 mmol) and chloroform (55 mL) were mixed and cooled at 0 ºC using ice/water bath. *m*-chloroperbenzoic acid (70% in water, 441 mg, 1.78 mmol) was added to the solution and stirred at 0 ºC. After 2.5 h of stirring, the reaction was quenched by adding a saturated aqueous solution of sodium bicarbonate (50 mL) followed by the addition of a saturated aqueous solution of sodium thiosulfate (50 mL). The organic layer was separated off and washed with a saturated aqueous solution of sodium bicarbonate (50 mL × 3) and dried over anhydrous sodium sulfate. After evapolation of solvent, the resulting solid was washed with hexane (9 mL) using ultrasonic bath for 5 min. The solid was collected and washed on a funnel using hexane (18 mL) to furnish white solids of compound **5** (293 mg, 1.17 mmol) in 69% yield.

^{1}H NMR ($CDCl_3$, 400 MHz, 298 K): δ = 6.51 (s, 2H, vinylene), 2.82 (s, 4H, ethylene), 1.40 ppm (s, 12H, dimethylmethylene); $^{13}C\{^{1}H\}$ NMR ($CDCl_3$, 100 MHz, 298 K): δ = 207.0, 201.7, 133.9, 62.6, 35.8, 22.0 ppm; IR (ATR, neat): 2985, 2945, 1694, 1674, 1608, 1416, 1383, 1364, 1091, 1044 cm^{-1}; HR-ESI-TOF-MS: m/z calcd. for $C_{14}H_{18}O_4Na^+$, 273.1097 $[M+Na]^+$; found 273.1098; Elemental analysis calcd.(%) for $C_{14}H_{18}O_4$: C 67.18; H 7.25, N 0.00; found: C 66.97, H 7.32, N 0.01; mp: 130-133 ºC; R_f = 0.43 (Ethyl acetate/hexane = 1/3).

· Synthesis of compound **1**

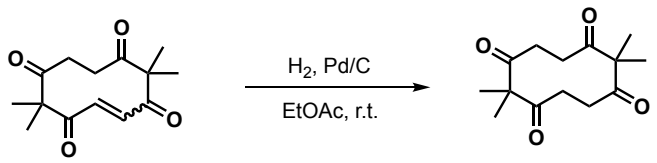

5 **1**

In a 100 mL round-bottomed flask, tetraketone **5** (300 mg, 1.20 mmol) and 210 mg of 10% Pd on carbon in 60 mL of ethyl acetate was stirred under H_2 gas for 2 h at room temperature. The reaction mixture was filtered through celite pad using CH_2Cl_2 (40 mL), and the filtrate was concentrated under reduced pressure. The resulting solid was added ethanol (60 mL) and heated to 73 ºC. After the removal of insoluble materials by hot filtration, filtrate was concentrated to dryness under reduced pressure. Then the resulting solid was dissolved in boiling ethanol (40 mL) and then cooled at 0 ºC. The precipitated crystals were collected by suction filtration. The crystals on funnel were further washed using cold ethanol (20 mL) to provide compound 9 (130 mg, 43%) as colorless crystals.

^{1}H NMR ($CDCl_3$, 400 MHz, 298 K): δ = 2.69 (s, 8H, ethylene), 1.30 ppm (s, 12H, dimethylmethylene); $^{13}C\{^1H\}$ NMR ($CDCl_3$, 100 MHz, 298 K): δ = 207.0, 63.5, 34.3, 21.4 ppm; IR (ATR, neat): 2979, 2959, 1691, 1410, 1246, 1099, 1057 cm^{-1}; HR-ESI-TOF-MS: m/z calcd. for $C_{14}H_{20}O_4Na^+$, 275.1254 $[M+Na]^+$; found 275.1247; Elemental analysis calcd.(%) for $C_{14}H_{20}O_4$: C, 66.65; H, 7.99; N, 0.00; found: C, 66.56; H, 8.05; N, 0.02; mp: 125-128 ºC; R_f = 0.74 (Ethyl acetate/hexane = 1/1).

· Synthesis of compound **8**

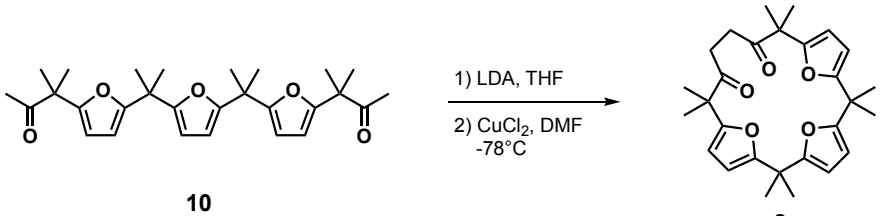

10 **8**

In a 50 mL three-neck flask equipped with a dropping funnel, lithium diisopropylamide (2.0 M in THF/heptane/ethylbenzene, 0.91 mL, 1.82 mmol) was added and cooled to –78 ºC under N_2 atmosphere. A solution of linear trifuran **10** (250 mg, 0.550 mmol) in anhydrous THF (10 mL) was added dropwise using a dropping funnel over 15 min. After 15 min of stirring, a solution of anhydrous $CuCl_2$ (244 mg, 1.82 mmol) in anhydrous DMF (4.0 mL) was added at once. The reaction mixture was stirred for an hour at –78 ºC in a cooling bath, and then allowed to reach room temperature. The reaction was quenched by adding a 3% aqueous solution of hydrochloric acid (5 mL), transferred to a separatory funnel, and extracted with diethyl ether (10 mL × 3). The combined organic layer was washed with a 3% aqueous solution of hydrochloric acid (10 mL × 2) and dried over anhydrous sodium sulfate. After concentration under reduced pressure, the crude product was purified by silica gel column chromatography (column diameter: 2.0 cm, height: 25 cm, eluent: ethyl acetate/hexane = 1/10) to furnish compound **8** (31 mg, 12% yield) as white solids.

^{1}H NMR ($CDCl_3$, 400 MHz, 298 K): δ = 6.02 (s, 2H, furyl), 6.01 (s, 4H, furyl), 2.17 (s, 4H, ethylene), 1.55 (s, 12H, dimethylmethylene), 1.37 ppm (s,12H, dimethylmethylene); ^{13}C{^{1}H} NMR ($CDCl_3$, 100 MHz, 298 K): δ = 210.4, 159.7, 158.1, 155.7, 106.3, 104.8, 104.3, 49.0, 37.0, 32.0, 25.7, 22.9 ppm; IR (ATR, neat): 2957, 1749, 1660, 1596, 1508, 1332, 1216, 1159, 1120, 1107, 1010 cm^{-1}; HR-ESI-TOF-MS: m/z calcd. for $C_{28}H_{34}O_5Na^+$, 473.2299 $[M+Na]^+$; found 473.2295; mp: 107-110 ºC; R_f = 0.38 (Ethyl acetate/hexane = 1/10).

2.5.3 X-ray crystallographic analysis

· Crystallographic data for **4**

Single crystals of **4** suitable for X-ray diffraction analysis were obtained by slow evaporation of a *n*-hexane solution of **4**.

$C_{14}H_{18}O_3$, $M = 234.28$, crystal size: $0.62 \times 0.36 \times 0.20$ mm^3, monoclinic, space group $P2_1/n$, $a = 11.3044(4)$, $b = 8.8083(3)$, $c = 13.4649(6)$ Å, $\beta = 112.723(5)$ º, $V = 1236.67(9)$ Å^3, $Z = 4$, $T = 123(2)$ K, $\mu = 0.087$ mm^{-1}, $D_{calc} = 1.258$ g/cm^3, $2.835^o \leq \theta \leq 26.491^o$, 2364 unique reflections out of 2548 with $I > 2\sigma(I)$, GOF = 1.061, $R_1 = 0.0372$, $wR_2 = 0.0935$, CCDC: 2223944

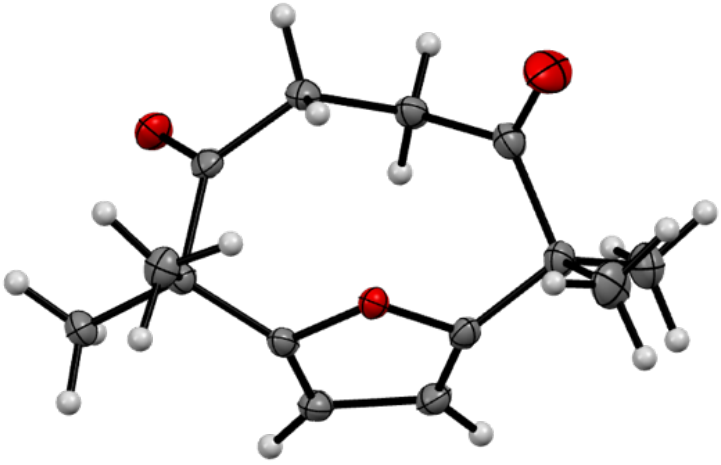

Figure 2-5. ORTEP drawing of the crystal structure of **4** at the 50% thermal probability levels (C: gray, H: white, O: red).

· Crystallographic data for **1**

Single crystals of **1** suitable for X-ray diffraction analysis were grown by vapor diffusion of *n*-hexane into a chloroform solution of **1**.

$C_{14}H_{20}O_4$, $M = 252.30$, crystal size: 0.70 × 0.10 × 0.08 mm^3, monoclinic, space group $P2_1/n$, a = 5.7594(3), b = 10.2138(6), c = 10.8502(6) Å, α = 90, β = 101.341(6), γ = 90º, V = 625.80(6) Å^3, Z = 2, T = 123(2) K, μ = 0.097 mm^{-1}, D_{calc} = 1.339 g/cm^3, 2.765º ≤ θ ≤ 27.498º, 1295 unique reflections out of 1431 with $I > 2\sigma(I)$, GOF = 1.059, R_1 = 0.0366, wR_2 = 0.1031, CCDC: 2223945

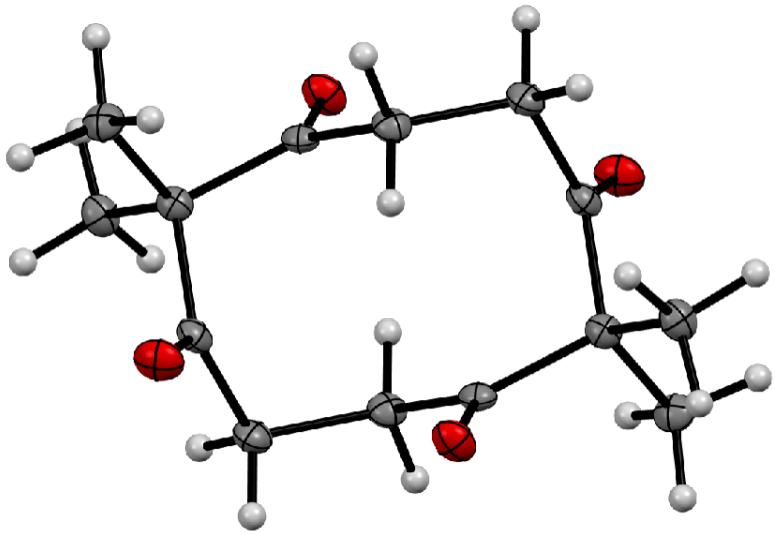

Figure 2-6. ORTEP drawing of the crystal structure of **1** at the 50% thermal probability levels (C: gray, H: white, O: red).

· Crystallographic data for **8**

Single crystals of **8** suitable for X-ray diffraction analysis were grown by vapor diffusion of *n*-heptane into a dichloromethane solution of **8**.

$C_{56}H_{68}O_{10}$, $M = 901.10$, crystal size: 0.30 × 0.05 × 0.05 mm^3, triclinic, space group P–1, a = 10.2761(5), b = 10.3420(6), c = 13.4935(8) Å, α = 112.254(5), β = 92.850(5), γ = 105.854(5)º, $V = 1257.69(13)$ Å^3, $Z = 1$, $T = 93(2)$ K, $\mu = 0.080$ mm^{-1}, $D_{calc} = 1.190$ g/cm^3, $1.655º \leq \theta \leq 30.539º$, 3858 unique reflections out of 5996 with $I > 2\sigma(I)$, GOF = 1.043, R_1 = 0.0722, wR_2 = 0.1872, CCDC: 2223946

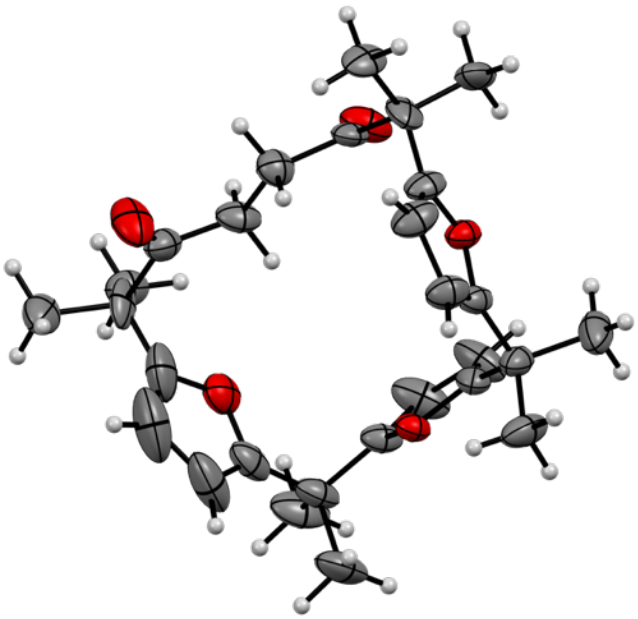

Figure 2-7. ORTEP drawing of the crystal structure of **8** at the 50% thermal probability levels (C: gray, H: white, O: red).

2.6 Reference

[1] Cafeo, G.; Kohnke, F.H.; La Torre, G.L.; White, A.J.P.; Williams, D.J., From Large Furan-Based Calixarenes to Calixpyrroles and Calix[n]furan[m]pyrroles: Syntheses and Structures. *Angew. Chem. Int. Ed*. **2000**, *39*, 1496-1498.

[2] Inaba, Y.; Nomata, Y.; Ide, Y.; Pirillo, J.; Hijikata Y.; Yoneda, T.; Osuka, A.; Sessler, J. L.; Inokuma, Y. Calix[3]pyrrole: A Missing Link in Porphyrin-Related Chemistry. *J. Am. Chem. Soc*. **2021**, *143*, 12355-12360.

[3] Uesaka, M.; Saito, Y.; Yoshioka, S.; Domoto, Y.; Fujita, M.; Inokuma, Y. Oligoacetylacetones as Shapable Carbon Chains and Their Transformation to Oligoimines for Construction of Metal-organic Architectures. *Commun. Chem*. **2018**, *1*, 23.

[4] Hazell, A. The Structure of Octamethyltetraoxaquaterene. *Acta Cryst*. **1989**, *C45*, 137-140.

[5] (a) Amarnath, V.; Anthony, D. C.; Amarnath, K.; Valentine, W. M.; Wetterau, L. A.; Graham, D. G. Intermediates in the Paal-Knorr Synthesis of Pyrroles. *J. Org. Chem*. **1991**, *56*, 6924-6931. (b) Amarnath, V.; Amarnath, K. Intermediates in the Paal-Knorr Synthesis of Furans. *J. Org. Chem*. **1995**, *60*, 301-307.

[6] Sheldrick, G. M. Crystal Structure Refinement with *SHELXL. Acta Crystallogr. Sect. C* **2015**, *71*, 3-8.

[7] Grimme, S.; Antony, J.; Ehrlich, S.; Krieg, H. A Consistent and Accurate *ab initio* Parametrization of Density Functional Dispersion Correction (DFT-D) for the 94 Elements H-Pu. *J. Chem. Phys.* **2010**, *132*, 154104.

[8] Gaussian 16, Revision C.01, Frisch, M. J.; Trucks, G. W.; Schlegel, H. B.; Scuseria, G. E.; Robb, M. A.; Cheeseman, J. R.; Scalmani, G.; Barone, V.; Petersson, G. A.; Nakatsuji, H.; Li, X.; Caricato, M.; Marenich, A. V.; Bloino, J.; Janesko, B. G.; Gomperts, R.; Mennucci, B.; Hratchian, H. P.; Ortiz, J. V.; Izmaylov, A. F.; Sonnenberg, J. L.; Williams-Young, D.; Ding, F.; Lipparini, F.; Egidi, F.; Goings, J.; Peng, B.; Petrone, A.; Henderson, T.; Ranasinghe, D.; Zakrzewski, V. G.; Gao, J.; Rega, N.; Zheng, G.; Liang, W.; Hada, M.; Ehara, M.; Toyota, K.; Fukuda, R.; Hasegawa, J.; Ishida, M.; Nakajima, T.; Honda, Y.; Kitao, O.; Nakai, H.; Vreven, T.; Throssell, K.; Montgomery, J. A., Jr.; Peralta, J. E.; Ogliaro, F.; Bearpark, M. J.; Heyd, J. J.; Brothers, E. N.; Kudin, K. N.; Staroverov, V. N.; Keith, T. A.; Kobayashi, R.; Normand, J.; Raghavachari, K.; Rendell, A. P.; Burant, J. C.; Iyengar, S. S.; Tomasi, J.; Cossi, M.; Millam, J. M.; Klene, M.; Adamo, C.; Cammi, R.; Ochterski,

J. W.; Martin, R. L.; Morokuma, K.; Farkas, O.; Foresman, J. B.; Fox, D. J. Gaussian, Inc., Wallingford CT, 2016.

Chapter 3

Structural evaluation and macrocycle design by StrainViz analysis

Abstract

In this chapter, the character of StrainViz analysis in the field of contracted porphyrin related compound was revealed with the comparison with result from homodesmotic reaction method. Using the visualization of strain energy distribution, StrainViz was also used for investigation of highly strained calix[2]pyrrole and newly designed [2.2](2,5)pyrrolophane cores.

3.1 Introduction

3.1.1 Ring strain evaluation

Considering the important effect of ring strain, several methods for evaluating ring strain energy have been developed. One of the most conventional method is combustion calorimetry that has been utilized for some typical strained macrocycles, such as [2.2]paracyclophane[1]. Unfortunately, such experimental methods are difficult to operate and do not easily obtain accurate data. With the continuous improvement of the accuracy of calculation methods, evaluating ring strain energy through theoretical calculations has now become the standard method. This is a type of analysis method that focuses on individuals, unlike the calculations in Chapter 2 show the overall energy change of the system. Nowadays, the most well-known calculational method for analyzing macrocyclic ring strain is homodesmotic reaction method[2]. The diagram of this method is shown in **Figure 3-1**.

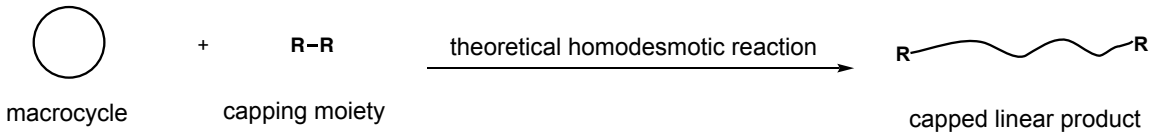

Figure 3-1. Diagram of theoretical homodesmotic reaction.

And the strain energy (E_{strain}) is defined as energy difference between the starting materials (macrocycle and capping moiety) and resulting linear product which is described with equation as follow:

$$E_{strain} = \left(E_{macrocycle} + E_{capping\ moiety}\right) - E_{linear\ product}$$

However, the information of strain energy obtained from this method is total strain energy. If local strain is required, this method can't provide useful result. Further, local strain is also an important factor to determinate reactivity (or stability) of the molecule. It is reasonable to image that two molecules with same strain energy, the molecule with strain energy spread over more atoms will be more stable that the molecule with concentrated strain in fewer atoms.

With the demand for local strain energy analysis, in 2020, Jasti group reported an advancement based on fragments to estimate strain energy that named StrainViz[3] that make it possible to analyze local strain and relative properties.

3.1.2 StrainViz method for local strain energy

This method was developed that identify the strain energy local to every coordinate (bond lengh, bond angle, and torsional angle) in a molecule. The general procedure of this method can be summarized as follows (**Figure 3-2**):

1. Freeze the molecular structure and cut out multiple molecular fragments

2. Cap the fragments with hydrogen atoms

3. Calculate the strain energy of each fragment

4. Map each obtained strain energy onto the original molecular structure

5. Fit and average strain energy in multiple fragments

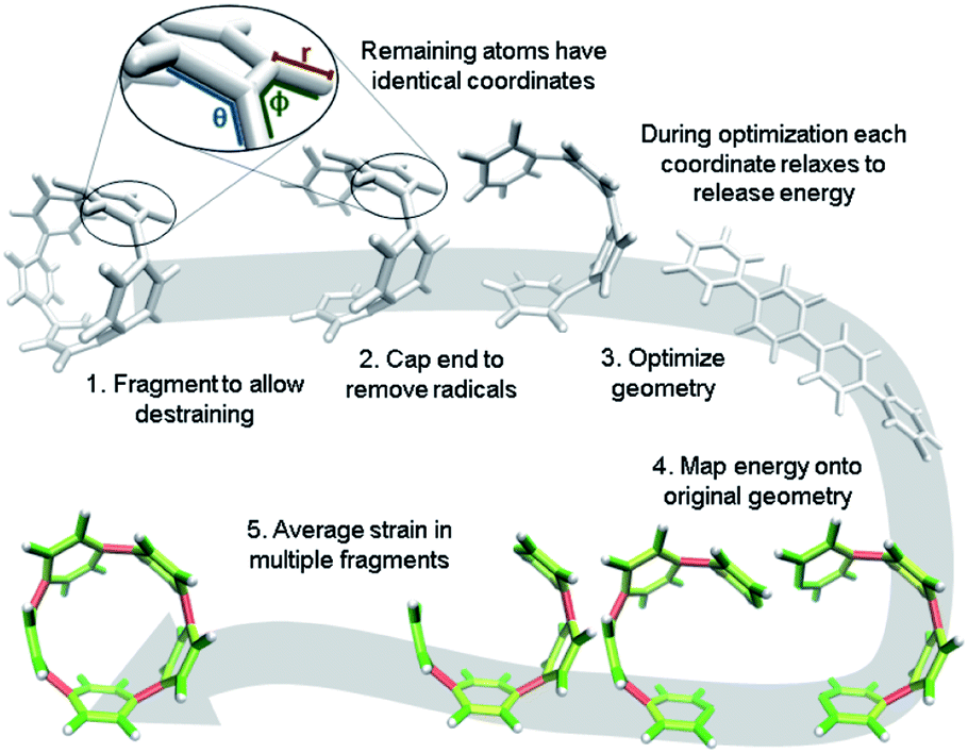

Figure 3-2. Workflow for StrainViz method[3].

The program calculates three strain energy including bond strain, angle strain and dihedral strain. The bond strain evaluated from bond length, the angle strain evaluated

from angle between three atoms, and the dihedral strain evaluated from torsional angle between four atoms of the aromatic ring. The sum of these strain energy so called total energy. And the energy distribution method as follows. The bond strain is assigned to the located bond. For the angle strain, the energy is divided in half among the two contributing bonds. For the torsional strain between four atoms, the energy is split evenly among the three bonds. Finally, the three types of energy are summed and a total strain map is produced and the degree of ring strain energy from low to high is represented by green to red.

Since the method of using fragments obviously introduces errors, there has requirements for the fragment. For obtaining accurate results, it requires create fragments as many symmetrically as possible, and create the fragment as large as possible to reduce error.

In this chapter, the further investigation about utilization of StrainViz in the field of contracted porphyrin analogues will be conducted.

3.2 StrainViz analysis for calix[*n*]pyrrole and related derivatives

StrainViz already used for strain comparison of calix[3]pyrrole and its derivatives that reported by our group recently[4]. However, as the 3.1.1 section mentioned, homodesmotic reaction method is the most conventional method. There is no comparison about StrainViz method and homodesmotic reaction method yet in the field of contracted porphyrin related macrocycles, while this should be important for understanding utilization of this two method.

In another work reported by our group[5], the ring strain of calix[3]pyrrole and its derivatives were investigated by homodesmotic reaction method. Therefore, here using StrainViz method investigated same molecules including calix[3]pyrrole, calix[1]furan[2]pyrrole and calix[3]furan for comparison, which summarized in **Figure 3-3**.

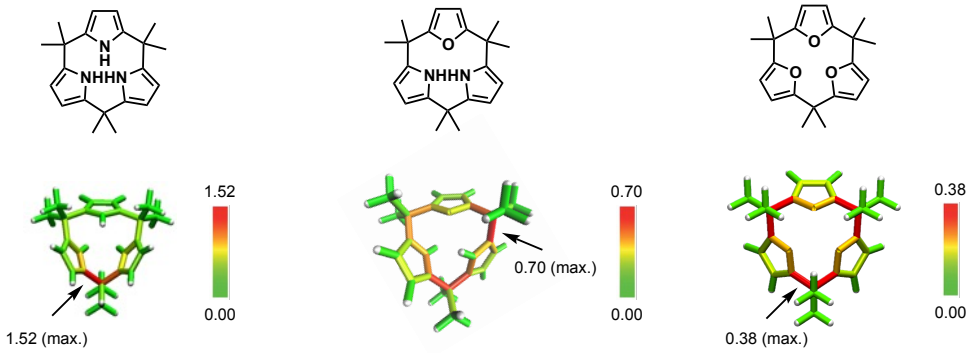

Total strain (in kcal mol^{-1})	13.4	11.6	6.2
Homodesmotic reaction method (in kcal mol^{-1})	20.0	17.7	16.4

Figure 3-3. StrainViz analysis for calix[3]pyrrole[4], calix[1]furan[2]pyrrole and calix[3]furan with the ring strain data obtained from homodesmotic reaction method[5].

It is clearly shown that StrainViz method will provide smaller energy strain values than homodesmotic reaction method but the tendency can be ensured for strain comparison. This relatively small value may be due to the information loss caused by the fragmentation process mentioned above. Regardless of possible information lost, StrainViz still a useful

method that allows for a clearer visualization of local strain energy which is benefit for understanding of molecules.

In chapter 2, the large destabilization energy increase in the Paal-Knorr process for calix[2] type compounds was proposed. It is reasonable to attribute this increase in energy to the high ring strain of the calix[2] type product. However, the molecular ring strain state cannot be intuitively understood. In the sense of use StrainViz analysis, it is clearly shown that the energy distribution located on the bridge moiety and two chemical bonds between α position and nitrogen.

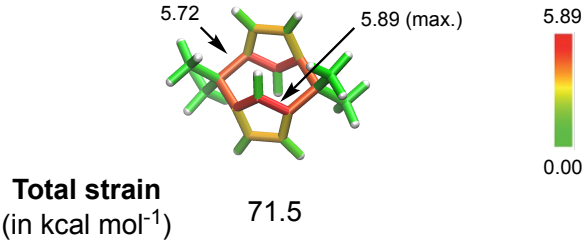

Figure 3-4. StrainViz analysis of calix[2]pyrrole.

The result implies StrainViz is a useful method for understanding strain structure of macrocycle. Next, the novel macrocycle design will also by means of StrainViz to distinguish subtle differences in ring strain distribution.

3.3 Molecule design of novel [2,2](2,5)pyrrolophane-type macrocycle

In the pervious chapter, the synthetic attempts for calix[2]-type macrocycles were described. The failure to produce the target compounds was not too surprising if compare the situation of cyclophane field such as the two typical paracyclophane molecules shown in **Figure 3-5**.

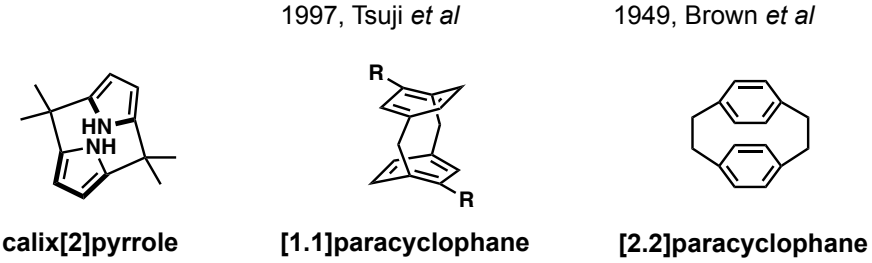

Figure 3-5. Structural of calix[2]pyrrole, [1.1]paracyclophane and [2.2]paracyclophane.

The calix[2]-type macrocycles also can be defined as [1.1]cyclophane-type macrocycles that two aromatic rings connected by one carbon atoms each side bridging chain. In the case of [1.1]paracyclophane, this highly strained molecule was reported by Tsuji *et al*[6] with photochemical condition at a very low temperature (**Scheme 3-1a**). And this [1.1]paracyclophane only stable at low temperature that can't be isolated unless the molecular structure is modified to form a kinetically stable species[7]. In contrast, [2.2]paracyclophane was found long before[8] and can be prepared by Hofmann elimination[9] easily (**Scheme 3-1b**). Although the formation of [1.1] type molecules is not impossible, the extremely special conditions and elusive stability make it difficult to research property in detail.

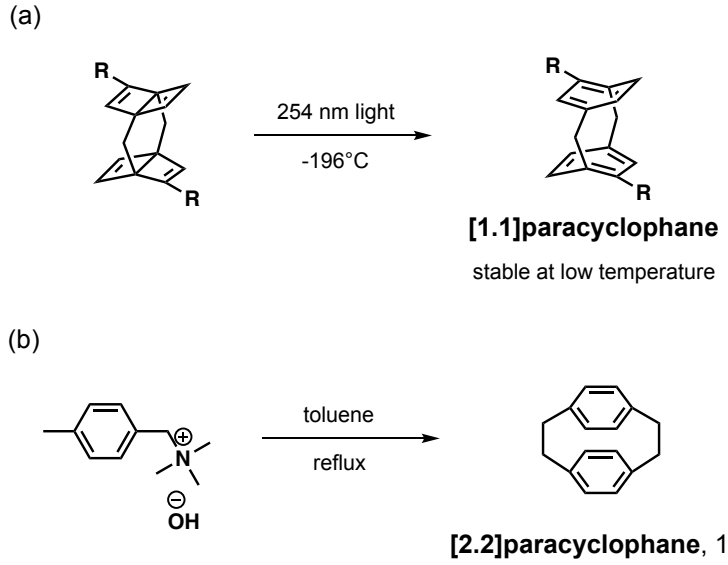

Scheme 3-1. (a) Photochemical synthesis of [1.1]paracyclophane[6] and (b) synthesis of [2.2]paracyclophane by Hofmann elimination[9].

If add one more carbon atom into the bridging chain of calix[2]pyrrole, the synthesis difficulty caused by ring strain will be significantly reduced. And the resulting [2.2]cyclophane-type molecule (**Figure 3-6**) is promising candidate for molecular machinery or molecular switch because of the ring flipping ability. However, Haley *et al*[10] have conducted early exploration that proved this type of molecules has very high ring flipping energy barrier by variable temperature NMR (VTNMR). And a recent computational work also indicated the difficulty of ring flipping[11].

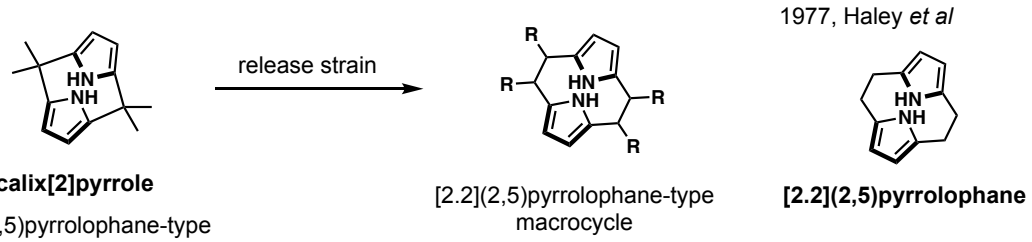

Figure 3-6. Ring strain releasing strategy by extending bridging chain.

It seems difficult to achieve molecular conformational switch through physical process that simply change temperature. Therefore, chemical processes are considered to achieve reversible conformational transformations. For pyrrole compounds, the most widely

reported reversible chemical reaction should be redox process, from small bi-, tri-, tetrapyrrole molecules[12] to macromolecular polypyrrole[13]. Such redox process can act as a driving force to change the molecular conformation combined with electronic structure change.

Hence, the molecule design is using pyrrole ring as bridge chain to generate the novel [2.2](2,5)pyrrolophane-type compound with four directly linked pyrroles. Because of the potential flexibility of cyclophane-type skeleton, the conformational change in redox process also be expected. This will promote the fundamental research and application of flexible π-conjugated skeleton.

However, the different bond lengths and angles at the α and β positions of pyrrole[14] will result in different isomers (**Figure 3-7**). In such highly contracted structure, even the minor structural difference may cause different strain energy and energy distribution. The ideal target should have less ring strain and averaged distribution. Therefore, the ring strain of these isomers was evaluated by StrainViz to determine the total strain energy, maximum energy site, and uniformity of energy distribution.

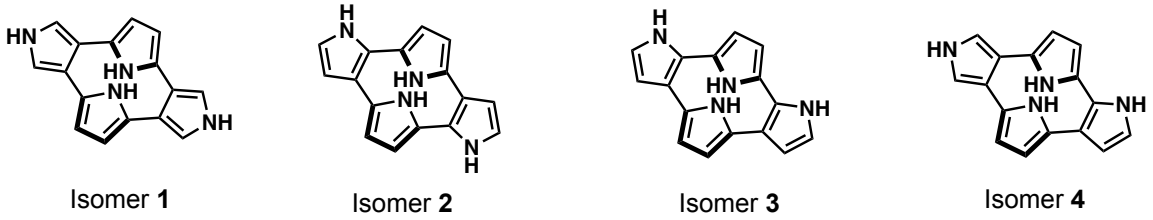

Figure 3-7. The structure of four isomers of designed [2.2](2,5)pyrrolophane-type macrocycles.

It can be observed very intuitively that, among all isomers, the sites with the highest ring strain energy distribution are all located on the chemical bonds connecting the two pyrrole rings (**Figure 3-8**). For specific values, isomer **1**, due to its highly symmetrical structure, has the same maximum ring strain energy distribution among the chemical bonds between its four pyrrole rings. For isomers **2** and **3**, the sites with the maximum distribution of ring strain energy both appear at the pyrrole α - pyrrole β bond, while the energy distribution at the pyrrole β - pyrrole β bond is slightly smaller. For isomer **4**, due to the asymmetric structure, the chemical bonds connecting the two pyrrole rings exhibit different energy distributions, but the maximum value also appears at the pyrrole α - pyrrole β bond.

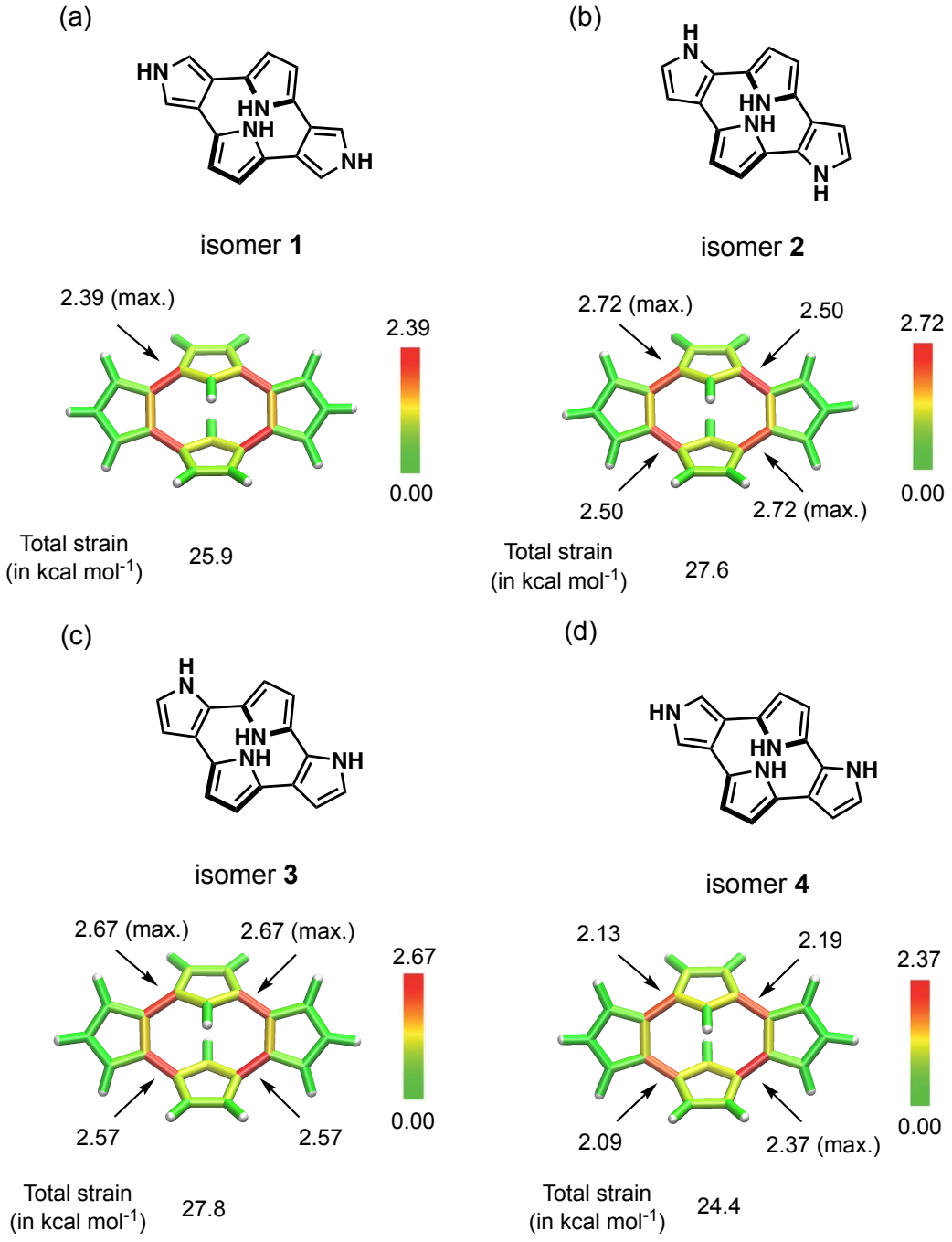

Figure 3-8. Visualization of the ring strain distribution of (a) isomer **1**; (b) isomer **2**; (c) isomer **3**; (d) isomer **4** at B3LPY/6-31G(d) level.

All the total strain values indicated that the conventional thermal chemical condition is possible for generation of such contracted core structure. After obtaining the ring strain evaluation data for the four isomers, and considering the ease of synthesis, isomer **1** was selected as the target core structure for actual synthesis of next chapter. Although isomer **4** has the lowest total ring strain energy and smallest maximum energy distribution, the asymmetric structure will make the design of synthetic route challenge. Among the other three isomers with symmetry, isomer **1** has the lowest total ring strain energy and smallest maximum energy distribution, therefore selected isomer **1** as target core structure for actual synthesis.

3.4 Conclusion

By analyzing several calix[3]pyrrole derivatives, the character of StrainViz analysis was revealed with the comparison with result from homodesmotic reaction method. The StrainViz method was further used for investigation of highly strained calix[2]pyrrole and newly designed [2.2](2,5)pyrrolophane cores with the visualization of strain energy distribution.

3.5 Experimental Section

3.5.1 General procedure of StrainViz calculation

1. Create the molecular structure in Gaussview and optimized the structure at B3LYP/6-311G(2d, p) level by Gaussian 16[15].
2. Transfer the obtained ".chk" files into ".mol2" files and opened by Avogadro 2 software.
3. In Avogadro 2, make several fragments from the original structure, and save the original structure and all fragments as ".xyz" files.
4. The ".xyz" files are uploaded to the WPI-ICReDD server for computation[16], and then the corresponding "output" file is downloaded for analysis.
5. Visual analysis is performed by loading the "total_force.tcl" file from the "output" folder using VMD software. The distribution of ring strain energy is located with date described from "total_force.txt" file.

3.5.2 Detail Strain energy composition

Table 3-1. The total strain energy (in kcal mol^{-1}) of calix[n]pyrrole derivatives predicted by StrainViz method at B3LPY/6-31G(d) level.

	Calix[1]furan[2]pyrrole	Calix[3]furan	Calix[2]pyrrole
Bond strain	1.10	0.49	4.96
Angle strain	1.00	0.82	3.55
Dihedral strain	9.47	4.89	62.96
Total strain	11.57	6.21	71.46

Table 3-2. The total strain energy (in kcal mol^{-1}) of four isomers predicted by StrainViz method at B3LPY/6-31G(d) level.

	Isomer **1**	Isomer **2**	Isomer **3**	Isomer **4**
Bond strain	1.54	1.50	1.54	1.37
Angle strain	6.92	7.17	7.27	4.55
Dihedral strain	17.44	18.92	19.00	18.43
Total strain	25.90	27.59	27.81	24.35

3.6 Reference

[1] Meijere, A. de; Kozhushkov, S. I.; Rauch, K.; Schill, H.; Verevkin, S. P.; Kümmerlin, M.; Beckhaus, H.; Rüchardt, C.; Yufit, D. S. Heats of Formation of [2.2]Paracyclophane-1-ene and [2.2]Paracyclophane-1,9-diene − An Experimental Study. *J. Am. Chem. Soc*. **2003**, *125*, 15110-15113.

[2] Wheeler, S. E.; Houk, K. N.; Schleyer, P. v. R.; Allen, W. D. A Hierarchy of Homodesmotic Reactions for Thermochemistry. *J. Am. Chem. Soc*. **2009**, *131*, 2547-2560.

[3] Colwell, C. E.; Price, T. W.; Stauch, T.; Jasti, R. Strain Visualization for Strained Macrocycles. *Chem. Sci*. **2020**, *11*, 3923-3930.

[4] Watanabe, K.; Shibata, K.; Ichino, T.; Ide, Y.; Yoneda, T.; Maeda, S.; Inokuma, Y. Strain-based Design, Direct Macrocyclization, and Metal Complexation of Thiazole-Containing Calix[3]pyrrole Analogues. *Inorg. Chem. Front*. **2024**, *11*, 3548-3554.

[5] Inaba, Y.; Kakibayashi, Y.; Ide, Y.; Pirillo, J.; Hijikata, Y.; Yoneda, T.; Inokuma, Y. Strain-Induced Ring Expansion Reactions of Calix[3]pyrrole-Related Macrocycles. *Chem. Eur. J*. **2022**, *28*, e202200056.

[6] Tsuji, T.; Ohkita, M.; Konno, T.; Nishida, S. [1.1]Paracyclophane. Photochemical Generation from the Corresponding Bis(Dewar benzene) Derivative and Theoretical Study of Its Structure and Strain Energy. *J. Am. Chem. Soc*. **1997**, *119*, 8425-8431.

[7] Kawai, H., Suzuki, T., Ohkita, M.; Tsuji, T. A Kinetically Stabilized [1.1]Paracyclophane: Isolation and X-Ray Structural Analysis. *Angew. Chem. Int. Ed*. **1998**, *37*, 817-819.

[8] Brown, C. J.; Farthing, A. C. Preparation and Structure of Di-*p*-Xylylene. *Nature* **1949**, *164*, 915-916.

[9] Winberg, H. E.; Fawcett, F. S. [2.2]Paracyclophane. *Org. Synth*. **1962**, *42*, 83.

[10] Haley J. F. Jr.; Rosenfeld, S. M.; Keehn, P. M. Cyclophanes. 10. Synthesis and Conformational Behavior of [2.2](2,5)pyrrolophanes. *J. Org. Chem*. **1977**, *42*, 1379-1386.

[11] Bezoari, M. D.; Bourgeois, C. Conformational Analysis of Selected [2.2]heterophanes: A Comparison of Stereochemical Switching via Computational Chemistry. *IJURCA*, **2023**, *12*, article 1.

[12] E, W.; Ohkubo, K.; Sanchez-Garcia, D.; Zhang, M.; Sessler, J. L.; Fukuzumi, S.; Kadish, K. M. Electron-Transfer Oxidation Properties of Substituted Bi-, Ter-, and Quaterpyrroles. *J. Phys. Chem. B* **2007**, *111*, 4320-4326.

[13] Li, Y. On the Large Overpotential of the First Reduction of Polypyrrole Perchlorate Films in Organic Solutions. *Electrochim. Acta* **1997**, *42*, 203-210.

[14] Nygaard, U.; Nielsen, J. T.; Kirchheiner, J.; Maltesen, G.; Rastrup-Andersen, J.; Sørensen, G.O. Microwave spectra of isotopic pyrroles. Molecular Structure, Dipole Moment, and ^{14}N Quadrupole Coupling Constants of Pyrrole. *J. Mol. Structure* **1969**, *3*, 491-506.

[15] Gaussian 16, Revision C.01, Frisch, M. J.; Trucks, G. W.; Schlegel, H. B.; Scuseria, G. E.; Robb, M. A.; Cheeseman, J. R.; Scalmani, G.; Barone, V.; Petersson, G. A.; Nakatsuji, H.; Li, X.; Caricato, M.; Marenich, A. V.; Bloino, J.; Janesko, B. G.; Gomperts, R.; Mennucci, B.; Hratchian, H. P.; Ortiz, J. V.; Izmaylov, A. F.; Sonnenberg, J. L.; Williams-Young, D.; Ding, F.; Lipparini, F.; Egidi, F.; Goings, J.; Peng, B.; Petrone, A.; Henderson, T.; Ranasinghe, D.; Zakrzewski, V. G.; Gao, J.; Rega, N.; Zheng, G.; Liang, W.; Hada, M.; Ehara, M.; Toyota, K.; Fukuda, R.; Hasegawa, J.; Ishida, M.; Nakajima, T.; Honda, Y.; Kitao, O.; Nakai, H.; Vreven, T.; Throssell, K.; Montgomery, J. A., Jr.; Peralta, J. E.; Ogliaro, F.; Bearpark, M. J.; Heyd, J. J.; Brothers, E. N.; Kudin, K. N.; Staroverov, V. N.; Keith, T. A.; Kobayashi, R.; Normand, J.; Raghavachari, K.; Rendell, A. P.; Burant, J. C.; Iyengar, S. S.; Tomasi, J.; Cossi, M.; Millam, J. M.; Klene, M.; Adamo, C.; Cammi, R.; Ochterski, J. W.; Martin, R. L.; Morokuma, K.; Farkas, O.; Foresman, J. B.; Fox, D. J. Gaussian, Inc., Wallingford CT, 2016.

[16] https://github.com/CurtisColwell/StrainViz

Chapter 4

Synthesis and property investigation of designed [2.2](2,5)pyrrolophane, the cyclo[4]pyrrole with α-β direct linkage

Abstract

In this chapter, the designed [2.2](2,5)pyrrolophane-type macrocycle, cyclo[4]pyrrole with α-β direct linkage, was successfully synthesized by a 6-step route combined carbonyl related reaction and Pd-catalyzed cross-coupling reaction. This newly obtained compound exhibited a non-planar and highly strained conjugated structure. Detail investigation of this new compound was performed for the unique spectral changes during the reversible oxidation process. The conformational and electronic structure changes during the oxidation process were revealed through theoretical calculations.

4.1 Introduction

The designed [2,2](2,5)pyrrolophane skeleton is the structure that all pyrroles connect directly. This type of compound has a more common name: cyclo[*n*]pyrrole that *n* means the number of pyrrole rings in the macrocycle. All previously reported cyclo[*n*]pyrrole compounds (**Figure 4-1**) were expended porphyrin analogs that from cyclo[6] to cyclo[10]pyrroles[1-4]. These compounds were obtained through a similar "one-pot" synthetic strategy, that is, in the presence of anion template, pyrrole or bipyrrole were directly dehydrogenative coupling to form macrocyclic compounds with oxidant. For example, the cyclo[6]pyrrole was synthesized from bipyrrole precursor with $FeCl_3$ as oxidant and chloride anion as templet as shown in **Scheme 4-1a**.

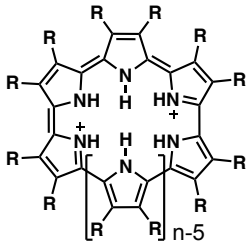

Cyclo[8]pyrrole: 2002, Seidel *et al*

Cyclo[6]pyrrole and cyclo[7]pyrrole: 2003, Köhler *et al*

Cyclo[10]pyrrole: 2016, Okujima *et al*

Cyclo[9]pyrrole: 2021, Matsumoto *et al*

Figure 4-1. Summary of reported cyclo[n]pyrrole.

The target compound cyclo[4]pyrrole will be the first contracted example for the family of cyclo[*n*]pyrrole. However, the conventional synthetic method is definitely unsuitable for this molecule because the small cavity makes template-based synthesis impractical. Further, as a strained macrocycle, the "one-pot" method that simultaneously forming multiple chemical bonds for cyclization is obviously extremely difficult. Therefore, stepwise synthesis would be reasonable and "3+1" strategy was selected here (**Scheme 4-1b**). For the construction of terpyrrole subunit with alpha-beta linkage, refer the synthesis of terpyrrole with alpha-alpha linkage[5], it is possible be obtained from beta-acetyl pyrrole by enolate coupling and Paal-Knorr reaction. For the cyclization process, transition metal-catalyzed coupling reactions are considered attractive because they play a crucial role in the cyclization of some important contracted porphyrin analogues, such as Ni-catalyst coupling for norcorrole[6] and Pd-catalyst coupling for free base subporphyrin[7]. Certainly, in the specific synthesis process, appropriate substituents will be added to the pyrrole unit to make the multi-step synthesis more efficient.

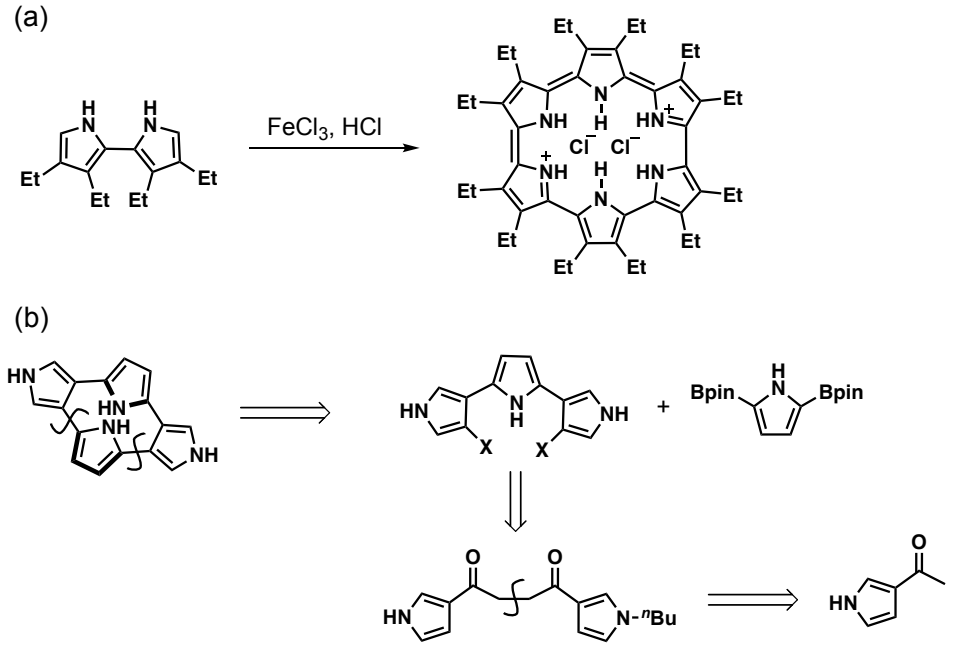

Scheme 4-1. (a) The conventional "one-pot" synthesis of cyclo[6]pyrrole[2]; (b) Retrosynthetic analysis of cyclo[4]pyrrole skeleton.

4.2 Synthesis of cyclo[4]pyrrole

The specific synthetic route was described in **Scheme 4-2**. Firstly, the β-acetyl pyrrole **3** was obtained efficiently from Paal-Knorr pyrrole synthesis of tetraacetylethane **1**[8] and *p*-toluenesulfonic acid (*p*-TsOH) catalyst β deacylation reaction[9] of compound **2**. Here, the reason for choosing *n*-butylamine as the starting material for the Paal-Knorr reaction is to enhance the solubility of the final compound. Although using 2,5-substituted pyrrole for the Vilsmeier-Haack reaction is also possible[10], the reaction reported with moderate yields and requires the irritating phosphorus oxychloride.

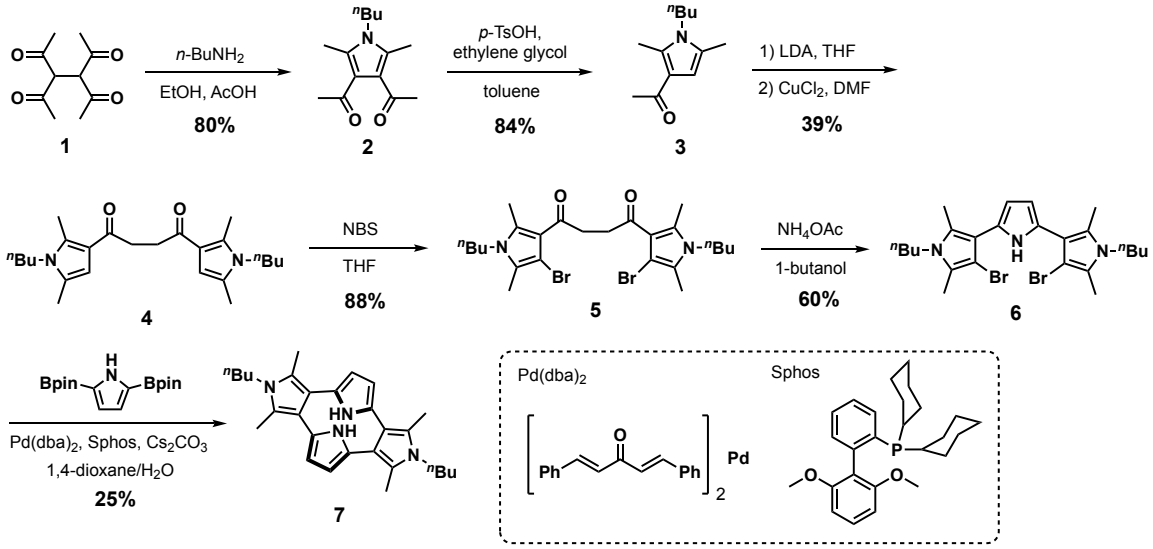

Scheme 4-2. Stepwise synthetic route for cyclo[4]pyrrole **7**.

Enolate coupling of compound **3** was conducted with conventional lithium diisopropylamide (LDA)/$CuCl_2$ condition to provide compound **4**, and followed by bromination with *N*-bromosuccinimide (NBS) in THF to provide compound **5**.

The next Paal-Knorr pyrrole synthesis of compound **5** with ammonium acetate was found very slow in ethanol, so changed the solvent to 1-butanol and performed the reaction at higher temperature to accelerate the reaction. Furthermore, reaction time was crucial because the product appears to be unstable under this acidic, high-temperature condition, with the yield initially increasing and then decreasing over time. By monitoring the

reaction, 1.5 hours was determined as most suitable reaction time that can provide compound **6** with best yield.

Finally, Suzuki-Miyaura coupling was used for the cyclization step. $Pd(dba)_2$/Sphos/Cs_2CO_3 system was found most suitable in this reaction after several condition screening. During the condition screening process, it was also found that concentration was crucial. At normal concentrations (e.g., 100 mM), 2,5-diborylpyrrole[11] was rapidly consumed while compound **6** remained in large quantities in the reaction mixture. The reason for this phenomenon should be steric hindrance of substrate **6** which has two adjacent substituents at its bromide position that makes oxidative insertion of Pd(0) species difficult. Further increasing the concentration accelerated the consume of compound **6**, thereby increasing the yield of target compound and obtained 25% yield of cyclo[4]pyrrole **7** at 285 mM concentration.

During the synthesis, another alternative route (**Scheme 4-3**) was also explored, which involved compound **5** and changing the order of Paal-Knorr reaction and Suzuki reaction. The terpyrrole diketone compound **8** was successfully obtained from Suzuki reaction while the followed Paal-Knorr pyrrole synthesis can't provide cyclo[4]pyrrole **7** using the same condition generated compound **6**, while only intramolecular addition product was observed (see experimental section). Increased ring strain was considered an important factor hindering the reaction, and the detailed analysis will be discussed in the next section.

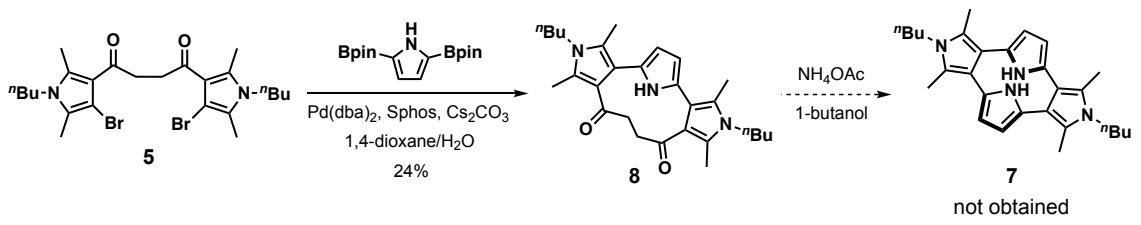

Scheme 4-3. Alternative synthetic routes from compound **5**.

4.3 Ring strain analysis

Single crystal X-ray diffraction analysis revealed a non-planar macrocyclic structure of compound **7** (**Figure 4-2**). The two N-butylated pyrrole moieties were positioned on the same plane, and the other two pyrrole units were arranged almost parallel with a mean interplanar distance of 2.4 Å, which is larger than the typical sum of van der Waals radius of two carbon atoms (3.4 Å) or two nitrogen atoms (3.10 Å). The dihedral angle between the two adjacent pyrrole units was 54.78°. The dihedral angle between the pyrrole and benzene planes in the o-phenylene-linked pyrrolophane **9**[12] was slightly larger (57.78°), while both **7** and **9** exhibited C_{2h}-symmetric conformations with two pyrrole-2,5-diyl units slip-stacked in an anti-parallel fashion with a mean distance of 2.4 Å.

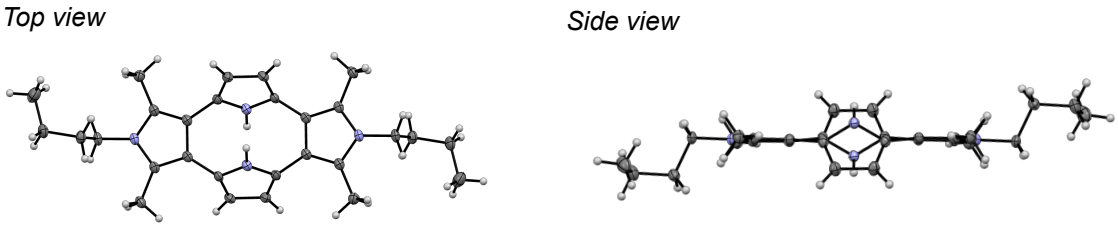

Figure 4-2. X-ray crystal structure of compound **7**, thermal ellipsoids are set at the 50% probability.

Compound **8** also exhibited a non-planar conformation for the 3,2':5',3''-terpyrrole unit indicated by Single crystal X-ray diffraction analysis (**Figure 4-3**) that the dihedral angles between the two adjacent pyrrole units were 53.18° and 68.58°.

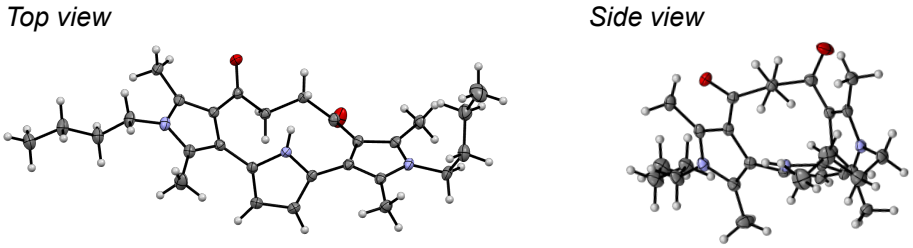

Figure 4-3. X-ray crystal structure of compound **8**, thermal ellipsoids are set at the 50% probability.

For analyzing the ring strain of newly obtained macrocycles **7** and **8**, comparing their pyrrole subunit deformation in their crystal structures firstly, and utilized the crystal data of compounds **9**[12] as a supplementary comparison. The deformation angles α and β represent the deformation of the pyrrole ring from planarity and the displacement of the carbon atom externally connected to the pyrrole–α position from the bow of the pyrrole ring (**Figure 4-4**).

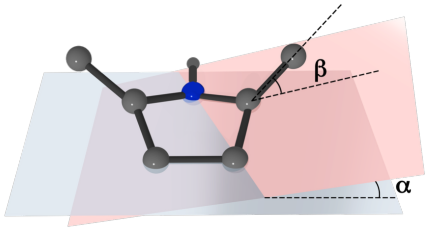

Figure 4-4. Definition of deformation angles α and β of pyrrole subunit in macrocycle.

Cyclo[4]pyrrole **7** showed the largest deformation angle α (5.95°) in the series, while its angle β (17.48°) was comparable to that of **9** (17.55°). Considering deformation angles, cyclo[4]pyrrole **7** is a more strained macrocycle than calix[3]pyrrole (α = 2.52°, β = 9.20°)[13], another typical contracted porphyrin analogue. In contrast, diketone-linked terpyrrole **9** exhibited notably smaller α and β of 2.09° and 10.01°, respectively, which indicated the smaller ring strain. The detailed deformation angle data was summarized in **Table 4-1**.

Table 4-1. Deformation angles comparison between compound **7**, **8** and **9**. The selected pyrrole subunit for each compound is marked with blue color.

	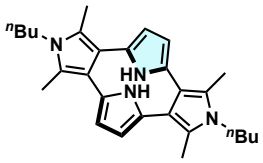	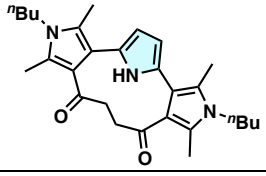	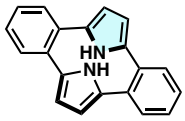
Deformation angle	Compound **7**	Compound **8**	Compound **9**
α (°)	5.95	2.09	5.07
β (°)	17.48	10.01	17.55

Then, StrainViz[14], the calculation method used in Chapter 3 was also used here for evaluating their strain and strain distribution quantitatively by using DFT calculations at

the M06-2X[15]/6-311+G(2d,p) level of theory. StrainViz analysis revealed that all the compounds exhibited the maximum strain energy around the C–C single bonds between two aromatic rings as shown in **Figure 4-5**, which agree with the result in chapter 3 using simulated structure. One reason for this energy distribution pattern should be the repulsion of the two central pyrroles in which the small distance is proved by crystal structure.

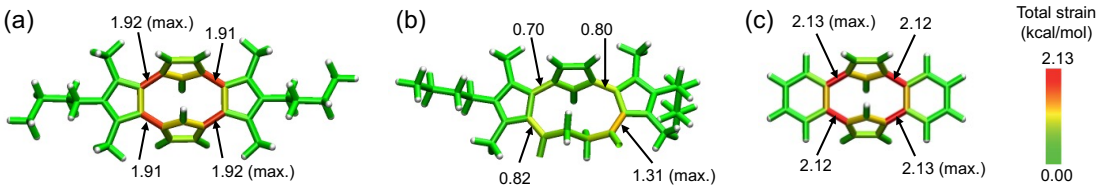

Figure 4-5. Strain energy distribution of (a) compound **7**; (b) compound **8**; (c)compound **9** indicated by StrainViz.

As for the total strain energy, **7** and **9** have approximately twice larger energy than that of **9**, and the bond and angle strain energies were similar. The dihedral strain greatly contributed to the total strain of these macrocycles. Although **7** exhibited the largest deformation angle α in the crystal structure, the maximum and total strain (1.92 and 20.8 kcal mol^{-1}, respectively) were slightly smaller than that of **9** (2.12 and 22.7 kcal mol^{-1}, respectively). Possible reason is the steric effect of the methyl group in **7** affected the strain energy and torsional motion, which resulted in less strain. Furthermore, **9** has a smaller macrocyclic cavity than **7**, which resulted in a larger total strain. All quantitative strain energy values were summarized in **Table 4-2**.

Table 4-2. The total, bond, angle and dihedral strain energies (in kcal mol^{-1}) revealed by StrainViz.

	7	**8**	**9**
Total strain	20.8	11.4	22.7
Bond strain	0.9	0.9	1.2
Angle strain	4.2	3.2	4.8
Dihedral strain	15.7	7.3	16.7

Both the deformation angle data from crystal structure and calculational data from StrainViz indicated large difference in strain state between **7** and **8**, which is one of the possible reasons for unsuccessful conversion of **8** to **7** in the Paal-Knorr reaction. In other words, the Suzuki-Miyaura coupling is a more powerful synthetic tool for cyclization step to overcome increased strain energy.

4.4 Property investigation

As a novel synthesized conjugated skeleton, the electronic properties of compound **7** were investigated in detail.

The UV-vis absorption spectrum of **7** (**Figure 4-6**, black line) was recorded in acetonitrile that shown an absorption band at 276 nm with an absorption coefficient ε of 4.25×10^4 M^{-1} cm^{-1} and the absorption edge reached to 350 nm. No absorption occurs in the longer wavelength region should be attribute to the large dihedral angle between each pyrrole unit that prevent the generation of larger conjugated structure. Upon photoexcitation at 270 nm, cyclo[4]pyrrole **7** exhibited fluorescence emission at 434 nm (**Figure 4-6**, red line) with a fluorescence quantum yield (Φ) of 2.6%. The fluorescence decay measurement revealed that the emission lifetime (τ) of **7** in acetonitrile was 3.05 ns.

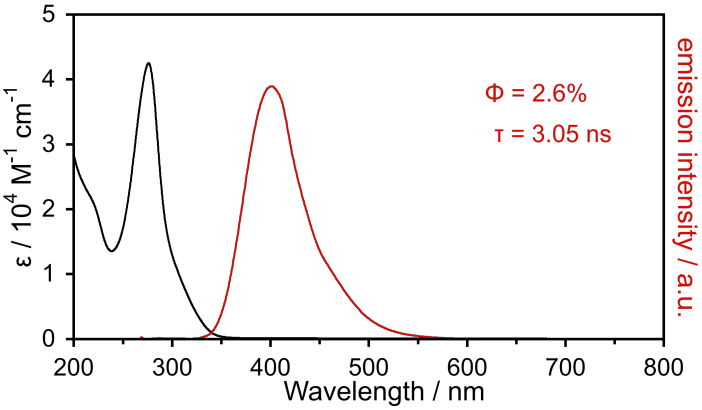

Figure 4-6. UV-vis absorption (black) and fluorescence (red) spectra of **7** in acetonitrile.

The cyclic voltammogram of **7** was recorded in dichloromethane containing 0.1 M tetrabutylammonium hexafluorophosphate (**Figure 4-7**), and the reversible oxidation waves were observed at –0.20 V and 0.28 V *vs*. ferrocene/ferrocenium (Fc/Fc^+) ion couple.

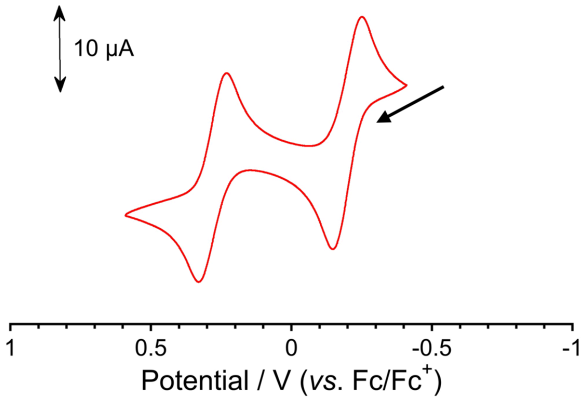

Figure 4-7. Cyclic voltammogram of **7** in dichloromethane electrolyte, scan rate: 0.05 V/s.

This two-step reversible redox process of compound **7** contrasted with the single irreversible oxidation process of compound **9** occurred at 0.47 V *vs*. Fc/Fc^+ ion couple[10]. This clear distinction demonstrated the success of the strategy in Chapter 3, which involved using pyrrole to replace the phenyl moiety to introduce more abundant oxidation states.

Further, the difference in oxidation potential between compound **7** and **9** can be well explained by theoretical calculations. The molecular orbital calculation (**Figure 4-8**) at the B3LYP/6-311G(d,p) level revealed that **7** exhibited relatively high HOMO and HOMO-1 energy levels as compared with **9**, consistent with the lower electrochemical oxidation potentials. And the orbital coefficients of both **7** and **9** were well-spread over the four aromatic rings.

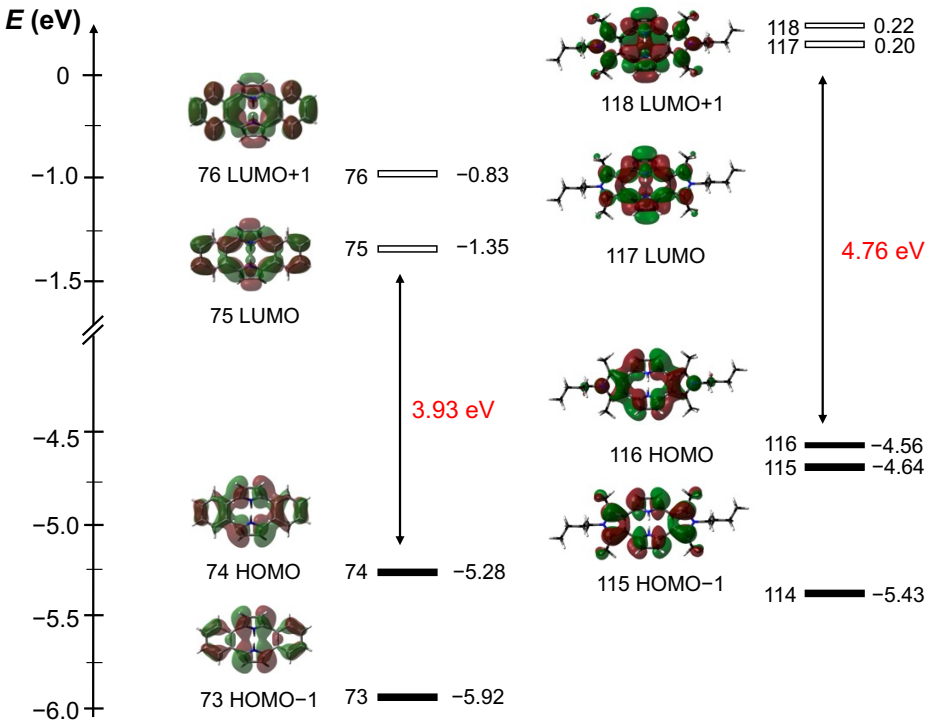

Figure 4-8. Frontier orbitals of **9** (left) and **7** (right) calculated at the B3LYP/6-311G(d,p) level.

Given the reversible two-electron oxidation processes of **7** observed by cyclic voltammetry, the electrochemical oxidation of **7** was further investigated using spectroelectrochemical and theoretical analyses.

The UV-vis absorption spectra recorded in dichloromethane during electrochemical oxidation at 0.6 V (vs. Ag/Ag^{+}) showed two-step spectral changes (**Figure 4-9**). At lower oxidation potentials (0.2-0.5 V), new intense bands at 350-500 nm and broad bands covering the 700-1000 nm region appeared, concomitant with a decrease in the absorption at 278 nm, assignable to neutral state of **7**. During the first spectral changes, an isosbestic point was observed at 322 nm. The application of a higher voltage (0.5-0.6 V) led to the appearance of other new absorption bands at 300 nm and 500-600 nm, resulting in a broad absorption spectrum covering from the ultraviolet to the near-infrared region.

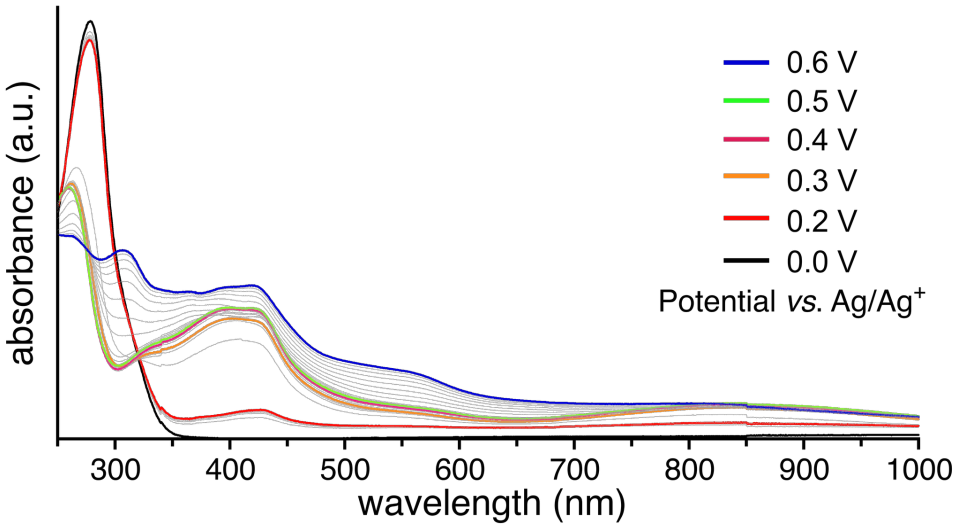

Figure 4-9. UV-vis absorption spectra during the electrochemical oxidation of **7** in dichloromethane.

To analyze the observed stepwise oxidation events of cyclo[4]pyrrole **7**, the theoretical calculations for the oxidized species were conducted.

For the first oxidation process, the optimized structure (**Figure 4-10a**) of radical cation $\mathbf{7}^{\bullet+}$ showed increased dihedral angles around one pyrrole-2,5-diyl unit (> 65°), while the other three pyrrole units underwent coplanarization with dihedral angles of ca. 38°. These structural features suggest that the π-electronic conjugation in $\mathbf{7}^{\bullet+}$ is roughly divided across the 3,2':5',3''-terpyrrole and single pyrrole units. Indeed, the calculated spin density is mainly spread over the terpyrrole segment (**Figure 4-10b**).

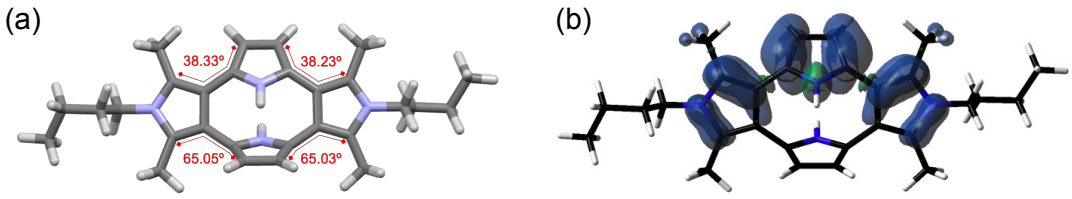

Figure 4-10. (a) Optimized geometry of $\mathbf{7}^{\bullet+}$; (b) Spin density distribution plots for $\mathbf{7}^{\bullet+}$ with an isovalue of 0.001. Calculation level: UB3LYP/6-311G(d,p).

For the dication $\mathbf{7}^{2+}$, however, the situation becomes complicated. Both closed-shell state and open-shell of $\mathbf{7}^{2+}$ were investigated by calculation. Unexpectedly, the total energy comparison indicates that the triplet diradical dication state is 1.14 kcal mol^{-1} more stable than the closed-shell dication state (R/U)B3LYP/6-311G(d,p) level. While the open-shell singlet diradical dication state is higher in energy (+1.39 kcal mol^{-1} relative to the triplet state). To minimize errors, other calculation methods were also used for comparison (**Table 4-3**), that the result indicate open-shell triplet state and closed-shell singlet state have more similar energy level.

Table 4-3. Comparison of the total energy (sum of electronic and zero-point energies) of $\mathbf{7}^{2+}$ with various functional with SMD continuum solvation model (CH_2Cl_2). The basis set was set at 6-311G(d,p) level. (in kcal/mol)

Relative energy	(R/U)B3LYP	(R/U)ωB97XD	(R/U)CAM-B3LYP
Closed-shell, singlet	+1.14	0	+0.46
Open-shell, singlet	+1.39	+1.32	+1.30
Open-shell, triplet	0	+0.12	0

When the structural optimization was conducted at the RB3LYP/6-311G(d,p) level, the structure of closed-shell dication $\mathbf{7}^{2+}$ (**Figure 4-11a**) changed to the terpyrrole-type structure similar to $\mathbf{7}^{\bullet+}$ with the dihedral angles between the two adjacent pyrrole units of 32° and 67° and the bond length alternation indicates quinoid-type π-electronic conjugation (**Figure 4-11b**).

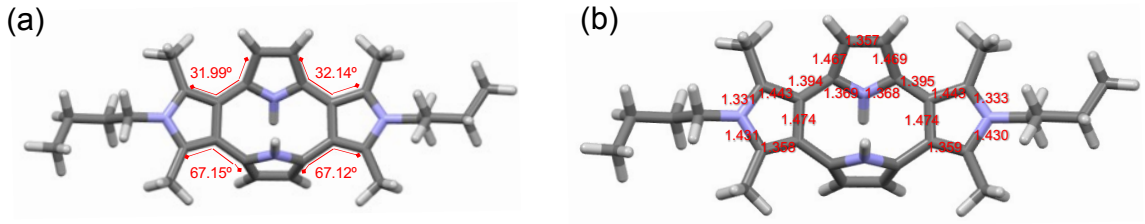

Figure 4-11. (a) Optimized geometry of closed-shell dication $\mathbf{7}^{2+}$; (b) bond length of quinoid-type terpyrrole moiety of closed-shell dication $\mathbf{7}^{2+}$. Calculation level: RB3LYP/6-311G(d,p).

When the structural optimization was conducted at the UB3LYP/6-311G(d,p) level revealed that the triplet diradical dication $\mathbf{7}^{2+}$ have essentially similar structures to neutral

7 (**Figure 4-12a**) with with the spin density delocalized onto the four pyrrole units (**Figure 4-12b**).

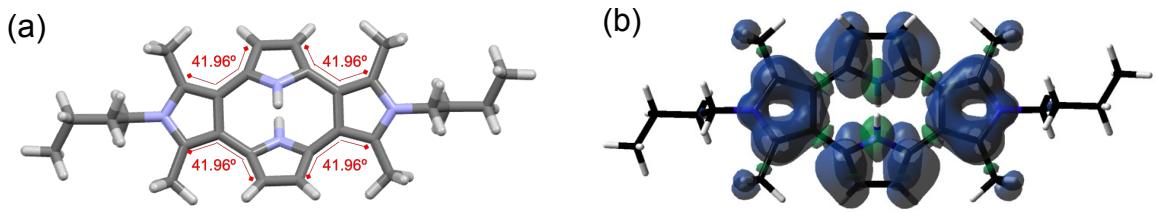

Figure 4-12. (a) Optimized geometry of triplet diradical dication $\mathbf{7}^{2+}$; (b) Spin density distribution plots for $\mathbf{7}^{2+}$ with an isovalue of 0.001. Calculation level: UB3LYP/6-311G(d,p).

The time-dependent density functional theory (TDDFT) calculation well-reproduced the absorption profiles of **7** (**Figure 4-18**) and $\mathbf{7}^{\cdot+}$ (**Figure 4-19**), while those of $\mathbf{7}^{2+}$ could not be assigned to the experimental spectra (**Figure 4-20** and **Figure 4-21**). Given the extremely close energy levels, it is conceivable that the conformational changes between the quinoidal form in the closed-shell state and the cyclophane form in the open-shell triplet state are fast under ambient conditions. The second stage absorption change in **Figure 4-9** can be assigned to the contribution from both the triplet diradical and closed-shell forms of $\mathbf{7}^{2+}$. The aromatic nature of the pyrrole segments in the dication state was compared using the Anisotropy of the Induced Current Density (ACID) and Nucleus-Independent Chemical Shifts (NICS) calculations (**Figure 4-22** and **Figure 4-23**). Accordingly, the terpyrrole-like segment is only weakly aromatic and the pyrrol-2,5-diyl segment remains aromatic.

Unfortunately, the attempt for generation of the oxidated species of **7** using tris(4-bromophenyl) ammoniumyl hexachloroantimonate (magic blue) which is a common single-electron oxidant, was unsuccessful. For the chemical oxidation and isolation of the oxidated species required more investigation.

4.5 Conclusion

In summary, the ring strained cyclo[4]pyrrole **7** was successfully synthesized by a 6-step route combined carbonyl related reaction and Pd-catalyzed cross-coupling reaction. As a result of the ring-contraction effect, **7** exhibited a non-planar and highly strained macrocyclic structure and the strain energy was investigated by theoretical calculation quantitative. Two reversible oxidation processes of **7** were identified in cyclic voltammetry and unique optical spectral changes during electrochemical oxidation was observed by spectroelectrochemical mearsument. Further theoretical analysis revealed effect of ring strain energy in **7**. In the radical cation $\mathbf{7}^{\cdot+}$, the dihedral angles around the pyrrol-2,5-diyl segment increased, which interrupted π-conjugation, resulting in the formation of a 3,2':5',3''-terpyrrole-localized radical cation. In contrast, dication $\mathbf{7}^{2+}$ mainly consisted of the triplet diradical dication form with the spin density delocalized onto the four pyrrole units bearing similar cyclophane-type conformation as neutral **7**. Further investigation about chemical oxidation should be necessary for understanding better about the oxidated species of **7**.

4.6 Experimental section

4.6.1 General information

Solvents and reagents were purchased from Fujifilm Wako Pure Chemical Industries Ltd., TCI Co., Ltd., Kanto Chemical Co., Inc., or Sigma-Aldrich Co., and used without further purification unless otherwise mentioned. All ^{1}H and ^{13}C NMR spectra were recorded using JEOL JNM-ECS400 spectrometers, and chemical shifts were reported in parts per million (ppm) relative to an internal standard tetramethylsilane (δ = 0.00 ppm for ^{1}H NMR in $CDCl_3$) or a solvent residual peak (δ = 77.16 ppm for ^{13}C NMR in $CDCl_3$, δ = 2.50 ppm for ^{1}H NMR in DMSO-*d*$_6$, 39.52 ppm for ^{13}C NMR in DMSO-*d*$_6$, and δ = 2.05 ppm for ^{1}H NMR in Acetone-*d*$_6$). Infrared spectra were measured using a JASCO Co. FT/IR-4600. ESI-TOF-MS spectra were recorded on a Thermo Scientific Executive spectrometer. Elemental analyses were carried out using an Exceter Analytical, Inc. CE440. Melting points were recorded using Yanaco MP-S3. Thin layer chromatography (TLC) was performed on silica gel sheets, MERCK silica gel 60 F254. Preparative scale separations were performed by means of gravity column chromatography over silica gel (Cica-Reagent, 60N, 63-210 μm). UV-vis absorption spectra were recorded on a Shimadzu UV-1800 spectrophotometer. Fluorescence emission spectra were recorded on a JASCO FP-8550 spectrophotometer. Fluorescence lifetime was recorded on EDINBURGH INSTRUMENTS FLS1000 photoluminescence spectrometer. Quantum yields were measured using a HAMAMATSU Quantaurus-QY Absolute PL quantum yield spectrometer: C11347-01. Analytical HPLC chromatograms were recorded using a JASCO MD-2018 photodiode array detector quipped with a JASCO PU-2089 pump, JASCO AS-2059 sampler, JASCO CO-2060 column thermostat. Recycling HPLC LaboACE LC-5060 equipped with two JAIGEL-2HR columns. Cyclic voltammograms were recorded by ALS Model660E electrochemical analyzer with an electrochemical system utilizing the three-electrode configuration consisting of platinum (working electrode), platinum wire (counter electrode) and $Ag/AgNO_3$ (reference electrode) in dichloromethane containing 0.1 M tetra-*n*-butylammonium hexafluorophosphate ($TBAPF_6$) as a supporting electrolyte. Spectroelectrochemical measurements were conducted on a JASCO V-770 spectrophotometer using a CH Instrument Model 700E (ALS) in dichloromethane solutions with 0.3 M tetra-*n*-butylammonium hexafluorophosphate as a supporting electrolyte. Measurements were made with an optically transparent thin-layer electrode cell containing a degassed sample solution using a Pt mini-grid as a working electrode, a

Pt wire as a counter electrode, and an Ag/AgCl wire as a reference electrode. Single crystal X-ray diffraction data were obtained using Rigaku XtaLAB P200 diffractometer equipped with a PILATUS200K detector, which uses a multilayer mirror (MoKa radiation l = 0.71073 Å). All structures were solved using a dual-space algorithm (SHELXTS2[16]) and refined using full-matrix least-squares method (SHELXLS3[17]).

4.6.2 Synthetic procedures

· Synthesis of compound **2**

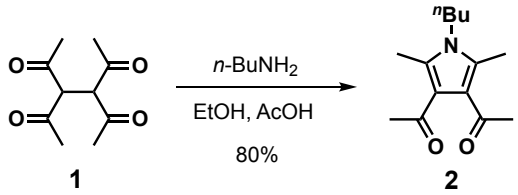

Tetraacetylethane **1**[8] (7.93 g, 40.0 mmol) was dissolved in a 1:1 (v/v) mixture (200 mL) of EtOH and AcOH in a 500 mL round bottom flask equipped with a reflux condenser. To the solution, *n*butylamine (4.00 mL, 40.0 mol) was added, and the mixture was refluxed overnight. After cooling the reaction mixture to room temperature, the solvent was removed with a rotary evaporator. 200 mL of saturated aqueous $NaHCO_3$ solution was added to the residue, and the products were extracted by washing with dichloromethane (50 mL × 3). The combined organic layer was dried over Na_2SO_4 followed by rotary evaporation to dryness. The residue was chromatographed on a silica gel column (diameter: 6 cm, height: 15 cm, eluent: ethyl acetate/hexane = 1:1) to give compound 6 (7.56 g, 32.1 mmol) in 80% yield as a colorless solid.

R_f = 0.30 (silica gel, ethyl acetate/hexane = 1:1), m.p.: 45-48ºC; ^{1}H NMR (400 MHz, DMSO-*d*$_6$, 298 K): δ = 3.83 (t, J = 7.6 Hz, 2H, methylene), 2.29 (s, 6H, methyl), 2.26 (s, 6H, methyl), 1.52 (m, 2H, methylene), 1.33 (sext, J = 7.6 Hz, 2H, methylene) , 0.92 ppm (t, J = 7.2 Hz, 3H, methyl); ^{13}C{^{1}H} NMR (100 MHz, DMSO-*d*$_6$, 298 K): δ = 196.4, 131.5, 122.5, 42.8, 31.9, 30.8, 19.4, 13.5, 10.9 ppm; IR(ATR, neat) 2956, 2933, 2864, 1664, 1639, 1415, 1384, 1365, 1342, 1155, 593 cm^{-1}; HRMS(ESI): m/z calcd for $C_{14}H_{21}NO_2Na^+$: 258.1465 $[M+Na]^+$; found: 258.1459; elemental analysis calcd (%) for $C_{14}H_{21}NO_2$: C, 71.44; H, 9.00; N, 5.95; found: C, 71.38; H, 9.04; N, 5.93.

· Synthesis of compound **3**

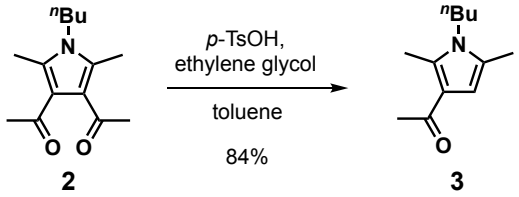

In a 300 mL round bottom flask equipped with a refluxing condenser, compound **2** (4.71 g, 20.0 mmol), ethylene glycol (1.12 mL, 20.0 mmol), *p*-toluenesulfonic acid monohydrate (0.38 g, 2.0 mmol) were dissolved in 100 mL of toluene. After refluxing the mixture for 1 h, the reaction solution was cooled to room temperature. The reaction solution was poured into a saturated aqueous $NaHCO_3$ solution (100 mL), and the organic layer was then separated. The aqueous layer was extracted with dichloromethane (50 mL × 2), and the combined organic layer was dried over anhydrous Na_2SO_4. After the removal of the solvent by rotary evaporator, the crude product was chromatographed on a silica gel column (diameter: 5.5 cm, height: 11 cm, eluent: ethyl acetate/hexane = 1:2) to give compound **3** (3.23 g, 16.7 mmol) in 84% yield as a pale yellow solid.

R_f = 0.46 (silica gel: ethyl acetate/hexane = 1:2), m.p.: 46-48 ºC; ^{1}H NMR (400 MHz, DMSO-d_6, 298 K): δ = 6.20 (s, 1H, pyrrole), 3.77 (t, J = 7.2 Hz, 2H, methylene), 2.44 (s, 3H, methyl), 2.22 (s, 3H, methyl), 2.17 (s, 3H, methyl), 1.51 (quint, J = 7.5 Hz, 2H, methylene), 1.30 (sext, J = 7.4 Hz, 2H, methylene), 0.90 ppm (t, J = 7.2 Hz, 3H, methyl); ^{13}C{^{1}H} NMR (100 MHz, DMSO-d_6, 298 K): δ = 193.3, 133.5, 127.0, 119.3, 108.0, 42.5, 32.0, 28.3, 19.5, 13.6, 11.8, 11.4 ppm; IR(ATR, neat) 2961, 2954, 2871, 1643, 1518, 1417, 1362, 1343, 1232, 1214, 1184, 945, 923, 774, 623 cm^{-1}; HRMS(ESI): *m/z* calcd for $C_{12}H_{19}NONa^+$: 216.1359 $[M+Na]^+$; found: 216.1356; elemental analysis calcd (%) for $C_{12}H_{19}NO$: C, 74.57; H, 9.91; N, 7.25; found: C, 74.62; H, 9.95; N, 7.23.

· Synthesis of compound **4**

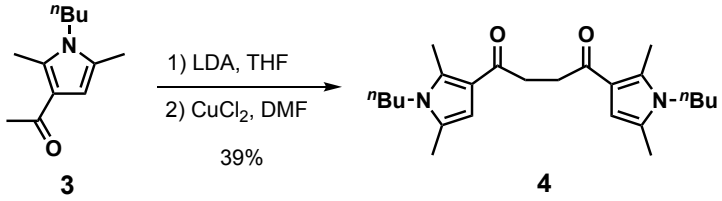

3 **4**

Compound **3** (1.74 g, 9.00 mmol) was added into a dropping funnel that equipped on a 200 mL three-neck flask. After the flask was cooled to −78ºC with N_2 atmosphere, lithium diisopropylamide (LDA) solution (2M, 5.80 mL, 11.7 mmol) was added. Then anhydrous THF (15 mL) was added into the dropping funnel and the result solution of **3** was slowly added into flask over 15 min. After stirring for 15 min, a solution of $CuCl_2$ (2.42 g, 18.0 mmol) in anhydrous DMF (40 mL) was added all at once. The reaction mixture was stirred for 1.5 h while kept the temperature at –78 ºC. The mixture was quenched by saturated NH_4Cl aqueous solution (90 mL) after warming to room temperature and extracted by ether (90 mL × 3). The combined ether layer was washed by water (90 mL) and dried over Na_2SO_4, then concentrated by rotary evaporation to provide the residue. The crude was chromatographed by a silica gel column (diameter: 4 cm, height: 15 cm, eluent: ethyl acetate/hexane = 1:3) to give compound **4** (0.67 g, 1.7 mmol) in 39% as pale yellow solid.

R_f = 0.29 (silica gel: ethyl acetate/hexane = 1:3), m.p.: 136-139ºC; ^{1}H NMR (400 MHz, $CDCl_3$, 298 K): δ = 6.31 (s, 2H, pyrrole), 3.74 (t, J = 7.6 Hz, 4H, methylene), 3.11 (s, 4H, ethylene), 2.54 (s, 6H, methyl), 2.20 (s, 6H, methyl), 1.36 (sext, J = 7.5 Hz, 4H, methylene), 0.96 ppm (t, J = 7.2 Hz, 6H, methyl), one methylene peak was overlapped with water peak; ^{1}H NMR (400 MHz, DMSO-d_6, 298 K): δ = 6.26 (s, 2H, pyrrole), 3.78 (t, J = 7.8 Hz, 4H, methylene), 2.90 (s, 4H, ethylene), 2.44 (s, 6H, methyl), 2.18 (s, 6H, methyl), 1.52 (m, 4H, methylene), 1.31 (sext, J = 7.4 Hz, 4H, methylene), 0.91 ppm (t, J = 7.4 Hz, 6H, methyl); ^{13}C{^{1}H} NMR (100 MHz, $CDCl_3$, 298 K): δ = 196.3, 134.7, 127.3, 119.6, 107.9, 43.3, 34.8, 32.7, 20.2, 13.9, 12.4, 12.0 ppm; IR(ATR, neat) 2967, 2918, 2872, 2856, 1635, 1519, 1417, 1361, 774, 418 cm^{-1}; HRMS(ESI): *m/z* calcd for $C_{24}H_{36}N_2O_2Na^+$: 407.2669 $[M+Na]^+$; found: 407.2657; elemental analysis calcd (%) for $C_{24}H_{36}N_2O_2$: C, 74.96; H, 9.44; N, 7.28; found: C, 75.12; H, 9.48; N, 7.24; UV-Vis (MeCN): λ_{max} (ε) = 212 (3.0×10^4), 250 (2.1×10^4), 285 nm (1.6×10^4 L mol^{-1} cm^{-1}).

· Synthesis of compound **5**

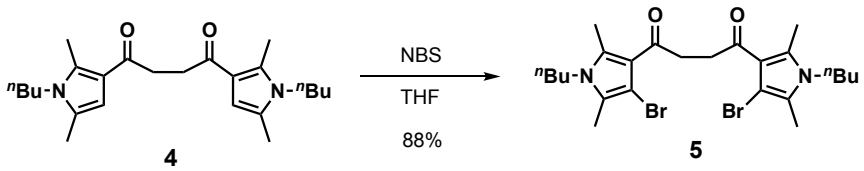

4 **5**

Compound **4** (461 mg, 1.20 mmol) was added to a 50 mL round bottom flask and dissolved in 12 mL THF (with 0.03% stabilizer). Then, a solution of 428 mg N-bromosuccinimide (NBS) (2.40 mmol) in 12 mL THF (with 0.03% stabilizer) was added dropwise. After keeping stirring 15 min, the solvent was removed by rotary evaporation. The residue was ultrasonic dispersed in EtOH (2.4 mL) and filtered. The result solid was washed by EtOH (1 mL) and water (10 mL) to provide compound **5** as pale solid (569 mg, 1.05 mmol) in 88% yield.

^{1}H NMR (400 MHz, $CDCl_3$, 298 K): δ = 3.78 (t, J = 7.8 Hz, 4H, methylene), 3.38 (s, 4H, ethylene), 2.48 (s, 6H, methyl), 2.23 (s, 6H, methyl), 1.36 (sext, J = 7.5 Hz, 4H, methylene), 0.96 ppm(t, J = 7.2 Hz, 6H, methyl), one methylene peak was overlapped with water peak; ^{1}H NMR (400 MHz, acetone-d_6, 298 K): δ = 3.92 (t, J = 7.8 Hz, 4H, methylene), 3.27 (s, 4H, ethylene), 2.44 (s, 6H, methyl), 2.25 (s, 6H, methyl), 1.62 (m, 4H, methylene), 1.39 (sext, J = 7.4 Hz, 4H, methylene), 0.95 ppm (t, J = 7.2 Hz, 6H, methyl); ^{13}C{^{1}H} NMR (100 MHz, $CDCl_3$, 298 K): δ = 196.2, 134.9, 126.4, 119.9, 94.8, 44.3, 37.2, 32.7, 20.1, 13.9, 12.5, 11.3 ppm; IR(ATR, neat) 2953, 2931, 2863, 1638, 1499, 1412, 1392, 1193, 968, 424 cm^{-1}; HRMS(ESI): *m/z* calcd for $C_{24}H_{34}Br_2N_2O_2Na^+$: 565.0859 [M+Na]$^+$; found: 565.0850; elemental analysis calcd (%) for $C_{24}H_{34}Br_2N_2O_2$: C, 53.15; H, 6.32; N, 5.17; found: C, 53.17; H, 6.30; N, 5.04; UV-Vis (MeCN): λ_{max} (ε) = 212 (2.5 × 10^4), 254 (1.8 × 10^4), 279 nm (1.2 × 10^4 L mol^{-1} cm^{-1}).

· Synthesis of compound **6**

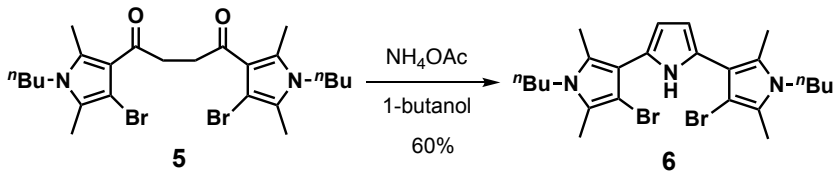

5 **6**

To a 100 mL Schlenk flask with flat stopper, compound **5** (864 mg, 1.60 mmol), NH_4OAc (2.47g, 32.0 mmol) and 1-butanol (27 mL) were added. Heating the flask to 105 °C then closed the switch and kept 90 min. The solution was cooled to room temperature and washed by 120 mL saturated $NaHCO_3$ aqueous solution. The organic layer was separated and extracted the aqueous layer by dichloromethane (40 mL × 2). The combined organic layer was dried over Na_2SO_4 and followed by rotary evaporation to obtain the concentrated residue. After a silica gel column chromatograph (diameter: 3 cm, height: 10 cm, eluent: dichloromethane/hexane = 1:2), compound **6** (500 mg, 0.955 mmol) in 60% yield as a colorless solid.

R_f = 0.35 (silica gel: dichloromethane/hexane = 1:2); ^{1}H NMR (400 MHz, $CDCl_3$, 298 K): δ = 8.88 (br, 1H, pyrrole), 6.19 (d, J = 2.0 Hz, 2H, pyrrole), 3.79 (t, J = 7.8 Hz, 4H, methylene), 2.36 (s, 6H, methyl), 2.25 (s, 6H, methyl), 1.61 (m, 4H, methylene), 1.38 (sext, J = 7.4 Hz, 4H, methylene), 0.97 ppm (t, J = 7.4 Hz, 6H, methyl); ^{13}C{^{1}H} NMR (100 MHz, $CDCl_3$, 298 K): δ = 125.00, 124.98, 124.5, 112.6, 107.4, 93.8, 44.7, 33.2, 20.2, 14.0, 11.6, 11.1 ppm; IR(ATR, neat) 3442, 2956, 2926, 2861, 1337, 1046, 762, 527 cm^{-1}; HRMS(ESI): *m/z* calcd for $C_{24}H_{32}Br_2N_3^-$: 522.0948 [M–H]$^-$; found: 522.0960; elemental analysis calcd (%) for $C_{24}H_{33}Br_2N_3$: C, 55.08; H, 6.36; N, 8.03; found: C, 55.02; H, 6.35; N, 7.89; UV-Vis (MeCN): λ_{max} (ε) = 278 nm (1.8 × 10^4 L mol^{-1} cm^{-1}).

· Synthesis of compound **7**

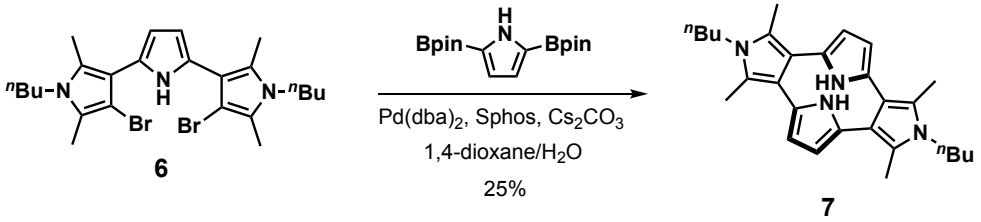

To a 50 mL 2-necked flask equipped with a reflux condenser, compound **6** (418 mg, 0.80 mmol), 2,5-bis(4,4,5,5-tetramethyl-1,3,2-dioxaborolan-2-yl)-1H-pyrrole[11] (281 mg, 0.88 mmol), bis(dibenzylideneacetone)palladium(0) ($Pd(dba)_2$) (46 mg, 0.080 mmol), dicyclohexyl(2',6'-dimethoxy[1,1'-biphenyl]-2-yl)phosphane (Sphos) (66 mg, 0.16 mmol), 1.56 g Cs_2CO_3 (4.80 mmol) were added. Fill the flask with N_2 then added degassed 1,4-dioxane (2.67 mL) and water (130 μL) into the flask by syringe. The mixture was heated to 100 °C for 90 min then remove the solvent under reduced pressure. Added 25 mL water into the flask and extracted the aqueous layer by dichloromethane (20 mL × 3). The combined dichloromethane layer was dried over Na_2SO_4 followed rotary evaporation to provide the crude. The crude was chromatographed on a silica gel column (diameter: 3 cm, height: 19 cm, eluent: dichloromethane/hexane = 2:1) to give compound **7** (87 mg, 0.20 mmol) in 25% yield as colorless solid.

R_f = 0.70 (silica gel: dichloromethane/hexane = 2:1); ^{1}H NMR (400 MHz, $CDCl_3$, 298 K): δ = 6.34 (br, 2H, pyrrole), 6.21 (d, J = 2.0 Hz, 4H, pyrrole), 3.77 (m, 4H, methylene), 2.40 (s, 12H, methyl), 1.69 (quint, J = 7.5 Hz, 4H, methylene), 1.44 (sext, J = 7.4 Hz, 4H, methylene), 1.00 ppm (t, J = 7.4 Hz, 6H, methyl); ^{13}C{^{1}H} NMR (100 MHz, $CDCl_3$, 298 K): δ = 130.1, 122.9, 116.5, 113.5, 44.0, 33.4, 20.4, 14.0, 10.9 ppm; IR(ATR, neat) 3422, 2950, 2925, 2864, 1595, 1473, 1403, 1031, 762 cm^{-1}; HRMS(ESI): *m/z* calcd for $C_{28}H_{36}N_4Na^+$: 451.2833 [M+Na]$^+$; found: 451.2822; UV-Vis (MeCN): λ_{max} (ε) = 276 nm (4.3×10^4 L mol^{-1} cm^{-1}).

· Synthesis of compound **8**

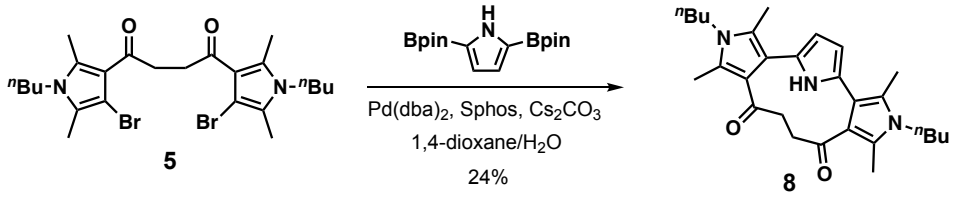

To a 50 mL 2-necked flask equipped with a reflux condenser, compound **5** (245 mg, 0.450 mmol), 2,5-bis(4,4,5,5-tetramethyl-1,3,2-dioxaborolan-2-yl)-1H-pyrrole[11] (156 mg, 0.490 mmol), bis(dibenzylideneacetone)palladium(0) ($Pd(dba)_2$) (26 mg, 0.045 mmol), dicyclohexyl(2',6'-dimethoxy[1,1'-biphenyl]-2-yl)phosphane (Sphos) (37 mg, 0.090 mmol), Cs_2CO_3 (880 mg, 2.70 mmol) were added. Fill the flask with N_2 atmosphere then added degassed 1,4-dioxane (1.5 mL) and water (75 µL). The mixture was heated to 100 °C for 1 h, then remove the solvent under reduced pressure. Added 10 mL water into the flask and extracted by dichloromethane (10 mL × 3). The combined dichloromethane layer provided the crude after drying by Na_2SO_4 and rotary evaporation. The crude was chromatographed on a silica gel column (diameter: 3 cm, height: 15 cm, eluent: ethyl acetate/hexane = 2:3) to provide a fraction (R_f = 0.21). From this fraction, compound **8** (48 mg, 0.107 mmol, 24%) was obtained as grey powder by recrystallization in MeOH (7.5 mL).

R_f = 0.21 (silica gel: ethyl acetate/hexane = 2:3); ^{1}H NMR (400 MHz, $CDCl_3$, 298 K): δ = 8.15 (br, 1H, pyrrole), 6.09 (d, J = 2.8 Hz, 2H, pyrrole), 3.79 (t, J = 8.0 Hz, 4H, methylene), 2.40 (s, 6H, methyl), 2.35 (s, 4H, ethylene), 2.34 (s, 6H, methyl), 1.41 (sext, J = 7.4Hz, 4H, methylene), 0.98 ppm (t, J = 7.4Hz, 6H, methyl), one methylene peak was overlapped with water peak; ^{1}H NMR (400 MHz, acetone-d_6, 328 K): δ = 9.81 (br, 1H, pyrrole), 6.00 (d, J = 2.0 Hz, 2H, pyrrole), 3.91 (t, J = 7.8 Hz, 4H, methylene), 2.39 (s, 6H, methyl), 2.34 (s, 6H, methyl), 2.25 (s, 4H, ethylene), 1.68 (m, 4H, methylene), 1.45 (sext, J = 7.4Hz, 4H, methylene), 1.00 ppm (t, J = 7.4Hz, 6H, methyl); ^{13}C{^{1}H} NMR (100 MHz, $CDCl_3$, 298 K): δ = 199.8, 134.4, 125.4, 125.3, 123.4, 112.5, 110.8, 43.8, 40.1, 32.8, 20.3, 13.9, 11.7, 10.6 ppm; IR(ATR, neat) 3338, 2957, 2929, 2869, 1646, 1606, 1508, 1407, 784, 769 cm^{-1}; HRMS(ESI): *m/z* calcd for $C_{28}H_{37}N_3O_2Na^+$: 470.2778 $[M+Na]^+$; found:

470.2768; elemental analysis calcd (%) for $C_{28}H_{37}N_3O_2$: C, 75.13; H, 8.33; N, 9.39; found: C, 74.96; H, 8.39; N, 9.30; UV-Vis (MeCN): λ_{max} (ε) = 241 nm (2.6×10^4 L mol^{-1} cm^{-1}).

· Attempt of Paal-Knorr pyrrole synthesis of compound **8**

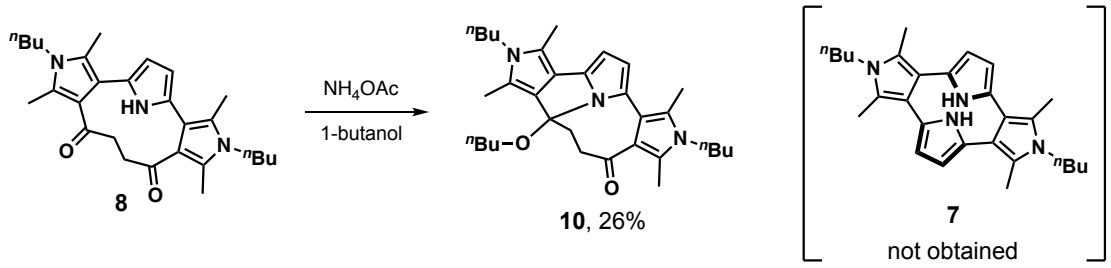

In a 10 mL Schlenk flask with flat stopper, compound **8** (48.0 mg, 0.100 mmol), NH_4OAc (154 mg, 2.00 mmol) and 1-butanol (1.70 mL) were added. Heating the flask to 115 °C then closed the switch and kept 6 h. Meanwhile, compound **8** was slowly consumed and generated a new compound during the process, but not completely consumed after 6 h. The solution was cooled to room temperature and washed by 100 mL saturated $NaHCO_3$ aqueous solution. The organic layer was separated and extracted the aqueous layer by dichloromethane (5 mL × 3). The combined organic layer was dried over Na_2SO_4 and followed by rotary evaporation to obtain the concentrated residue. After a silica gel column chromatograph (diameter: 2 cm, height: 13 cm, eluent: ethyl acetate/hexane = 2:3), compound **10** (13.0 mg, 0.0258 mmol, 26%) was obtained as yellow oil.

R_f=0.61 (silica gel: ethyl acetate/hexane = 2:3); ^{1}H NMR (400 MHz, $CDCl_3$, 298 K): δ = 6.14 (d, J = 3.2 Hz, 1H, pyrrole), 6.00 (d, J = 3.6 Hz, 1H, pyrrole), 3.86-3.75 (m, 2H, methylene), 3.67 (t, J = 7.4 Hz, 2H, methylene), 3.18-3.10 (m, 1H, ethylene), 3.07-3.02 (m, 1H, ethylene), 2.89-2.81 (m, 1H, ethylene), 2.67-2.61 (m, 1H, ethylene), 2.59 (s, 3H, methyl), 2.30 (s, 6H, methyl), 2.21-2.16 (m, 2H, methylene), 2.14 (s, 3H, methyl), 1.45-1.31 (m, 6H, methylene), 0.99-0.92 (m, 6H, methyl), 0.59 ppm (t, J = 7.0 Hz, 3H, methyl), one methylene peak overlap with water peak; ^{13}C{^{1}H} NMR (100 MHz, $CDCl_3$, 298 K): δ=199.0, 133.8, 132.5, 127.8, 125.4, 124.9, 120.1, 119.7, 115.8, 115.7, 113.6, 112.0, 95.9, 95.2, 63.6, 43.5, 41.8, 37.6, 33.3, 32.9, 31.5, 20.3, 20.2, 19.0, 14.0, 13.94, 13.92, 11.9, 11.8, 11.4, 10.4 ppm, one pyrrolic carbon peak may overlapped; HRMS(ESI): *m/z* calcd for $C_{32}H_{45}N_3O_2Na^+$: 526.3404 $[M+Na]^+$; found: 526.3394.

4.6.3 Single Crystal X-ray Diffraction Analysis

· Crystallographic data for compound **7**

Single crystals suitable for X-ray diffraction analysis were grown by vapor diffusion of hexane into a dichloromethane solution of compound **7**.

$C_{28}H_{36}N_4$, M = 428.61, crystal size: 0.50 × 0.15 × 0.04 mm^3, triclinic, space group P-1, a = 9.0906(8), b = 9.1054(5), c = 9.2735(5) Å, α = 62.149(6), β = 61.589(7), γ = 65.472(7)º, V = 578.30(9) Å^3, Z = 1, T = 123(2) K, μ = 0.073 mm^{-1}, D_{calc} = 1.231 g/cm^3, 2.612 ≤ θ ≤ 26.999°, 2268 unique reflections out of 2469 with I > 2σ(*I*), GOF = 1.039, R_1 = 0.0407 and wR_2 = 0.1035 for all data. CCDC deposit number: 2382889.

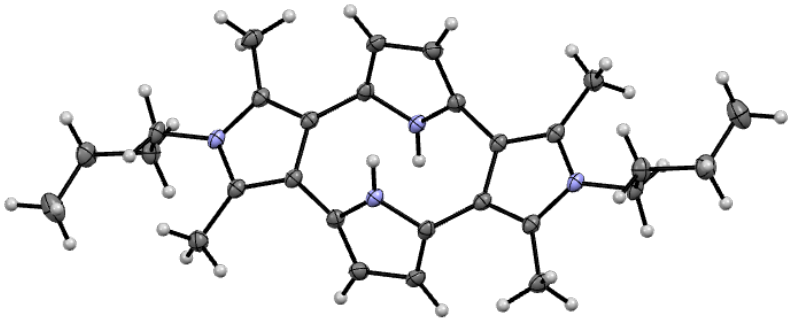

Figure 4-13. ORTEP drawing of crystal structure of compound **7** at the 50% thermal probability level.

· Crystallographic data for compound **8**

Single crystals suitable for X-ray diffraction analysis were grown by vapor diffusion of hexane into a chloroform solution of compound **8**.

$C_{28}H_{37}N_3O_2$, M = 447.60, crystal size: 0.68 × 0.35 × 0.22 mm^3, monoclinic, space group $P2_1/n$, a = 12.8130(5), b = 13.3344(5), c = 14.2787(6) Å, α = 90, β = 91.632(4), γ = 90º, V = 2438.58(17) Å^3, Z = 4, T = 123(2) K, μ = 0.077 mm^{-1}, D_{calc} = 1.219 g/cm^3, 2.090 ≤ θ ≤ 27.498, 4750 unique reflections out of 5478 with I > 2σ(I), GOF = 1.004, R_1 = 0.0419 and wR_2 = 0.1063 for all data, CCDC deposit number: 2382890.

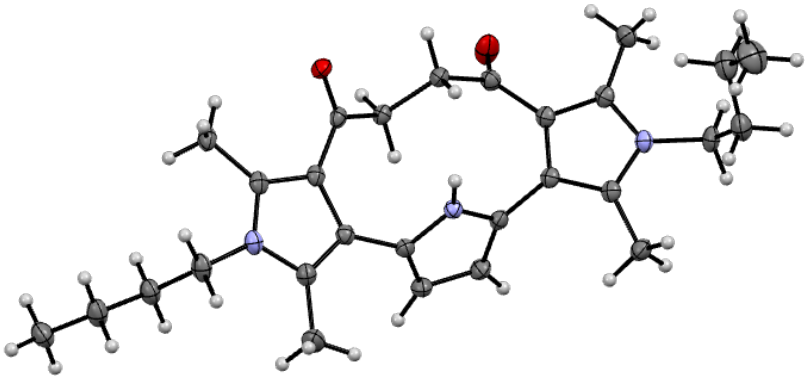

Figure 4-14. ORTEP drawing of crystal structure of compound **8** at the 50% thermal probability level.

4.6.4 StrainViz analysis

Geometry optimization and vibration analysis of the three compounds (**7**, **8**, and **9**) were performed by the global reaction route mapping (GRRM) program[18]. The initial structures were prepared from the crystal structures. The vibrational frequencies were computed to confirm whether the optimized geometry corresponded to stationary or saddle points on potential energy surface. The density functional theory (DFT) calculations were carried out at the M06-2X[15]/6-311+G(2d,p) level of theory implemented in the Gaussian 16 program[19]. Strains of each macrocycle were computed by the StrainViz program[14] at the same DFT level of theory as the geometry optimization calculations. The DFT structure was divided into four fragments with same manner to evaluate four types of strain (total, bond, angle, and dihedral). The strain representation was visualized by the visual molecular dynamics (VMD) software[20]. The fragments prepared for StrainViz and the corresponding energy changes are shown in **Figure 4-15**, **4-16**, **4-17**.

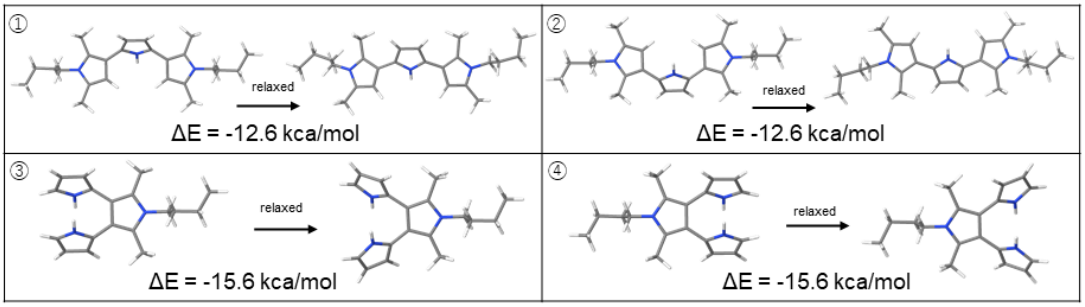

Figure 4-15. Fragments for StrainViz analysis of compound **7**.

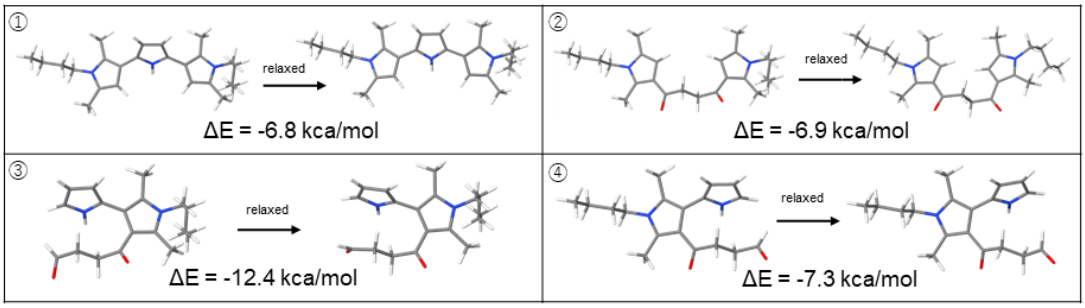

Figure 4-16. Fragments for StrainViz analysis of compound **8**.

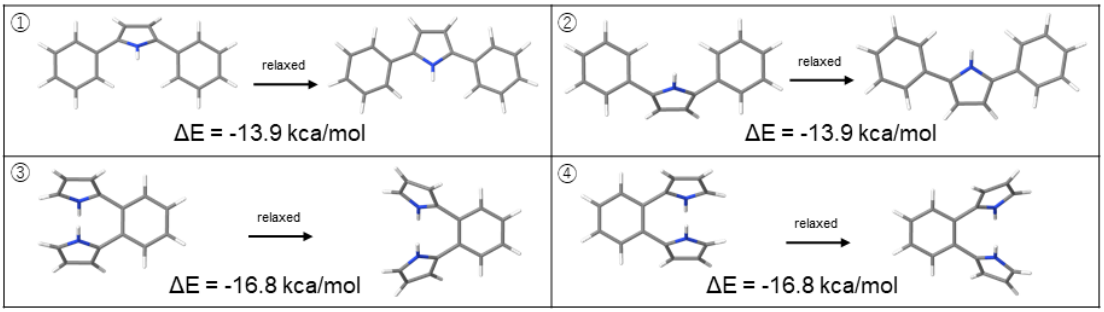

Figure 4-17. Fragments for StrainViz analysis of compound **9**.

4.6.5 Other DFT analysis

All calculations were carried out using the Gaussian 16 program[19]. The calculations were performed by the density functional theory (DFT) method with the indicated functional (B3LYP, ωB97XD, or CAM-B3LYP), employing a basis set 6-311G(d) for C, H, and N. SMD solvation model with CH_2Cl_2 as a continuum description of the solvent was applied for the relative energy comparison and simulation of the UV/Vis spectra via time-dependent DFT method. All structures were fully optimized without any symmetry restriction. Calculated frequencies were used to verify the nature of all stationary points as minima (no imaginary frequencies). The NICS values were obtained with the GIAO method. The ring centers for the NICS values were designated at the nonweighted means of the carbon and nitrogen coordinates[21]. The anisotropy of the induced current density (ACID) calculation was conducted with the CSGT method, in which the external magnetic field was applied in the direction from the back of the paper to the surface[22].

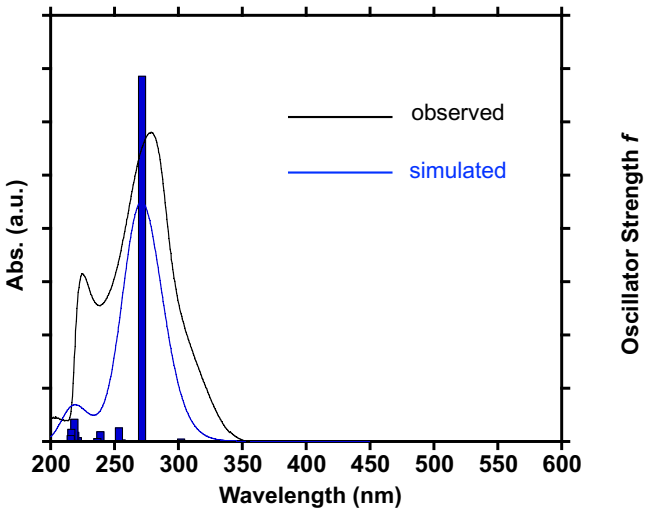

Figure 4-18. Calculated UV/Vis absorption spectra of **7** at B3LYP/6-311G(d,p) level.

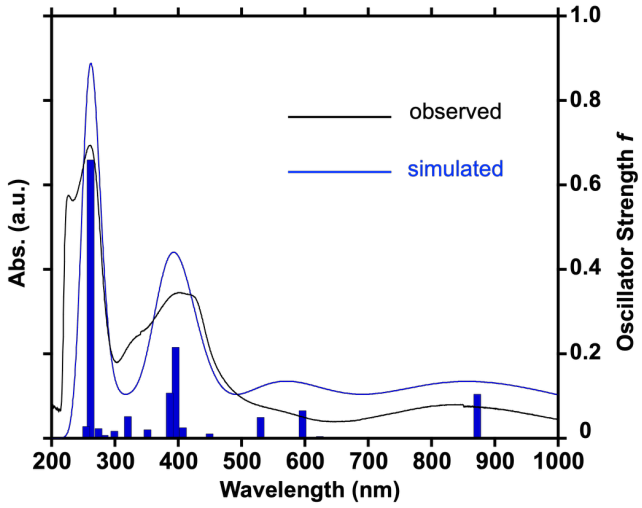

Figure 4-19. Calculated UV/Vis absorption spectra of $\mathbf{7}^{\bullet+}$ at UB3LYP/6-311G(d,p) level.

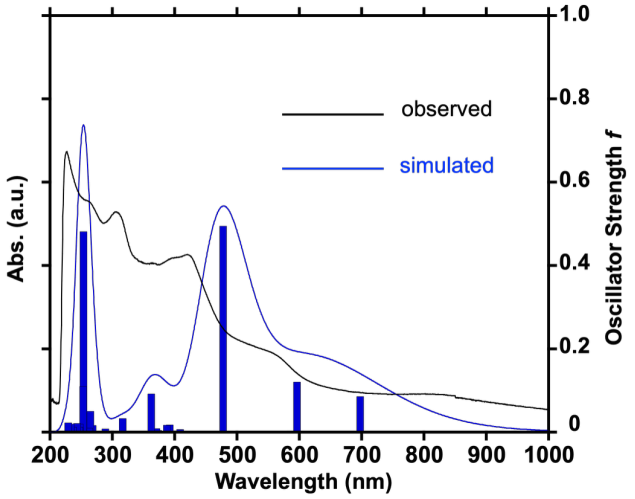

Figure 4-20. Calculated UV/Vis absorption spectra of closed-shell $\mathbf{7}^{2+}$ at RB3LYP/6-311G(d,p) level.

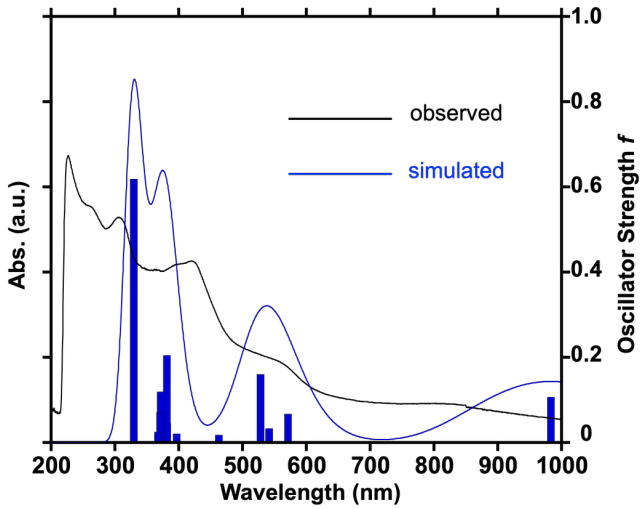

Figure 4-21. Calculated UV/Vis absorption spectra of open-shell triplet $\mathbf{7}^{2+}$ at UB3LYP/6-311G(d,p) level.

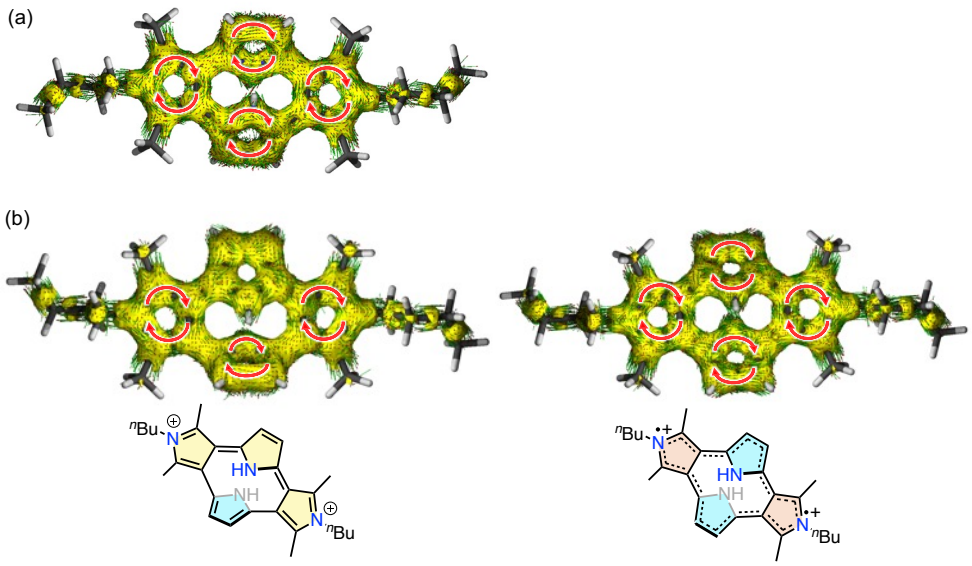

Figure 4-22. ACID isosurfaces for (a) **7** and (b) $\mathbf{7}^{2+}$ (left: closed-shell, right: open-shell triplet). Isosurface value: 0.05.

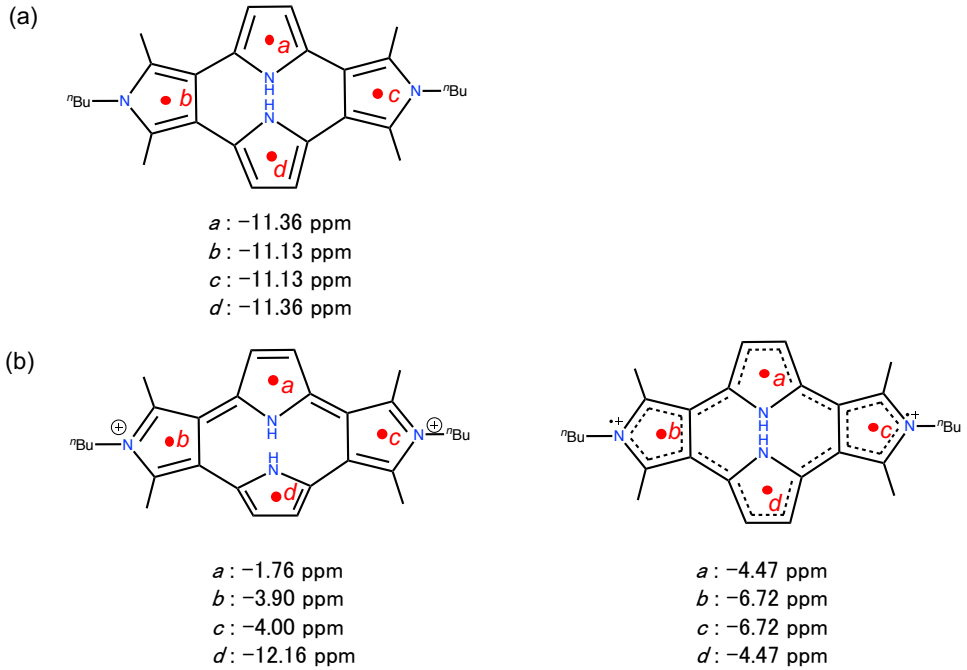

Figure 4-23. NICS(0) values for (a) **7** and (b) $\mathbf{7}^{2+}$ (left: closed-shell, right: open-shell triplet).

4.7 Reference

[1] Seidel, D.; Lynch, V.; Sessler, J. L. Cyclo[8]pyrrole: A Simple-to-Make Expanded Porphyrin with No Meso Bridges. *Angew. Chem. Int. Ed*. **2002**, *41*, 1422-1425.

[2] Köhler, T.; Seidel, D.; Lynch, V.; Arp, F. O.; Ou, Z.; Kadish, K. M.; Sessler, J. L. Formation and Properties of Cyclo[6]pyrrole and Cyclo[7]pyrrole. *J. Am. Chem. Soc*. **2003**, *125*, 6872-6873.

[3] Okujima, T.; Ando, C.; Agrawal, S.; Matsumoto, H.; Mori, S.; Ohara, K.; Hisaki, I.; Nakae, T.; Takase, M.; Uno, H.; Kobayashi, N. Template Synthesis of Decaphyrin without Meso-Bridges: Cyclo[10]pyrrole. *J. Am. Chem. Soc*. **2016**, *138*, 7540-7543.

[4] Matsumoto, H.; Okujima, T.; Mori, S.; Bacilla, A. C. C.; Takase, M; Uno, H.; Kobayashi, N. Cyclo[9]pyrrole: Selective Synthesis of [34]Nonaphyrin(0.0.0.0.0.0.0.0.0). *Org. Lett*. **2021**, *23*, 3442-3446.

[5] Sessler, J. L.; Weghorn, S. J.; Hiseada, Y.; Lynch, V. Hexaalkyl Terpyrrole: A New Building Block for the Preparation of Expanded Porphyrins. *Chem. Eur. J*. **1995**, *1*, 56-67.

[6] Ito, T.; Hayashi, Y.; Shimizu, S.; Shin, J.; Kobayashi, N.; Shinokubo, H. Gram-Scale Synthesis of Nickel(II) Norcorrole: The Smallest Antiaromatic Porphyrinoid. *Angew. Chem. Int. Ed*. **2012**, *51*, 8542-8545.

[7] Liu, L.; Kim, J.; Xu, L.; Rao, Y.; Zhou, M.; Yin, B.; Oh, J.; Kim, D.; Osuka, A.; Song, J. Synthesis of Subporphyrin Free Bases. *Angew. Chem. Int. Ed*. **2022**, *61*, e202214342.

[8] Charles, R. G. Tetraacetylethane. *Org. Synth*. **1959**, *39* , 61.

[9] (a) Smith, K. M.; Miura, M; Tabba, H. D. Deacylation and Deformylation of Pyrroles. *J. Org. Chem*. **1983**, *48*, 4779-4781. (b) Moon, M. W.; Wade, R. A. Deacylation of Pyrrole and Other Aromatic Ketones. *J. Org. Chem*. **1984**, *49*, 2663-2669.

[10] Pindur, U.; Flo, C. First Reactions of Dialkoxycarbenium Tetrafluoroborates with Pyrroles, 5H-dibenz[b,f]azepines, and Electron-rich arenes. *J. Heterocycl. Chem*. **1989**, *26*, 1563-1568.

[11] Hoque, M. E.; Bisht, R.; Haldar, C.; Chattopadhyay, B. Noncovalent Interactions in Ir-Catalyzed C-H Activation: L-Shaped Ligand for Para-Selective Borylation of Aromatic Esters. *J. Am. Chem. Soc*. **2017**, *139*, 7745-7748.

[12] Morimoto, Y.; Koo, Y. H.; Otsubo, K.; Kitakado, H.; Seki, S.; Osuka, A.; Tanaka, T. Dibenzodiazapyracylenes: Doubly N-Doped Cyclopenta-Fused Polycyclic

Molecules That Exhibit High Carrier Mobility. *Angew. Chem. Int. Ed*. **2022**, *61*, e202200341.

[13] Inaba, Y.; Nomata, Y.; Ide, Y.; Pirillo, J.; Hijikata Y.; Yoneda, T.; Osuka, A.; Sessler, J. L.; Inokuma, Y. Calix[3]pyrrole: A Missing Link in Porphyrin-Related Chemistry. *J. Am. Chem. Soc*. **2021**, *143*, 12355-12360.

[14] Colwell, C. E.; Price, T. W.; Stauch, T.; Jasti, R. Strain Visualization for Strained Macrocycles. *Chem. Sci*. **2020**, *11*, 3923-3930.

[15] Zhao,Y.; Truhlar, D. G. The M06 Suite of Density Functionals for Main Group Thermochemistry, Thermochemical kinetics, Noncovalent Interactions, Excited States, and Transition Elements: Two New Functionals and Systematic Testing of Four M06-class Functionals and 12 Other Functionals. *Theor. Chem. Acc*. **2008**, *120*, 215-241.

[16] Sheldrick, G. M. SHELXT – Integrated Space-group and Crystal-structure Determination. *Acta Cryst*. **2015**, *A71*, 3-8.

[17] Sheldrick, G. M. Crystal structure refinement with SHELXL. *Acta Cryst*. **2015**, *C71*, 3-8.

[18] https://global.hpc.co.jp/products/grrm23/ (accessed August 26, 2024)

[19] Gaussian 16, Revision C.01, Frisch, M. J.; Trucks, G. W.; Schlegel, H. B.; Scuseria, G. E.; Robb, M. A.; Cheeseman, J. R.; Scalmani, G.; Barone, V.; Petersson, G. A.; Nakatsuji, H.; Li, X.; Caricato, M.; Marenich, A. V.; Bloino, J.; Janesko, B. G.; Gomperts, R.; Mennucci, B.; Hratchian, H. P.; Ortiz, J. V.; Izmaylov, A. F.; Sonnenberg, J. L.; Williams-Young, D.; Ding, F.; Lipparini, F.; Egidi, F.; Goings, J.; Peng, B.; Petrone, A.; Henderson, T.; Ranasinghe, D.; Zakrzewski, V. G.; Gao, J.; Rega, N.; Zheng, G.; Liang, W.; Hada, M.; Ehara, M.; Toyota, K.; Fukuda, R.; Hasegawa, J.; Ishida, M.; Nakajima, T.; Honda, Y.; Kitao, O.; Nakai, H.; Vreven, T.; Throssell, K.; Montgomery, J. A., Jr.; Peralta, J. E.; Ogliaro, F.; Bearpark, M. J.; Heyd, J. J.; Brothers, E. N.; Kudin, K. N.; Staroverov, V. N.; Keith, T. A.; Kobayashi, R.; Normand, J.; Raghavachari, K.; Rendell, A. P.; Burant, J. C.; Iyengar, S. S.; Tomasi, J.; Cossi, M.; Millam, J. M.; Klene, M.; Adamo, C.; Cammi, R.; Ochterski, J. W.; Martin, R. L.; Morokuma, K.; Farkas, O.; Foresman, J. B.; Fox, D. J. Gaussian, Inc., Wallingford CT, 2016.

[20] Visual Molecular Dynamics. https://www.ks.uiuc.edu/Research/vmd/. (accessed August 26, 2024)

[21] (a) Schleyer, P. v. R.; Maerker, C.; Dransfeld, A.; Jiao, H.; Hommes, N. J. R. v. E. Nucleus-Independent Chemical Shifts: A Simple and Efficient Aromaticity Probe. *J. Am. Chem. Soc*. **1996**, *118*, 6317-6318. (b) Chen, Z.; Wannere, C. S.; Corminboeuf, C.; Puchta, R.; Schleyer, P. v. R. Nucleus-Independent Chemical Shifts (NICS) as an Aromaticity Criterion. *Chem. Rev*. **2005**, *105*, 3842-3888.

[22] (a) Herges, R.; Geuenich, D. Delocalization of Electrons in Molecules. *J. Phys. Chem. A* **2001**, *105*, 3214-3220. (b) Geuenich, D.; Hess, K.; Köhler, F.; Herges, R. Anisotropy of the Induced Current Density (ACID), a General Method To Quantify and Visualize Electronic Delocalization. *Chem. Rev*. **2005**, *105*, 3758-3772.

Chapter 5

Promising bipyrrole precursor synthesis for elusive cyclic tetrapyrrole with cyclooctatetraene core

Abstract

In this chapter, another situation of four pyrrole connected directly was considered and for this elusive tetrapyrrole-fused cyclooctatetraene compound, a novel designed synthetic route was proposed the structure was evaluated by calculation in advance. A facile and effective 4-step synthesis was performed toward promising bipyrrole precursor, which laid the foundation for subsequent reactions. And a preliminary attempt for homocoupling of bipyrrole was conducted.

5.1 Introduction

With the successful synthesis of cyclo[4]pyrrole that described in chapter 4, this chapter focus on another situation of four pyrrole connected directly. By changing the linkage, the cyclic tetrapyrrole compound can converse to less strained macrocycle with cyclooctatetraene (COT) skeleton (**Figure 5-1**). The small strain primarily from its ability to release strain energy through a tub-shaped conformation[1].

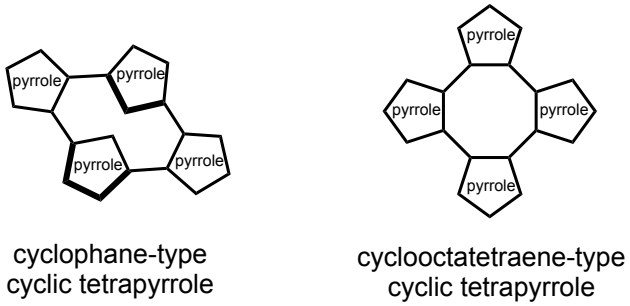

Figure 5-1. Different types of cyclic tetrapyrrole with different linkage mode.

The COT compounds with tetra-fused arenes are important subjects for aromaticity research not only because the intrinsic interesting properties derived from COT core, but also because the better thermal stability and modified electronic structure derived from fused arene[1]. Several types arenes be introduced into COT structure (**Figure 5-2**) such as benzene ring[2], thiophane ring[3], indole ring[4] and thiazole ring[5].

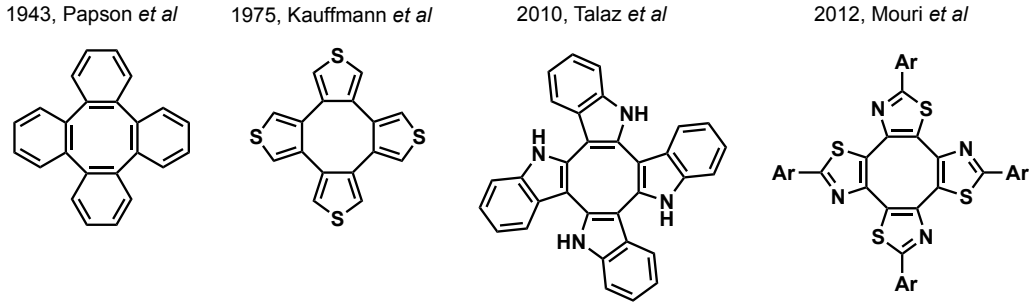

Figure 5-2. Several reported COT core with different fused arenes.

However, in the case of pyrrole, the COT core with tetra-fused pyrrole looks still elusive. To the best knowledge of me, such structure only reported as substructure in parent compounds. For example, the substructure in porphyrin sheet reported by Nakamura *et al*[6]

and the substructure in Tetrabenzotetraaza[8]circulene reported by Chen *et al*[7] (**Figure 5-3**). Obviously, the property of these substructure is highly affected by the parent structure including the resonance patterns and conformational behavior.

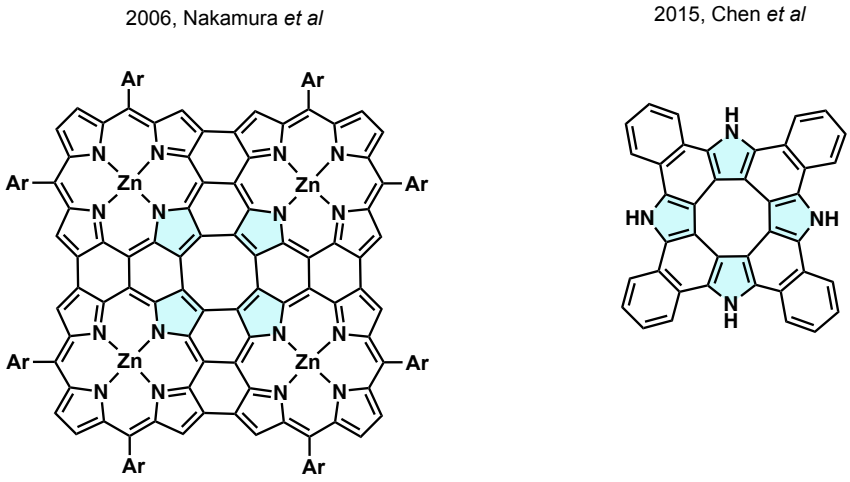

Figure 5-3. The COT core (marked in blue) with tetra-fused pyrrole existed as substructures.

Independent structure of tetrapyrrole fused COT will be an attractive target for investigating the intrinsic property of this type of compound. Here, a multi-step synthetic route was proposed (**Scheme 5-1**) from the compound **1** obtained in chapter 4. This route combining carbonyl chemistry[8], transition metal catalytic reductive coupling[9], and oxidative coupling[9], which all these reactions are common in bond formation between pyrrole rings.

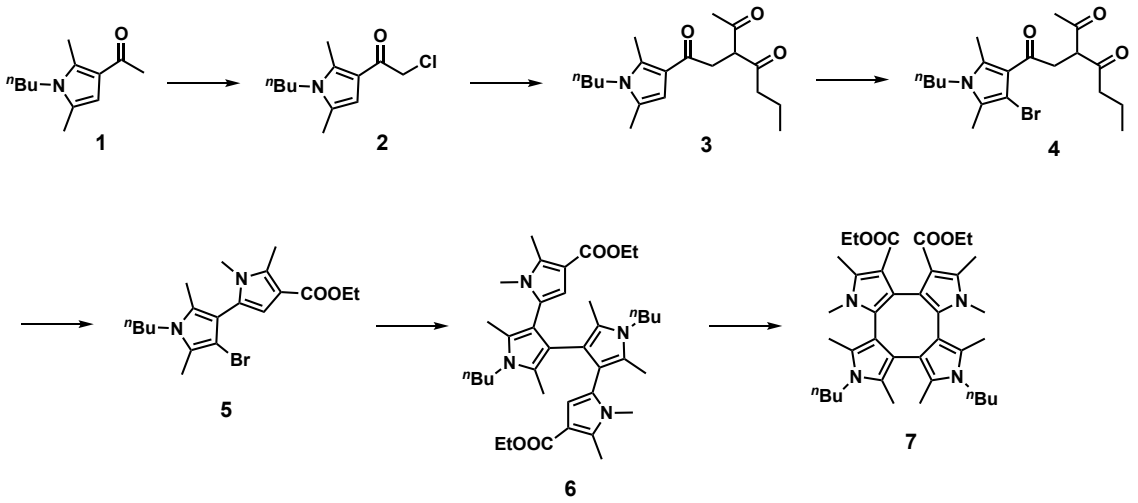

Scheme 5-1. Proposed synthetic route for tetrapyrrole fused COT compound.

The structure and strain state of final target cyclooctatetraene **7** was investigated by calculation in advance (**Figure 5-4**). The typical tub-conformation was confirmed by simulation and small strain energy value suggested by StrainViz method confirmed the strain release compared to the cyclo[4]pyrrole skeleton.

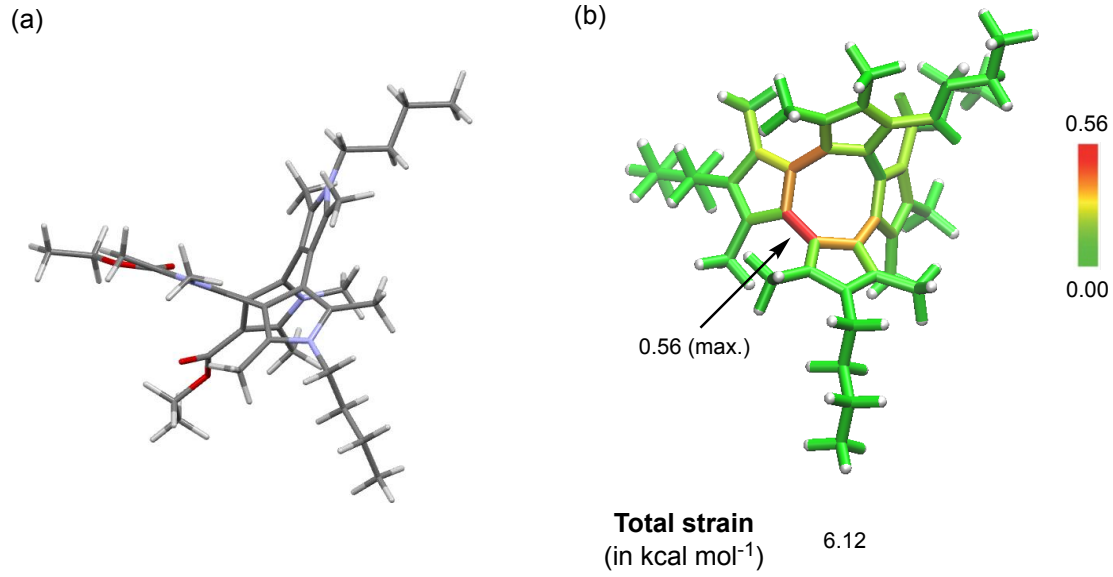

Figure 5-4. (a) Simulated structure of compound **7** at B3LYP/6-31G(d) level; (b) StrainViz analysis of compound **7** at B3LYP/6-31G(d) level.

5.2 Synthesis of bipyrrole precursor

From the compound **1** obtained in chapter 4, a facile 4-step synthesis was conducted as shown in **Scheme 5-2**. The strategy is from aryl α-haloketone substrate to make 1,4-diketone structure by S_N2 reaction with enolate and followed by Paal-Knorr reaction to build biaryl structure. The first step is the key step because the ketone α-halogenation of compound **1** will suffer from side reaction like electrophilic substitution reactions and free radical halogenation reactions[10].

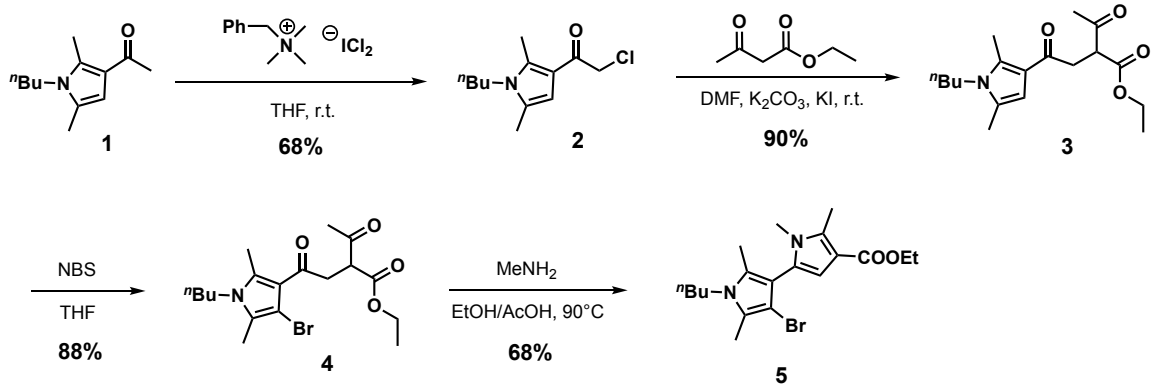

Scheme 5-2. Synthetic route to bipyrrole precursor **5**.

The dichloroiodate reagent was found as suitable halogenation reagent for compound **1**. This iodine-mediated chlorination reaction[11] was mild enough to provide acceptable yield for compound **2**. The followed S_N2 reaction with ethyl acetoacetate was conducted with K_2CO_3 as base and KI as nucleophilic catalyst in DMF and provided an excellent 90% yield to compound **3**. Before Paal-Knorr reaction, brominated the pyrrole β position firstly using the normal condition with *N*-bromosuccinimide (NBS) in THF. Then, treated compound **4** with methylamine in ethanol/acetic acid mix solvent to furnish target bipyrrole **5** with 68% yield.

The structure of bipyrrole precursor **5** is well-designed for the next steps. Firstly, the ester group act as electron-withdrawing group can stabilize the bipyrrole. Then, the nitrogen of pyrrole is capped with alkyl group that can make it tolerance with basic condition in some Cu or Ni catalyst homocoupling reaction for the formation of linear tetrapyrrole **6**. Finally, the remained two free pyrrole-H can be conducted by intramolecular oxidative coupling. Although using transition metal catalyst coupling is

also possible, but this type of response is not efficient in crowded spaces, such as the synthesis of cyclic thiazole reported by Mouri *et al*[5], the final intramolecular cyclization by Pd-catalyst thiazole C-H arylation required 4 days reaction time at 140°C.

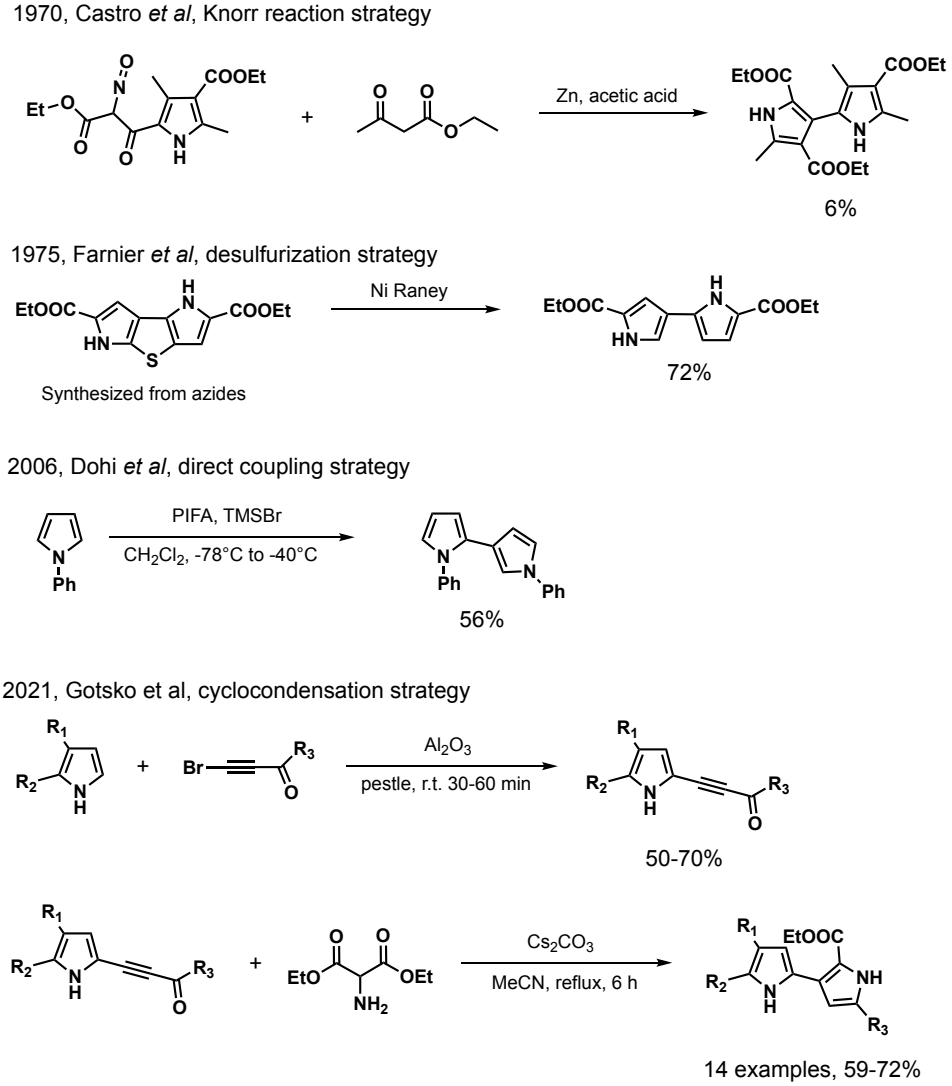

Scheme 5-3. Some representative works for 2,3'-bipyrrole synthesis.

The efficient and facile synthesis of promising precursor **5** laid the foundation for subsequent reactions. In addition, this synthetic strategy also provides a new approach for creating 2,3'-bipyrrole. The synthetic strategy for 2,2'-bipyrrole was well developed[9]

while the synthetic strategy for 2,3'-bipyrrole still rare. Some representative works are summarized in **Scheme 5-3**. Early exploration by Castro *et al*[12] using the Knorr reaction strategy yielded only very low yield. Another early exploration by Farnier *et al*[13] used azide-related reaction for starting material synthesis although the formation of 2,3'-bipyrrole can provide good yield. In 2006, Dohi *et al*[14] reported a sample direct coupling for 2,3'-bipyrrole using phenyliodine bis(trifluoroacetate) (PIFA) with bromotrimethylsilane (TMSBr) while only one example demonstrated. The methodology reported by Gotsko *et al*[15] has wide scope of substrates but the 2-(acylethynyl)pyrroles required a special mechanochemical method.

5.3 Preliminary attempt for homocoupling of bipyrrole

With the brominated bipyrrole **5** in hand, the preliminary attempt for Ullmann reaction was conducted. Because of the steric hindrance of the substrate, this factor was fully considered when selecting the conditions. First, the most conventional high-temperature copper powder condition reported by Nelson *et al*[16] was selected, which has been reported to be effective in synthesizing a series of atropisomer (**Scheme 5-4a**). And another promising homogeneous condition reported by Lin *et al*[17] also be considered that using Ni(0) species as catalyst with NaH for suppressing dehalogenation side reaction (**Scheme 5-4b**). However, in these two conditions, the target homocoupling product was not found.

(a) Nelson *et al*

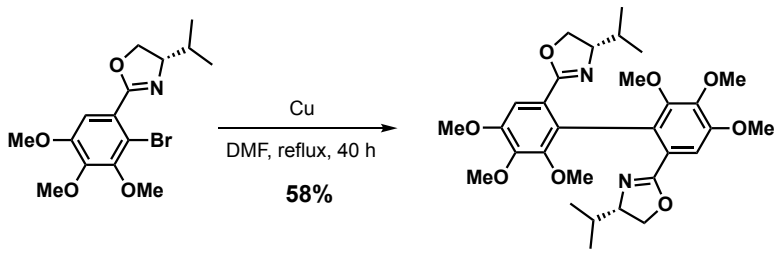

(b) Lin *et al*

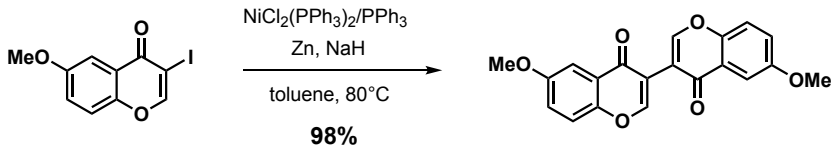

Scheme 5-4. (a) Copper powder condition[16]; (b) Ni(0) condition[17].

For the copper powder condition (**Scheme 5-5a**), the consume of substrate **5** was very slow even the reaction mixture heated up to 170°C. After 8 hours reaction, only some minor unidentified product generated with higher polarity. The second entry was conducted with higher temperature (around 190°C) while the compound **5** rapidly decomposed to some unidentified black product.

For the Ni(0) condition with NaH (**Scheme 5-5b**), the substrate **5** was no consume at 110°C. While just slightly increase temperature to 120°C, two new products will be slowly generated that one has similar polarity with compound **5** and another one has higher

polarity. But the ^{1}H NMR analysis indicated both products have phenyl group that the solvent toluene or the ligand triphenylphosphine looks involved in the reaction.

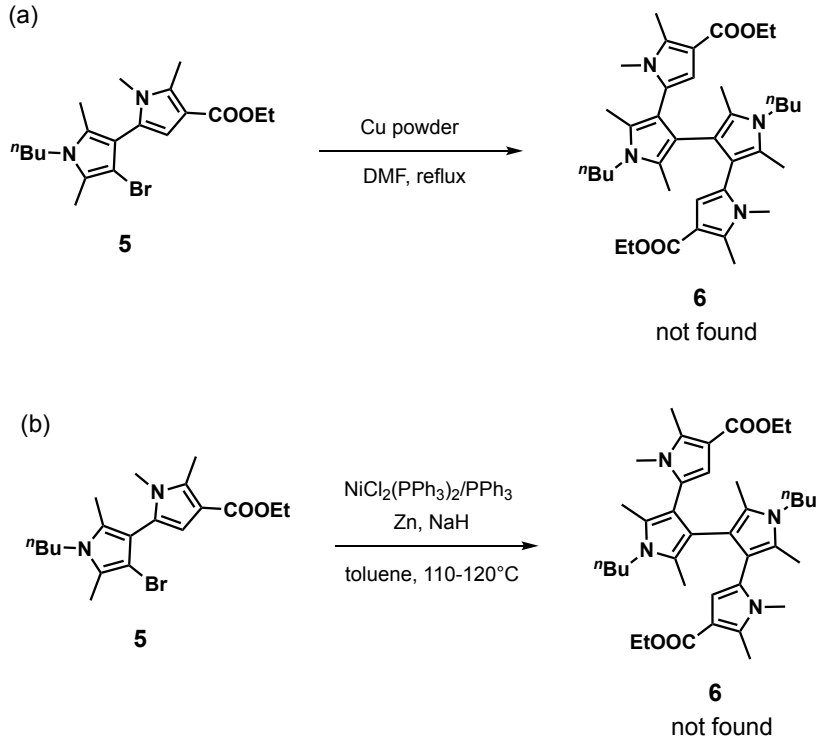

Scheme 5-5. Ullmann reaction for compound **5**. (a) Cu powder condition; (b) Ni(0) condition.

These preliminary explorations suggested that steric hindrance is indeed an important factor affecting homocoupling reactions, as the presence of steric hindrance hinders the oxidative insertion of metal species into carbon-halogen bond. Further improvements to the reaction conditions should include the selection of suitable ligands to lower the energy barrier of the metal oxidation insertion process. In addition, catalytic systems other than copper and nickel, such as palladium-catalyzed reaction conditions, are also worth considering.

5.4 Conclusion

For the elusive tetrapyrrole-fused COT compound, a novel designed synthetic route was proposed and the structure was evaluated by calculation in advance. From the starting material **1**, a facile and effective 4-step synthesis was performed toward promising bipyrrole **5**, among the key α-haloketone formation with dichloroiodate reagent. The efficient and facile synthesis of promising precursor **5** laid the foundation for subsequent reactions and provides a new approach for bipyrrole synthesis. The preliminary explorations about homocoupling of bipyrrole **5** indicated the selection of reaction conditions should fully consider steric hindrance factors.

5.5 Experimental section

5.5.1 General information

Solvents and reagents were purchased from Fujifilm Wako Pure Chemical Industries Ltd., TCI Co., Ltd., Kanto Chemical Co., Inc., or Sigma-Aldrich Co., and used without further purification unless otherwise mentioned. All ^{1}H and ^{13}C NMR spectra were recorded using JEOL JNM-ECS400 spectrometers, and chemical shifts were reported in parts per million (ppm) relative to an internal standard tetramethylsilane ($\delta = 0.00$ ppm for ^{1}H NMR in $CDCl_3$) or a solvent residual peak ($\delta = 77.16$ ppm for ^{13}C NMR in $CDCl_3$. ESI-TOF-MS spectra were recorded on a Thermo Scientific Executive spectrometer.

5.5.2 Calculation analysis

The simulated structure of the target cyclooctatetraene compound is carried out using the Gaussian 16 program[18] at B3LYP/6-31G(d) level. StrainViz analysis was carried out with B3LYP/6-31G(d) level using the open source script[19]. The general process is same as introduced at 3.5 section. The ring strain energy composition suggested by StrainViz are as follows: bond strain: 0.42 kcal mol^{-1}; angle strain: 1.63 kcal mol^{-1}; dihederial strain: 4.07 kcal mol^{-1}; total strain: 6.12 kcal mol^{-1}.

5.5.3 Synthetic procedure

· Synthesis of compound **2**

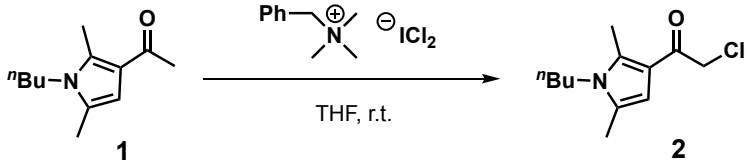

1 2

579 mg (3.00 mmol) of compound **1** was dissolved in 12 mL anhydrous THF in a 50 mL Schlenk flask under N_2. A solution of 2.19 g (6.30 mmol) benzyltrimethylammonium dichloroiodate in 15 mL anhydrous THF was slowly added. After addition, the reaction mixture was stirred at room temperature overnight. Then the mixture was quenched by 10% (w/w) $Na_2S_2O_3$ aqueous solution and extracted by CH_2Cl_2 (50 mL × 2). The combined CH_2Cl_2 layer was dried over Na_2SO_4 and remove the solvent under reduced pressure. The residue was separated by silica gel column (diameter: 4 cm, height: 15 cm, CH_2Cl_2/ethyl acetate = 40/1) and provide compound **2** as colorless solid with 68% yield.

^{1}H NMR (400 MHz, $CDCl_3$, 298 K): δ = 6.17 (d, *J* = 0.8 Hz, 1H, pyrrole), 4.42 (s, 2H, methylene), 3.76 (t, 2H, ethylene), 2.56 (s, 3H, methyl), 2.21 (d, *J* = 0.8 Hz, 3H, methyl), 1.64-1.56 (m, 2H, ethylene), 1.38 (sext, *J* = 7.6 Hz, 2H, ethylene), 0.96 ppm (t, *J* = 7.2 Hz, 3H, methyl); ^{13}C{1H} NMR (100 MHz, $CDCl_3$, 298 K): δ = 187.0, 137.0, 128.1, 116.7, 107.1, 47.4, 43.6, 32.6, 20.2, 13.9, 12.4, 12.1 ppm; HRMS(ESI): m/z calcd for $C_{12}H_{19}ClNO^+$: 228.1150 $[M+H]^+$; found: 228.1149. R_f = 0.66 (silica gel, CH_2Cl_2/ethyl acetate = 40/1)

· Synthesis of compound **3**

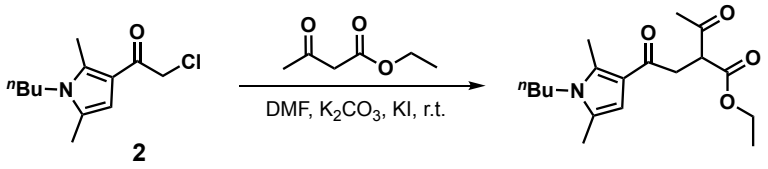

455 mg (2.00 mmol) of compound **2**, 304 mg (2.20 mmol) K_2CO_3, 365 mg (2.2 mmol) KI were added in to 50 mL Schlenk flask under N_2. Then, 10 mL anhydrous DMF and 286 mg (2.20 mmol) ethyl acetoacetate were added. The mixture was stirred at room temperature overnight. After finish of reaction, the mixture was diluted with 200 mL ether and washed by water (200 mL × 2). Ether layer was dried over Na_2SO_4 and remove the solvent under reduced pressure. The crude mixture was separated by silica gel column (diameter: 4 cm, height: 12 cm, hexane/acetone = 5/1) and provide compound **3** as colorless oil with 90% yield.

^{1}H NMR (400 MHz, $CDCl_3$, 298 K): δ = 6.28 (d, *J* = 1.2 Hz, 1H, pyrrole), 4.24-4.13 (m, 3H, ethylene and methine), 3.73 (t, *J* = 7.8 Hz, 2H, ethylene), 3.45 (dd, ^2J = 18.0 Hz, ^3J = 8.6 Hz, 1H, methylene), 3.28 (dd, ^2J = 18.0 Hz, ^3J = 5.6 Hz, 1H, methylene), 2.50 (s, 3H, methyl), 2.40 (s, 3H, methyl), 2.20 (s, 3H, methyl), 1.36 (sext, *J* = 7.6 Hz, 2H, ethylene), 1.27 (t, *J* = 7.0 Hz, 3H, methyl), 0.95 ppm (t, *J* = 7.4 Hz, 3H, methyl), one ethylene peak overlapped with water peak. ^{13}C{1H} NMR (100 MHz, $CDCl_3$, 298 K): δ = 203.2, 193.0, 169.6, 135.1, 127.6, 118.8, 107.7, 61.5, 54.0, 43.4, 39.0, 32.7, 30.3, 20.2, 14.1, 13.8, 12.3, 12.0 ppm. HRMS(ESI): m/z calcd for $C_{18}H_{27}NNaO_4^+$: 344.1832 $[M+Na]^+$; found: 344.1830. R_f = 0.33 (silica gel, hexane/acetone = 5/1)

· Synthesis of compound **4**

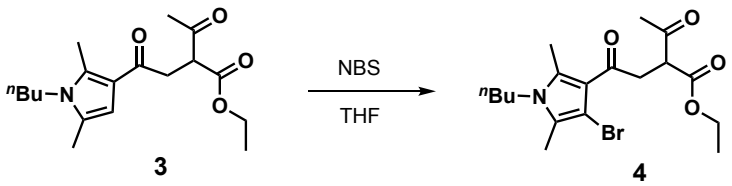

3 **4**

206 mg (0.640 mmol) compound **3** was dissolved in 12 mL THF, then the 114 mg (0.640 mmol) NBS was added slowly. After 15 min stir at room temperature, the THF was removed by evaporation. Added 30 mL water into the flask and extracted by ether (30 mL × 2). Ether layer was dried over Na_2SO_4 and remove the solvent by evaporation. The crude mixture was separated by silica gel column (diameter: 3 cm, height: 15 cm, hexane/ethyl acetate = 5/1) and provide compound **4** as yellow oil with 88% yield.

^{1}H NMR (400 MHz, $CDCl_3$, 298 K): δ = 4.24- 4.11 (m, 3H, ethylene and methine), 3.78 (t, J = 7.8 Hz, 2H, ethylene), 3.69 (dd, ^2J = 18.4 Hz, ^3J = 7.6 Hz, 1H, methylene), 3.57 (dd, ^2J = 18.4 Hz, ^3J = 5.6 Hz, 1H, methylene), 2.45 (s, 3H, methyl), 2.40 (s, 3H, methyl), 2.23 (s, 3H, methyl), 1.36 (sext, J = 7.2 Hz, 2H, ethylene), 1.28 (t, J = 7.0 Hz, 3H, methyl), 0.96 ppm (t, J = 7.2 Hz, 3H, methyl), one ethylene peak overlapped with water peak. ^{13}C{1H} NMR (100 MHz, $CDCl_3$, 298 K): δ = 203.2, 193.3, 169.7, 135.8, 126.9, 118.9, 94.8, 61.6, 54.3, 44.4, 41.6, 32.6, 30.2, 20.1, 14.2, 13.8, 12.5, 11.3. HRMS(ESI): m/z calcd for $C_{18}H_{26}BrNNaO_4^+$: 422.0937 $[M+Na]^+$; found: 422.0935. R_f = 0.46 (silica gel, hexane/ethyl acetate = 5/1)

· Synthesis of compound **5**

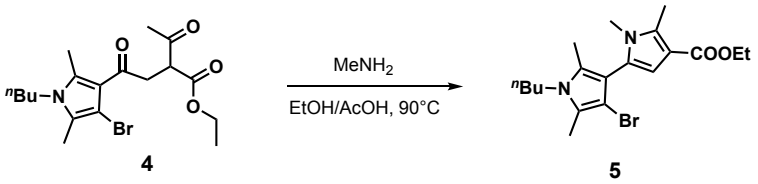

4 **5**

In a 200 mL flask, 720 mg (1.80 mmol) compound **4**, 1.08 g (9.00 mmol) $MgSO_4$, 9 mL ethanol and 9 mL acetic acid were added. Then methylamine (9.8 M in methanol, 0.551 mL) was added into the flask. The mixture was heated at 90°C for 2 h. The solvent was removed by evaporation and then the residue was washed by 100 mL saturated $NaHCO_3$ aqueous solution. The aqueous mixture was extracted by CH_2Cl_2 (60 mL × 2), and the CH_2Cl_2 layer dried over Na_2SO_4 and remove the solvent by evaporation. The crude mixture was separated by silica gel column (diameter: 4 cm, height: 10 cm, hexane/ethyl acetate = 4/1) and provide compound **5** as colorless oil with 68% yield.

^{1}H NMR (400 MHz, $CDCl_3$, 298 K): δ = 6.42 (s, 1H, pyrrole), 4.30-4.22 (m, 2H, ethylene), 3.80-3.76 (m, 2H, ethylene), 3.31 (s, 3H, methyl), 2.57 (s, 3H, methyl), 2.24 (s, 3H, methyl), 2.10 (s, 3H, methyl), 1.66-1.59 (m, 2H, ethylene), 1.43-1.31 (m, 5H, ethylene and methyl), 0.97 ppm (t, J = 7.2 Hz, 3H, methyl). ^{13}C{1H} NMR (100 MHz, $CDCl_3$, 298 K): δ = 166.0, 136.1, 127.6, 126.4, 124.8, 111.5, 111.2, 110.7, 97.0, 59.2, 44.9, 33.1, 31.3, 20.2, 14.7, 13.9, 11.93, 11.91, 11.1. HRMS(ESI): m/z calcd for C19H27BrN2NaO2+: 417.1148 $[M+Na]^+$; found: 417.1145.

5.6 Reference

[1] Nishinaga, T.; Ohmae, T.; Iyoda, M. Recent Studies on the Aromaticity and Antiaromaticity of Planar Cyclooctatetraene. *Symmetry* **2010**, *2*, 76-97.

[2] Rapson, W. S.; Shuttleworth, R. G. Niekerk, J. N. v. 89. Benzcyclooctatetraenes. Part III. Diphenylene and tetraphenylene. *J. Chem. Soc*. **1943**, 326-327.

[3] Kauffmann, T.; Greving, B.; König, J.; Mitschker, A.; Woltermann, A. Synthesis of Heterocyclic Cyclopolyaromatics Containing Similar Kinds of Nuclei. *Angew. Chem. Int. Ed*. **1975**, *14*, 713-714.

[4] Talaz, O.; Saracoglu, N. A study on the Synthesis of Structural Analogs of Bis-indole Alkaloid Caulerpin: A Step-by-step Synthesis of a Cyclic Indole-tetramer. *Tetrahedron* **2010**, *66*, 1902-1910.

[5] Mouri, K.; Saito, S.; Yamaguchi, S. Highly Flexible π-Expanded Cyclooctatetraenes: Cyclic Thiazole Tetramers with Head-to-Tail Connection. *Angew. Chem. Int. Ed*. **2012**, *51*, 5971-5975.

[6] Nakamura, Y.; Aratani, N.; Shinokubo, H.; Takagi, A.; Kawai, T.; Matsumoto, T.; Yoon, Z. S.; Kim, D. Y. Ahn, T. K.; Kim, D.; Muranaka, A.; Kobayashi, N.; Osuka. A. A Directly Fused Tetrameric Porphyrin Sheet and Its Anomalous Electronic Properties That Arise from the Planar Cyclooctatetraene Core. *J. Am. Chem. Soc*. **2006**, *128*, 4119-4127.

[7] Chen, F.; Hong, Y. S.; Shimizu, S.; Kim, D.; Tanaka, T.; Osuka, A. Synthesis of a Tetrabenzotetraaza[8]circulene by a "Fold-In" Oxidative Fusion Reaction. *Angew. Chem. Int. Ed*. **2015**, *54*, 10639-10642.

[8] Sessler, J. L.; Weghorn, S. J.; Hiseada, Y.; Lynch, V. Hexaalkyl Terpyrrole: A New Building Block for the Preparation of Expanded Porphyrins. *Chem. Eur. J*. **1995**, *1*, 56-67.

[9] Setsune, J. 2,2'-Bipyrrole-Based Porphyrinoids. *Chem. Rev*. **2017**, *117*, 3044-3101.

[10] Angelini, G.; Giancaspro, C.; Gabriello Illuminati, G.; Sleiter, G. Electrophilic Heteroaromatic Reactions. 3. The Alpha-side-chain Bromination of Some Polysubstituted Alpha-methylpyrroles in the Dark. Evidence for the Formation of Intermediate σ adducts. *J. Org. Chem*. **1980**, *45*, 1786-1790.

[11] Croce, P. D.; Ferraccioli, R.; Ritieni, A. Selective α-Chlorination of Acetylpyrroles. *Synthesis* **1990**, *3*, 212-213.

[12] Castro, A. J.; Giannini, D. D.; Greenlee, W. F. Synthesis of a 2,3'-bipyrrole. Denitrosation in the Knorr pyrrole synthesis. *J. Org. Chem*. **1970**, *35*, 2815-2816.

[13] Farnier, M.; Soth, S.; Fournari, P. Recherches en Série Hétérocyclique. XXVIII. Synthèse de Bipyrroles. *Can. J. Chem*. **1976**, *54*, 1083-1086.

[14] Dohi, T.; Morimoto, K.; Maruyama, A.; Kita, Y. Direct Synthesis of Bipyrroles Using Phenyliodine Bis(trifluoroacetate) with Bromotrimethylsilane. *Org. Lett*. **2006**, *8*, 2007-2010.

[15] Gotsko, M. D.; Saliy, I. V.; Sobenina, L. N.; Ushakov, I. A.; Kireeva, V. V.; Trofimov, B. A. Functionalized Bipyrroles and Pyrrolyl-Aminopyrones from Acylethynylpyrroles and Diethyl Aminomalonate. *Synthesis* **2022**, *54*, 1134-1144.

[16] Nelson, T. D.; Meyers. A. I. The Asymmetric Ullmann Reaction III. Application of a First-order Asymmetric Transformation to the Synthesis of C2-symmetric Chiral, Non-racemic Biaryls. *Tetrahedron Lett*. **1994**, *35*, 3259-3262.

[17] Lin, G.; Hong, R. A New Reagent System for Modified Ullmann-Type Coupling Reactions: $NiCl_2(PPh_3)_2/PPh_3/Zn/NaH/Toluene$. *J. Org. Chem*. **2001**, *66*, 2877-2880.

[18] Gaussian 16, Revision C.01, Frisch, M. J.; Trucks, G. W.; Schlegel, H. B.; Scuseria, G. E.; Robb, M. A.; Cheeseman, J. R.; Scalmani, G.; Barone, V.; Petersson, G. A.; Nakatsuji, H.; Li, X.; Caricato, M.; Marenich, A. V.; Bloino, J.; Janesko, B. G.; Gomperts, R.; Mennucci, B.; Hratchian, H. P.; Ortiz, J. V.; Izmaylov, A. F.; Sonnenberg, J. L.; Williams-Young, D.; Ding, F.; Lipparini, F.; Egidi, F.; Goings, J.; Peng, B.; Petrone, A.; Henderson, T.; Ranasinghe, D.; Zakrzewski, V. G.; Gao, J.; Rega, N.; Zheng, G.; Liang, W.; Hada, M.; Ehara, M.; Toyota, K.; Fukuda, R.; Hasegawa, J.; Ishida, M.; Nakajima, T.; Honda, Y.; Kitao, O.; Nakai, H.; Vreven, T.; Throssell, K.; Montgomery, J. A., Jr.; Peralta, J. E.; Ogliaro, F.; Bearpark, M. J.; Heyd, J. J.; Brothers, E. N.; Kudin, K. N.; Staroverov, V. N.; Keith, T. A.; Kobayashi, R.; Normand, J.; Raghavachari, K.; Rendell, A. P.; Burant, J. C.; Iyengar, S. S.; Tomasi, J.; Cossi, M.; Millam, J. M.; Klene, M.; Adamo, C.; Cammi, R.; Ochterski, J. W.; Martin, R. L.; Morokuma, K.; Farkas, O.; Foresman, J. B.; Fox, D. J. Gaussian, Inc., Wallingford CT, 2016.

[19] https://github.com/CurtisColwell/StrainViz

Chapter 6

Summary and outlook

6.1 Summary

In first Chapter of this thesis, the fundamental background of porphyrin and calix[4]pyrrole related compounds was introduced. The effects of ring strain on the synthesis and properties of contracted analogues were then described. And the objective of this thesis domesticated that further reveal the effect of ring strain on synthesis and explore new strain-induced properties for the development of functional macrocycle.

In chapter2, two promising precursors including cyclic tetraketone and furanophane as plausible precursors for calix[2]type molecules were synthesized and their ring strain state were analyzed by X-ray single crystal structures. However, treatment with Paal–Knorr-type reaction condition did not proceed target calix[2]type molecules. The increased energy derived from ring strain was evaluated by theoretical calculations that the remarkably large value revealed that the second aromatic ring formation seems unfeasible for conventional thermal reactions. The result indicated synthesis of calix[2]type macrocycles is a more challenging task that require novel synthetic methodology.

In Chapter 3, StrainViz method was compared with homodesmotic reaction method by analyzing calix[3]pyrrole derivatives. Using the visualization of strain energy distribution, StrainViz was also used for investigation of highly strained calix[2]pyrrole and newly designed [2.2](2,5)pyrrolophane cores with four direct connected pyrrole rings.

In Chapter 4, the cyclo[4]pyrrole with core structure designed in Chapter 3, was successfully synthesized by a 6-step route combined carbonyl related reaction and Pd-catalyzed cross-coupling reaction. Cyclo[4]pyrrole exhibited a non-planar and highly strained macrocyclic structure, and the strain energy was investigated by theoretical calculation quantitatively. Two reversible oxidation processes of cyclo[4]pyrrole were identified in cyclic voltammetry and unique optical spectral changes during electrochemical oxidation was observed by spectroelectrochemical mearsument. Further theoretical analysis revealed unique conformational and electronic change in two steps oxidation. In the radical cation state, the dihedral angles around the pyrrol-2,5-diyl segment increased, which interrupted π-conjugation, resulting in the formation of a 3,2’:5’,3’’-terpyrrole-localized radical cation. In contrast, dication state mainly consisted of the triplet diradical dication form with the spin density delocalized onto the four pyrrole units bearing similar cyclophane-type conformation as neutral state.

In Chapter 5, a novel designed synthetic route was proposed for the elusive tetrapyrrole-fused COT compound. A facile and effective 4-step synthesis was performed toward promising bipyrrole precursors, among the key α-haloketone formation with dichloroiodate reagent. This efficient and facile synthesis of promising precursor laid the foundation for subsequent reactions and provides a new approach for bipyrrole synthesis.

6.2 Outlook

The failure of ring tightening approach in chapter 2 for calix[2] type macrocycle revealed new strategy is required. Referring some successful examples of other highly strained macrocycles, photochemical condition which used for [1.1]paracyclophane or elimination reaction used for cycloparaphenylene should be considered.

The research content in Chapters 2 and 3 demonstrates the practicality of using computational methods to predict and analyze ring tension. However, the relationship between ring strain energy, synthetic difficulty, and compound reactivity is not yet fully understood and worth to further investigate.

The important compound, cyclo[4]pyrrole as a new conjugated core, has many other properties waiting to be explored. After synthesizing the molecule, I explored its subsequent reactions, such as aromatic electrophilic bromination and intramolecular dehydrogenation N-N coupling reactions. However, this molecule exhibits very unusual reactivity under normal conditions, and further research is needed.

Finally, completing all the synthesis steps in Chapter 5 to generate tetrapyrrole-fused cyclooctatetraene will be expected and the resulting compound will become important subject for both porphyrin field and cyclooctatetraene field.

List of Publication

Chapter 2

Toward calix[2]-type macrocycles: Synthesis and structural analysis of cyclic tetraketone and highly strained furanophane

Sano, T.[†]; **Sun, Y.**[†]; Mukai, T.; Inaba, Y.; Yoneda, Y.; Ide, Y.; Pirillo, J.; Hijikata, Y.; Inokuma, Y. [†] = equal contribution

J. Porphyrins Phthalocyanines. **2023**, *27*, 1071-1073.

Chapter 4

Cyclo[4]pyrrole with *α–β* direct linkages.

Sun, Y.; Kitahara, R.; Ichino, T.; Ide, Y.; Senboku, H.; Shimizu, S.; Tanaka, T.; Inokuma, Y.

Chem. Sci. **2024**, *15*, 19571-19576.

Acknowledgement

Firstly, I would like to thank the staff of our group for the academic guidance, including Professor Yasuhide Inokuma, Associate Professor Hisanori Senboku, Assistant Professor Yuki Ide, and also the former staff including Assistant Professor Tomoki Yoneda and Assistant Professor Yusuke Kinoshita.

Secondly, I would like to thank the research collaborator, Prof. Yuh Hijikata, Prof. Jenny Pirillo and Dr. Tomoya Ichino from WPI-ICReDD, Prof. Soji Shimizu from Kyushu University, Prof. Takayuki Tanaka from Kyoto University.

Then, I would like to thank the reviewers for this thesis, including Prof. Hajime Ito, Prof. Takeshi Ohkuma and Prof. Takanori Suzuki.

I also would like to thank other members of our group. Particularly, Mr. Narito Ozawa provided me with a lot of help in my daily life when I arrived in Japan as an international student. And Dr. K. I. Shivakumar, Dr. Yumehiro Manabe, Dr. Yuya Inaba gave many suggestions for the experiments.

Finally, I would like to thank Hokkaido University for the financial support from EXEX doctoral fellowship.